LIGHT-WEIGHT STEELS BASED ON IRON-MANGANESE-ALUMINIUM-NICKEL: INFLUENCE OF BORON ADDITION ON MICROSTRUCTURES AND MECHANICAL PROPERTIES

Master of Science Thesis

Mohsen ZAMANI

Eskisehir 2019

LIGHT-WEIGHT STEELS BASED ON IRON-MANGANESE-ALUMINIUM-NICKEL: INFLUENCE OF BORON ADDITION ON MICROSTRUCTURES AND MECHANICAL PROPERTIES

Mohsen ZAMANI

MASTER OF SCIENCE THESIS

Department of Material Science and Engineering
Supervisor: Assoc. Prof. Hakan GAŞAN

Eskisehir
Anadolu University
Graduate School of Sciences
June 2019

FINAL APPROVAL FOR THESIS

This thesis titled "light-weight steels based on iron-manganese-aluminium-nickel: influence of boron addition on microstructures and mechanical properties" has been prepared and submitted by Mohsen ZAMANI in partial fulfillment of the requirements in "Anadolu University Directive on Graduate Education and Examination" for the Degree of Master of Science in Material Science and Engineering Department has been examined and approved on 18/06/2019.

Committee Members	Title, Name and Surname	Signature
Member (Supervisor)	: ASSOC. PROF. Hakan GAŞAN	
Member:	: ASSOC. PROF. ERHAN AYAS	
Member:	: DR. GÜL İPEK SELİMOĞLU	

Prof. Dr Murat TANIŞLI

Director of Graduate School of Sciences

ABSTRACT

LIGHT-WEIGHT STEELS BASED ON IRON-MANGANESE-ALUMINIUM-NICKEL: INFLUENCE OF BORON ADDITION ON MICROSTRUCTURES AND MECHANICAL PROPERTIES

Mohsen ZAMANI
Department of Material Science and Engineering
Anadolu University, Graduate School of Sciences, June 2019
Supervisor: Assoc. Prof. Hakan GASAN

A novel medium entropy alloy (MEA) based on Fe-Mn-Al-Ni has been designed adopting HEAs phase formation rules, and the effects of minor addition of boron on phase content have been also investigated using both theoretical and computational approaches. Boron-free $Fe_{(52.71-x)}Mn_{31.11}Al_{5.09}Ni_{11.08}B_x$ (x=0,0.05,0.2,0.5,0.7 wt%) MEA showed a single face-centered cubic (FCC) structure. XRD results indicated that with 0.05 and 0.2 wt% boron addition the system maintains its single-phase structure. Further boron addition leads to the formation of metal boride intermetallics by 4.62 and 6.14% of Fe_2B intermediate phase in as-cast and 2.7 and 5.4% in D&H samples due to Rietveld Analysis for 0.5 and 0.7 wt% boron doped alloys respectively. Boron addition has positive effect on grain size reduction of the system where just by 0.05 wt % boron addition the grain size has been almost halved compare to boron free as-cast sample. Moreover, it is observed that as the boron level increases, the hardness value increases. The thermomechanical process resulted in increasing the yield strength by ~50% (from 151 MPa to 222.5 MPa) and ultimate tensile strength by ~15% (from 476 MPa to 543 Mpa)- both in 0.7 wt % boron doped alloy- at comparable ductility(Ɛ>60%).

Keywords: Medium Entropy Alloys, Design and modeling, Vaccum arc melting, Boron addition, Mechanical properties

ÖZET

DEMİR-MANGAN-ALUMİNYUM-NİKEL ESASLI DÜŞÜK AĞIRLIKLI ÇELİKLER: BOR İLAVESİNİN MİKROYAPI VE MEKANİK ÖZELLİKLERE ETKİSİ

Mohsen ZAMANI
Malzeme Bilimi ve Mühendisliği Anabilim Dalı
Anadolu Üniversitesi, Fen Bilimler Enstitüsü, Haziran 2019
Danışman: Doç. Dr. Hakan GAŞAN

Yüksek entropili alaşım tasarımı anlayışı ile bor katkısız ve düşük miktarda bor ilaveleriyle, Fe-Mn-Al-Ni esaslı yeni bir orta entropili alaşımı hem teorik hem de CALPHAD yaklaşımları kullanılarak tasarlanmıştır. Bor içermeyen $Fe_{(52.71-x)}Mn_{31.11}Al_{5.09}Ni_{11.08}B_x$ (x = 0,0.05,0.2,0.5,0.7 ağ.%) alaşımının, tek fazlı YMK yapıda olduğu anlaşılmıştır. XRD sonuçları % 0.05 ve% 0.2 bor katkılı sistemin tek fazlı yapısını koruduğunu göstermiştir. Daha fazla bor ilavesi ile üretilen alaşımlara yapılan Rietveld analizi sonuçları % 0.5 ve % 0.7 bor katkılı alaşımlar için sırasıyla döküm sonrası % 4.62 ve % 6.14 ve ısıl işlem sonrası %2.7 ve %5.4 oranında Fe_2B metal borür ara fazının oluştuğunu göstermektedir. Yalnızca % 0.05 bor ilavesi ile borun katkısız numuneye kıyasla tanecik boyutunun neredeyse yarı yarıya azaldığı, bor katkılamanın tane boyutu üzerinde etkisini doğrulamıştır. Ayrıca, ilave edilen bor miktarı arttıkça sertlik değerinin de arttığı gözlenmektedir. Bor katkılı alaşımlara uygulanan termomekanik işlemler neticesinde bor katkısız alaşımlarla aynı süneklik seviyesinde kalmakla birlikte, akma dayanımında %50 (ağırlıkça % 0.7 bor katkılı alaşımda 151 MPa'dan 222.5 MPa'a) ve çekme dayanımında ~% 15'e kadar (yine % 0.7 bor katkılı alaşımda 476 MPa'dan 543 MPa'a) artış elde edilmiştir..

Anahtar Kelimeler: Orta Entropili Alaşımlar, Tasarım ve modelleme, Vakum ark ergitme, Bor ilavesi, Mekanik özellikler

ACKNOWLEDGEMENT

First of all, I would like to express my sincere gratitude and thanks to Assoc. Prof. Hakan GAŞAN for his unconditional support and guidance during this research.

I would like to extend my heartfelt thanks to Akın ÖZCAN, a doctoral student who has not deprived me of his assistance in any stage of my thesis.

I would like to thank to Dr. Gül İpek SELİMOĞLU to provide her laboratory for the thermomechanical process.

I would like to also thank to Orhan ÇETİN and İrem ÖZKIR for supporting me in XRD laboratory and Rietveld Analysis.

My sincere thanks go to Raheleh, Aydin and Derya for their friendship and all the memories and moments we have shared.

My most heartfelt acknowledgement must go to my parents and my brothers for their endless love and support.

18/06/2019

STATEMENT OF COMPLIANCE WITH ETHICAL PRINCIPLES AND RULES

I hereby truthfully declare that this thesis is an original work prepared by me; that I have behaved in accordance with the scientific ethical principles and rules throughout the stages of preparation, data collection, analysis and presentation of my work; that I have cited the sources of all the data and information that could be obtained within the scope of this study, and included these sources in the references section; and that this study has been scanned for plagiarism with "scientific plagiarism detection program" used by Anadolu University, and that "it does not have any plagiarism" whatsoever. I also declare that, if a case contrary to my declaration is detected in my work at any time, I hereby express my consent to all the ethical and legal consequences that are involved.

Signature

Mohsen ZAMANI

CONTENTS

Page

Page

LIST OF TABLES

LIST OF FIGURES

Page

Page

SYMBOLS AND ABBREVIATIONS INDEX

δ	: Delta
σ	: Sigma
Ω	: Omega
HEAs	: High-Entropy Alloys
MPEAs	: Multi-Principal Element Alloys
CCAs	: Complex Concentrated Alloys
MEAs	: Medium-Entropy Alloys
BMGs	: Bulk Metallic Glasses
FCC	: Face Centered Cubic
BCC	: Body Centered Cubic
HCP	: Hexagonal Close Packed
CALPHAD	: CALculation of PHAse Diagrams
GB	: Grain Boundary
D&H	: Deformed and Heat-treated

1. INTRODUCTION

High-entropy alloys (HEAs) have become one of the most interesting research fields in materials science and engineering in the last decade. These alloys, which are also known as multi-principal element alloys (MPEAs), or complex concentrated alloys (CCAs), unlike conventional alloys, are composed of at least four or five elements, with the possible number of high entropy compositions. With the advent of the HEAs, design and modeling (especially preparing the relevant phase diagrams) of modern alloys has changed consequently. Various studies have proved that HEAs, compare to traditional alloys, possess higher strength and good creep and softening resistance properties.

On the other hand, since the 2000s, much attention has been also concentrated on the developing of ductile low-density steels with higher strength than traditional ones especially for automotive applications; studies on light-weight steels and particularly Fe–Al–Mn–C system, as an alternative to traditional steels, have led to outstanding achievements in automotive applications. Although this alloy has shown superior mechanical properties- up to a yield strength of 730 MPa, an ultimate tensile strength of 1000 MPa and total elongation of 55% reported by Frommeyer and Brux and a yield strength of 915 MPa, an ultimate tensile strength of 1140 MPa and total elongation of 22% reported by Sutou et al. - the related microstructural and underlying metallurgical issues are problematic. Despite the fact that Fe–Al–Mn–C light-weight steels - also known as TRIPLEX steels - can have ferritic, austenitic or even a mixture of them depending on primary alloying elements of C, Mn or Al, careful thermodynamic and phase studies, now, have been clarified that based on the temperature and chemistry, even four of five equilibrium phases (γ-austenite, α-ferrite, κ-carbide, M_3C carbide (θ) and β-Mn) can coexist in a Fe–Al–Mn–C system [9] which makes the deformation mechanism and heat-treatment procedure even more complicated.

In this study, benefiting from the phase formation rules of HEAs and referring to the Fe–Al–Mn–C system, a medium entropy multi-component alloy based on Iron (Fe), Manganese (Mn), Aluminum (Al) and Nickel (Ni), with a single FCC phase has been designed. The motivation in the development of this MEA can be described as follows: ***Firstly***, Iron has been chosen as the major alloying element to reduce the cost. ***Secondly***, Manganese and Nickel were selected as the FCC phase stabilizers. ***Thirdly***, Aluminium is selected as the low-density element, which can reduce the density of the alloy.

Regarding HEAs with FCC crystal structures, the preliminary mechanical tests indicate that this type of alloys possesses good ductility but poor strength. To strengthen HEAs with FCC phases, lots of studies have been reported regarding to address the problem: solid solution strengthening, nitriding, deformation strengthening, and annealing are the methods have been used to strengthen this type of HEAs. In this study boron (B) as the minor alloying element has been selected due to the following reasons; ***firstly***, boron was nominated for its effective grain size reduction, which was reported in various studies. ***Secondly***, in this study as the influence of grain size reduction on mechanical properties was in a great deal of interest, boron as one and only microalloying element has been selected, and **not last but least**, the formation of possible M_2B and it's consequence on both microstructure and mechanical properties was supposed to investigate. In this study, carbon as another possible minor alloying element has been discarded for two reasons; (i) to prevent the formation of κ-carbide and M_3C carbide (θ) phases, and (ii) to prevent a complicated microstructure.

This study is firstly concerned with the thermodynamic and computational design of FeMnAlNi MEA. The objective of this work was to find a single FCC phase and calculate related thermodynamic parameters and phase diagram basically for undoped FeMnAlNi MEA and eventually boron doped alloys and also investigate the validity of calculations by X-ray diffraction (XRD) technique and Rietveld analysis for as-cast and thermomechanical treated samples to demonstrate whether the predicted phases has been formed. Secondly, microstructural and mechanical characterization has been carried out to investigate the influence of boron addition on microstructure and mechanical properties of the system.

2. HIGH ENTROPY ALLOYS

With the emergence of HEAs, some fundamental issues contradict with the theories, models, and methods proposed for traditional alloys. Accordingly, the emergence of HEAs, consist of a large number of major elements, indicates a paradigmatic change in the design of modern alloys.

In this chapter, varying definitions of HEAs and their historical development path, as well as their thermodynamic aspects, basic properties, fabrication routes and finally designing methods of HEAs, are being briefly discussed.

2.1. Introduction and Fundamentals

2.1.1. The use of different terms of HEA, MPEA, and CCA

Today HEAs have become strongly linked with finding single-phase structures by adjusting the configurational entropy of the system. This is mostly possible by exploring the central regions of hyper-dimensional composition space. The biggest difference between HEA definition with the other ones is that despite HEA definition, multi-principal element alloys (MPEAs), complex concentrated alloys (CCAs) and baseless alloy definitions do not come to any conclusion about the size of the entropy or the types of available phase(s).

To be more clear, the HEA definition is used when the configurational entropy or a single-phase product is important. Any other way, the terms MPEAs or CCAs are used to demonstrate the fundamentals of this field (Yeh, 2006).

The traditional alloy design approach is frequently based on one element and adding other minor elements to optimize the properties and performances. While HEAs as the revolutionary alloy design concept is proposing a multi-component system with equimolar or near equimolar ratios to enhance the configuration entropy and stabilize the single-phase structure (Gao et al.,2006).

2.1.2. Background

The first study on MPEAs and HEAs were published both in 2004, but the background work started much earlier. The first studies for MPEAs began as a bachelor thesis in the late 1970s and were continued in 1998 by another bachelor research. These pioneer studies were rearranged and published in 2002. HEA work started in 1996 as a series of academic studies which resulted in five publications in 2004. These alloys were defined as HEAs by Yeh (2004) and named by Cantor (2004) as multi-component alloys, both referring to the same concept. The basic concept of these studies was the synthesis of metallic alloys possessing five or more elements in a near-equiatomic ratio. The characterization of mentioned alloys showed much fewer phases comparing to predictions based on the Gibbs phase rule. As a consequence of these studies, it was revealed that some compositions in this alloying system can achieve a single-phase solid solution structure in which each component has an equal chance to occupy in a given lattice structure. These observations and the consequent reports have caused a great interest in HEAs. Since 2004, each day there is much greater interest on HEAs as far as the fact that in 2016 roughly 450 publication just based on HEAs had been published. The content of these publications focuses on the mechanisms of improving the ability to understand the underlying structure of the unique structure owned by these alloys, and to predict the HEA composition. A wide range of full review articles as well as two books had been published, providing inclusive information on HEAs (Gao et al.,2006; Murty et al., 2014).

2.1.3. Definitions of HEAs

Although there is no definition for the multicomponent alloys yet, there are various definitions of HEA. The number of HEA definitions creates some confusion that leads to the controversy over whether certain alloys are referred to as HEA. Avoiding confusing definitions, commonly used composition- and entropy-based definitions will be introduced and discussed in this section.

2.1.3.1. Composition-based definition

Yeh one of the pioneer researchers in this field, in one of his earlier articles (2004) defined HEAs as, "*alloys which are composed of five or more principal elements in equimolar ratios".* However, he mentioned in the same article that it is not essential to fabricate these alloys just in equimolar ratios. He expanded his definition as *"principal elements with the concentration of each element being between 35 and 5 at. -%."* Therefore, omitting such a restriction, led to a paradigmatic shift on the number of HEAs. Beside that HEAs could also contain minor elements to modify the properties which means the number of these alloys are not limited just by pure HEAs (Yeh,2006) and can increase continuously. Particularly, this definition indicates elemental restricts and ignores the configurational entropy, where it also does not mention the requirement of single-phase structures.

2.1.3.2. Entropy-based definition

First of all, the term high entropy inspires to define a definition based on the magnitude of entropy. Thus, this alternate definition divide all alloys to the afterward three categories; low entropy alloys ($S^{SS,ideal} < 0.69R$), medium entropy alloys ($0.69R < S^{SS,ideal} < 1.61R$) and high entropy alloys ($S^{SS,ideal} > 1.61R$). Ignoring the fact that the entropy of alloys can change with temperature, this definition promote the idea that each alloy has an individual value of configurational entropy. It is worthy to mention that the effect of temperature on entropy value can be either slight or dramatic considering the effect of temperature which could be even on the short-range atomic pattern or chemical partitioning in a first-order phase transition, respectively (Gao et al.,2006). Overall and considering all the facts, the entropy-based definition has presented by Yeh (2006). According to him, the high entropy alloys could be determined as the *"liquid solution and high-temperature solid solution states where the thermal energy is sufficiently high to cause different elements to have random positions within the structure*". This definition implies that an alloy can achieve the possible maximum entropy at high temperatures or in the liquid state. However, based on experimental approaches, even a binary metallic liquid cannot reach %100 random atomic positions at the melting point. (Tomlin and Kaloshkin, 2015). These issues are such a challenge in the use of this definition.

2.2. Phase Formation Rules: Thermodynamic Approach

Disregarding the kinetic factors, the Gibbs free energy, *G*, is the key parameter which thermodynamically controls the phase formation. Considering various alloys formation, the Gibbs free energy, itself, is related to the enthalpy, *H*, and the entropy, *S*, via the following equation:

$$\Delta\mathrm{G}_{mix} = \Delta\mathrm{H}_{mix} - \mathrm{T}\Delta\mathrm{S}_{mix} \tag{2.1}$$

Here ΔG_{mix} is the Gibbs free energy of mixing, ΔH_{mix} is the enthalpy of mixing, ΔS_{mix} is the entropy of mixing, and T is the melting temperature. Note that the term ΔS_{mix} includes all entropy sources such as configurational, vibrational, electronic, and magnetic contributions. Naturally, referring to Eq 2.1, the competition between ΔH_{mix} and $T\Delta S_{mix}$ will determine the phase selection in various alloys which comprises the thermodynamic consideration of phase formation rules (Gao et al, 2016).

The enthalpy of mixing, ΔH_{mix}, for a multicomponent alloying system with n elements could be estimated by the formula driven by Zhang et al (2008):

$$\Delta\mathrm{H}_{mix} = \sum_{i=1, i\neq j}^{N} 4\Delta\mathrm{H}_{AB}^{mix}\, c_i c_j \tag{2.2}$$

where $\Delta\mathrm{H}_{AB}^{mix}$, is the regular solution interaction parameter between the *ith* and *jth* elements, c_i or c_j is the atomic percentage of the *ith* or *jth* component, and ΔH is the enthalpy of mixing of the binary liquid alloys.

Another equation is proposed by Zhang et al. (2008) to calculate *the entropy of mixing*, ΔS_{mix} regarding a regular solution system with "*n*" elements;

$$\Delta S_{mix} = -R \sum_{i=1}^{n} c_i \ln c_i \tag{2.3}$$

Where *R* is the gas constant, and *n* the total number of the constituent elements.

The atomic size effect is another important factor in regard to the phase formation of multi-component systems such as HEAs, with plenty of elements in which each element has its own specific atomic size. When determining phase formation rules for HEAs, descriptors are typically collected from parameters related to thermodynamic and geometry, considered using the parametric approach. To establish an effective geometry rule to reduce the negative atomic size effects Zhang et al. (2008) has comprised both Hume-Rothery and the famous Inoue's three empirical rules and has proposed Delta (δ) parameter which is defined as;

$$\delta = 100\sqrt{\sum_{i=1}^{N} c_i \left(1 - \frac{r_i}{\bar{r}}\right)^2} \quad (2.4)$$

Here, r_i represent the atomic radius of the *ith* element, where the average atomic size can be calculated as; $\bar{r} = \sum_{i=1}^{n} c_i r_i$.

Figure 2.1 shows the relationship of ΔH_{mix}, Delta (δ), and ΔS_{mix} factors to select a single-phase solid solution based on o high entropy alloying systems (Zhang et al.,2008).

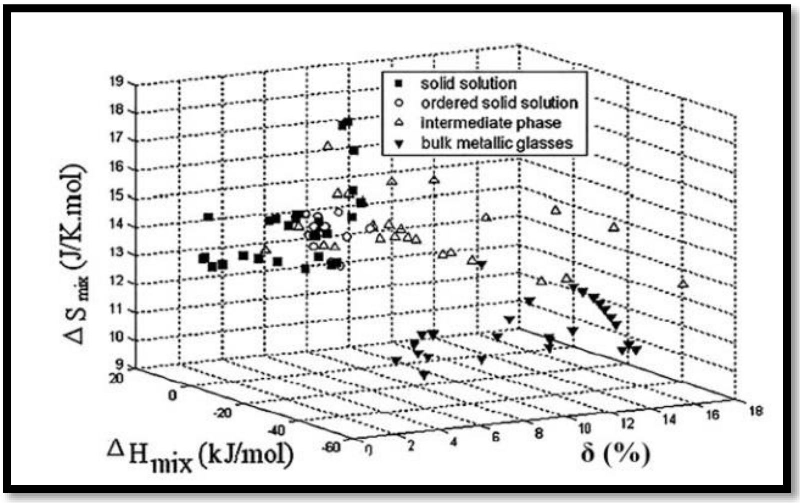

Figure 2.1. P*hase selection diagram of HEAs based on ΔH_{mix}, Delta (δ), and ΔS_{mix}* *(Zhang et al.,2008).*

Driven from Figure 2.1, the quantitative criterion for the formation of a single-phase solid solution due to Zhang et al. (2008) is:

- 12 J/K.mol ≤ ΔS_{mix} ≤ 17.5 J/K.mol
- -15kJ/mol < ΔH_{mix} < 5 kJ/mol *,and*
- δ < 6%.

Principally, in HEAs, high mixing entropy dominates the effects of mixing enthalpy and guarantees formation of the minimum number of possible phases. As a matter of better understanding of whether the mixing entropy dominates the effects of mixing enthalpy at the melting temperature, a new parameter, Ω, was proposed by Yang and Zhang (2012). The parameter Ω is defined by;

$$\Omega = \frac{T_m \Delta S_{mix}}{|\Delta H_{mix}|} \tag{2.5}$$

Where the melting temperature of the n-element alloy (T_m), can be calculated as the following equation;

$$T_m = \sum_{i=1}^{N} c_i (T_m)_i \tag{2.6}$$

Here $(T_m)_i$ is the melting temperature of each component.

On the other hand, in any temperature Ω parameter by a value greater than 1, can ensure that in that particular temperature the effect of the mixing entropy is greater than that of the enthalpy of mixing. Regarding equation 2.5 and considering that the calculated temperature was based on melting temperature of various components it can be concluded that if $\Omega > 1$, then at the melting temperature the high-entropy phase tends to form.

Based on analyzing the effects of Ω and δ parameters on the phase formation of various HEAs by Zhang et al. (2014), new criteria for forming solid solution phases were suggested: $\Omega \geq 1.1$ and $\delta \leq 6.6$ % (Figure 2.2).

This new attitude implies that the requirement of at least five element or high configurational entropy to form HEAs may not be necessary and as long as $\Omega > 1$ is satisfied high-entropy solid solution phase may form.

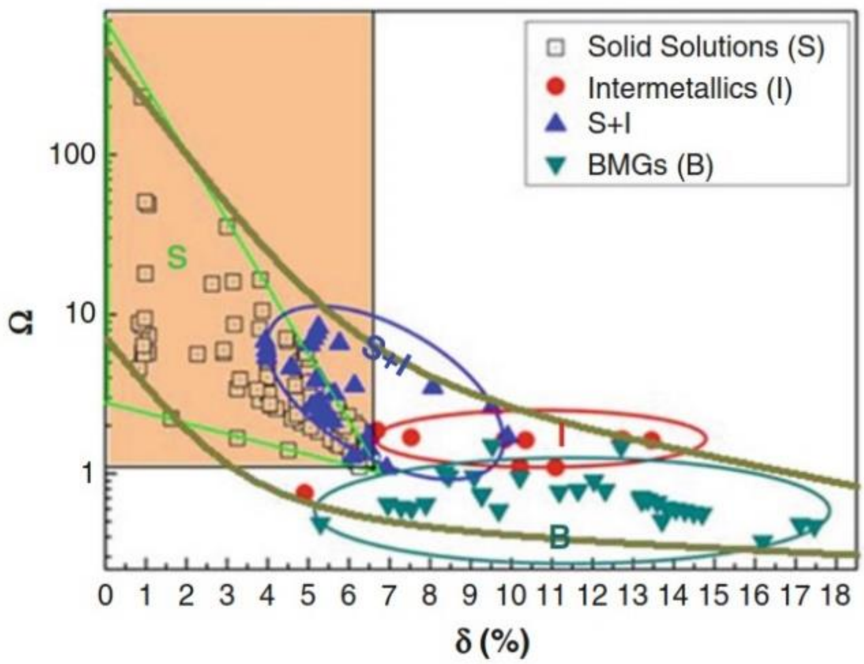

Figure 2.2. *Phase selection diagram of HEAs based on Ω and δ (Zhang et al., 2014)*

According to the Hume–Rothery rule where there is not a strong atomic size difference *the valence electron concentration (VEC)* of an alloy can influence the type of crystal structure of the alloy (Guo et al., 2011). This effect on the stability of FCC and BCC solid solution in HEAs has been analyzed by Guo et al. (2011).

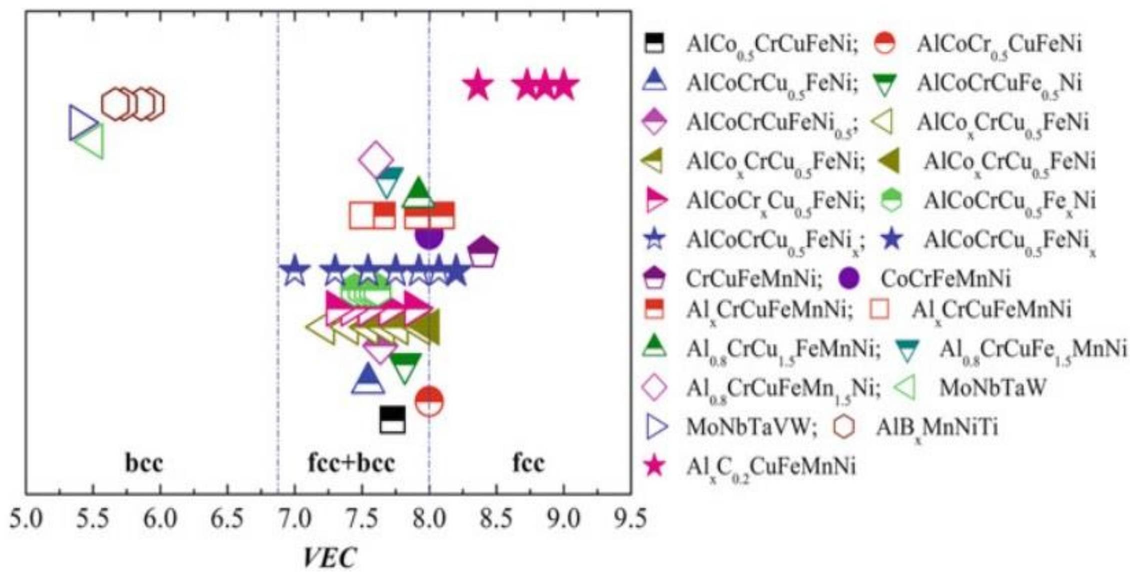

Figure 2.3. *Relationship between VEC and the phase stability of fcc and bcc phases in various HEAs (Guo et al.,2011).*

As it can be observed from Figure 2.3, a mixed of FCC and BCC phases coexist in the system as long as 6.87< VEC <8.0. FCC phases are stable at higher values (VEC≥8.0), whereas BCC phases are stable at lower (VEC 6.87) values. For HEAs, VEC is defined as;

$$VEC = \sum_{i=1}^{n} c_i (VEC)_i \quad (2.7)$$

Here, $(VEC)_i$ is VEC for the individual *ith* element.

2.3. For Core Effects of HEAs

The High-entropy effect, Sluggish diffusion effect, cocktail effect, and Severe lattice-distortion effect construct the four main characteristics of HEAs, also called as basic mechanisms of HEAs, that characterize the broad class of solid solution alloys (Oh et al., 2016).

2.3.1. High-entropy effect

The high-entropy effect indicates the tendency to stabilize the solid-solution phases. This effect was firstly proposed by Yeh (2004). The effect was highly contradictory since intermetallic phases were expected to be formed for equi- or near equi-molar alloy compositions which were placed at the center of the phase diagrams. (Murty, Yeh, and Ranganathan, 2014).

Based on the Gibbs phase rule which determines the number of phases (P) in a given alloy at constant pressure and equilibrium condition;

$$P = C+1-F \quad (2.8)$$

So, in a 6-component system at a given pressure, a maximum of 7 equilibrium phases is expected, however, with the concept of HEAs but only with carefully chosen compositions that satisfy the HEA-formation criteria, a single-phase solid solution can be achieved (Yeh et al., 2004).

As mentioned above high entropy effect tends to stabilize the high-entropy phases, i.e. solid-solution phases, rather than intermetallic phases. This can be explained by the maximum entropy production principle (MEPP) theory. This theory indicates that Intermetallics are mostly ordered phases which possess lower configurational entropy where the configurational entropy stoichiometric intermetallic compounds are zero, so are not stabilized through the solidification sequence of HEAs (Murty, Yeh, and Ranganathan, 2014).

As a result, this effect can increase the chance of formation of solution phases and make the microstructure much simpler than previously expected. Thus, this effect has the potential to improve the strength and ductility of the solution phases due to the solution hardening.

2.3.2. Sluggish diffusion effect

Due to many different kinds of atoms partitioning the same lattice structure and considering the highly limited vacancy concentration of HEAs diffusion process and consequently phase transformations in HEAs, comparing to traditional alloys, becomes much more difficult. In fact, a vacancy in the whole matrix is surrounded by so many atoms of different types during diffusion. As a result, the diffusion process and also phase transformation would be much slower in HEAs compare to conventional alloys. (Gao et al., 2016)

As a matter of fact, based on different field studies the sluggish diffusion effect can provide several important advantages compared to traditional alloys. These are; easiness to get supersaturated state, providing finer precipitates, higher recrystallization temperature, slower grain growth, a lower rate of particle coarsening, and better creep resistance. (Tong et al.,2005; Juan et al.,2013).

Comparing the diffusion coefficients for the elements in pure metals, stainless steels, and HEAs shows that HEAs have the lowest diffusion rate among these three different types of alloying system (Gao et al., 2016). Where;

HEAs < Stainless Steel < Pure Metal

2.3.3. The severe lattice distortion effect

The induced strain and stress in the lattice of HEAs is inevitable, as every atom in this multi-elemental matrix is surrounded by different kinds of atoms with different atomic sizes, different bonding energies, and different crystal structure tendencies. So, a lattice distortion as a result of this non-symmetrical neighboring atoms affects the atomic positions of each crystal (Tsai KY, Tsai MH, and Yeh, 2013). This effect is one of the main answers explaining the high strength of HEAs, especially the ones with BCC structures.

Severe lattice distortion affects properties of the alloy in two manners; firstly, it enhances the mechanical properties, and secondly, it reduces the thermal properties. Generally, it can effectively enhance hardness and strength by large solution hardening. However, it significantly reduces electrical and thermal conductivity due to its ability to disperse free electrons and phonons (Kao et al., 2011).

2.3.4. Cocktail effect

This effect indicates that mixing so many components in a single alloying system can bring unexpected properties that cannot be obtained from any independent element.

Tsai and Yeh (2014) showed that a certain property of a HEA can be greatly altered even by applying particular composition change and alloying manner, as shown in Figure 2.4. This figure indicates that the hardness of HEAs can be dramatically changed by adjusting the Al content in the $CoCrCuNiAl_x$ HEAs. In this study, they showed that by adjusting Al content, they can adjust the VEC value and transfer the crystal structure of the alloy to FCC, BCC + FCC or BCC structures. Adjusting Al content can help them to control the lattice constants for both the BCC and FCC and Consequently modify the hardness of the alloy (Tsai and Yeh, 2014).

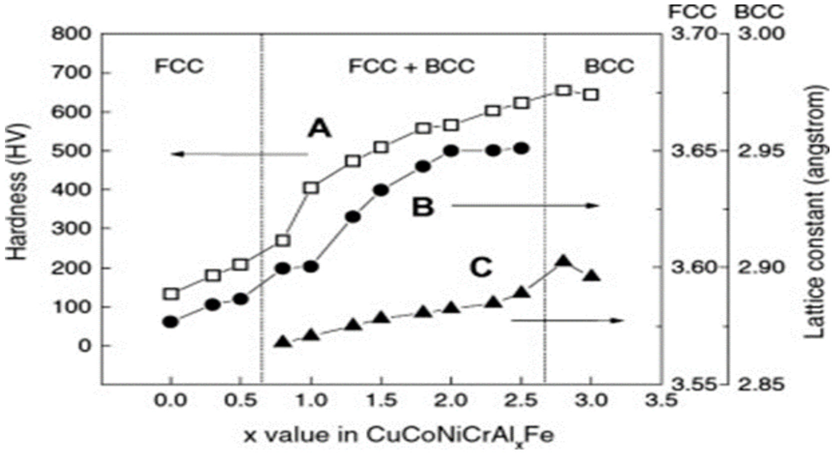

Figure 2.4. *Changes by adjusting the Al content in the $CoCrCuNiAl_xFe$ HEAs (Tsai and Yeh, 2014).*

2.4. Taxonomy

Miracle and Senkov (2017) has classified the 408 MPEAs into 7 alloying families. These families include 3d transition metals, refractory metals, light metals, 4f transition metals, brasses and bronzes, precious metals and finally interstitial compound i.e. borides, carbides, and nitrides. The alloy families are illustrated in Figure 2.5.

2.4.1. 3d transition metals

3d transition metals are the most widely studied alloy family in HEAs and approximately 85% of the MPEAs fall in this family. **Al**, **Co**, **Cr**, **Cu**, **Fe**, **Mn**, **Ni**, **Ti**, and **V** are 9 candidates for any 3d transition metals, which mostly contains at least 4 of these components. Fe is one of the most used elements in this family, where almost every MPEA (~ %96) include iron (Miracle and Senkov, 2017).

This alloying family used to consider as the extensions of stainless steels and superalloys.

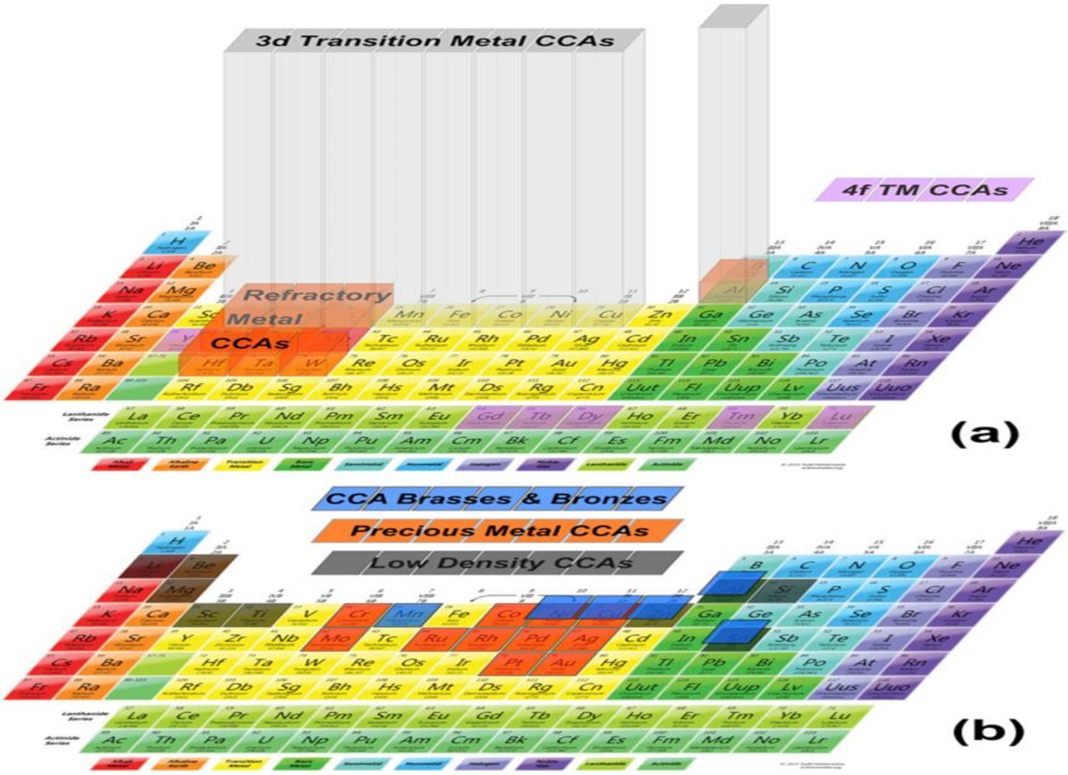

Figure 2.5. *Six of the seven HEA families.* ***(a)*** *3d transition metals, refractory metals, and 4f transition metals* ***(b)*** *light metals, precious metals and brasses and bronzes. (Miracle and Senkov, 2017).*

2.4.2. Refractory metals

Refractory HEAs were determined to establish new family high-temperature structural metals. This family offers outstanding mechanical properties such with a very wide range melting temperature, T_m, (2128–3695 K), with density (as low as 4.5 g/cm^3) and elastic moduli (up to 411 GPa for Young's modulus).

The refractory metal HEA family includes at least 4 of the 9 refractory elements: **Cr**, **Hf**, **Mo**, **Nb**, **Ta**, **Ti**, **V**, **W**, and **Zr**. **Al** and **Si** as non-refractory elements have been also observed as a part of this family to decrease density and increase intended properties (Miracle and Senkov, 2017).

According to Miracle and Senkov (2017), this family just covers 7% of total studied HEAs (29 refractory CCAs were reported by mid-2015). These refractory CCAs are based on Mo, Nb, Ta, W, Hf, Zr, Cr, and V element groupings, where other refractory elements (i.e. Ir, Os, Re, Rh, Ru) have not been used in refractory metal CCAs yet which offers new possibilities to investigate this family group.

2.4.3. Other alloy families

In the past 5-6 years and with the emergence of refractory HEAs investigations to introduce new family groups has been carried out. Since then several new alloying families have been introduced in various papers.

Light-weight structural metals base on **Al**, **Be**, **Li**, **Mg**, **Sc**, **Si**, **Sn**, **Ti** and **Zn** elements as *the third family* of HEAs was introduced to develop new alloys for aerospace and transportation applications. Seven alloys have been reported in this family by 2016. The most challenge in this family is the broad range of elemental melting and boiling points make processing difficult. To address this problem mechanical alloying or careful selection of elements is needed in primary processing (Miracle and Senkov, 2017).

4f transition as *the fourth family* of alloys contains at least 4 elements **Dy**, **Gd**, **Lu**, **Tb**, and **Tm**, plus the element **Y**. Scientist mostly investigates this family to discover a single-phase HCP solid-solution alloy. DyGdLuTbY and DyGdLuTbTm are the only HEAs in this family introduced by 2016 (Miracle and Senkov, 2017).

Complex concentrated brasses and bronzes as *the fifth family* of HEAs have recently been introduced. This family is being investigated to seek the possibility of achieving higher levels of strength in brasses and bronzes families. **Al**, **Cu**, **Mn**, **Ni**, **Sn**, and **Zn** are the elements in this family are (Miracle and Senkov, 2017).

precious metals are *the sixth family* of HEAs introduced so far and most interested family for catalysis applications. **Ag**, **Au**, **Co**, **Cr**, **Cu**, **Ni**, **Pd**, **Pt**, **Rh**, and **Ru** are the elements of this family. MoPdRhRu with a single-phase HCP structure is the first alloy of this family had been investigated by Paschoal, Kleykamp, and Thummler (1983) even before establishing the concept of HEAs.

The seventh family is those alloys which contain **B**, **C** or **N**. Miracle and Senkov (2017), had listed them as a separate family due to the dramatic effect of B, C or N on the phase content, microstructure, and properties. Most of the alloys in this family contain N, where only limited reports of alloys with C or B is available (Miracle and Senkov, 2017).

2.5. Fabrication Routes of HEAs

Various methods are used to produce high entropy alloys. These fabrication methods are classified into three major groups as illustrated in Figure 2.6. These routes include mixing elements from the liquid, solid and vapor states (Gao et al.,2016).

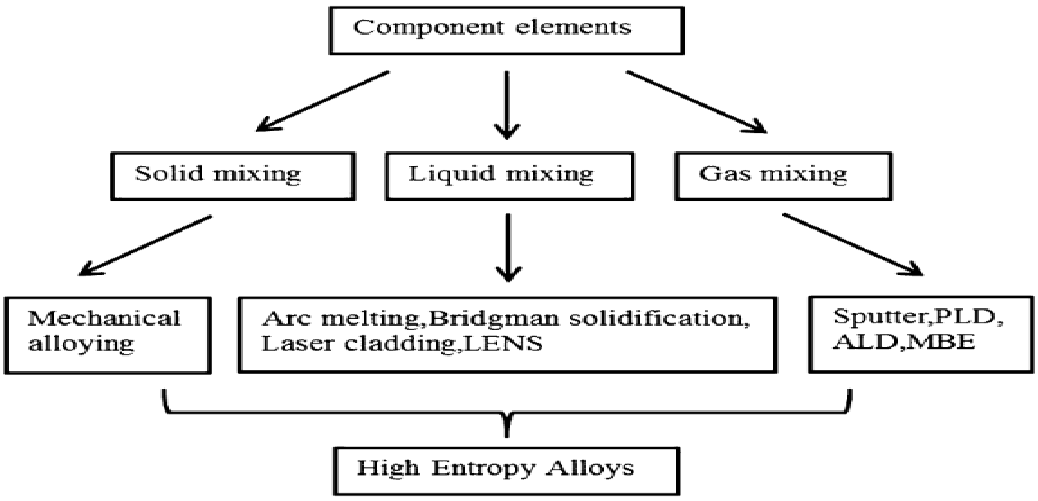

Figure 2.6. *Summary of the fabricating routes for HEAs (Gao et al., 2016).*

In this section, Arc melting and Bridgman Solidification, Mechanical alloying, and Physical vapor deposition (PVD) techniques will be summarized as the major routes of liquid state, solid state, and vapor state solidification techniques respectively.

2.5.1. Arc melting

The arc melting process is the most common technique to fabricate HEAs in which all alloying elements are completely mixed in a liquid state and then solidified in a copper or graphite crucibles.

In this technique, to ensure the chemical homogeneity of the alloys, multiple repeating melting and dissolution are usually carried out. The arc melting process can also lead to difficulties with the low melting point elements such as; Magnesium, Lead, and Manganese, which can make it difficult for the operator to control the composition. But one of the important reasons which have made arc melting many popular is that the temperature (about 3000℃) that is produced during arc melting is sufficient to melt most of the metals used in HEA production (Murty et al., 2014).

2.5.2. Bridgman solidification casting

The Bridgman solidification technique (BST) is less common than the arc melting method but is inevitable when controllable microstructures and properties are needed. In this method the temperature gradient and growth rate can be controlled by adjusting the heating power and withdrawal velocities, which assure the microstructural morphology and size, especially to fabricate rod-shaped samples (Gao et al.,2016).

2.5.3. Mechanical alloying

Mechanical alloying is a fabrication method to produce composite metal powders with controllable and extremely fine microstructures. In this method, the powder is obtained by repeated cold welding and fracture of initial powder particles until the targeted composition and percentage of the respective components are acquired (Gao et al., 2016).

The mechanical alloying process has the ability to synthesize various equilibrium and non-equilibrium alloys using one of the blended elemental or pre-alloyed powders. Mechanical alloying takes place in three stages. In the first stage, the materials are combined in a ball mill and ground into fine powders. The second stage is a sintering process to compress the obtained powders from the first stage. Finally, in the last stage different heat treatment process may carry out to remove any internal stresses induced during cold compression (Alaneme et al., 2016).

The mechanical alloying process is a highly adaptable fabricating method in which almost any material can be produced by this method. Mechanical alloying is typically performed at room temperature or below, resulting in surpassing the problems such as potential problems which can be produced in melting and casting methods. As the fabricated crystalline microstructures are typically very fine grained, this method is one of the most convenient methods for making nanocrystalline materials. Although some problems of contamination can be a serious disadvantage when a highly pure product is targeted (Gao et al., 2016).

2.5.4. Physical vapor deposition

Physical vapor deposition (PVD) provides a variety of vacuum deposition methods used to deposit thin films by the condensing a vaporized form of the desired film material onto various workpiece surfaces. It includes cathodic arc deposition, electron beam physical vapor deposition, evaporative deposition, pulsed laser deposition, and sputter deposition (Gao et al., 2016). Among them, magnetron sputtering deposition is the most popular method to fabricate HEA films, as shown in Figure 2.7.

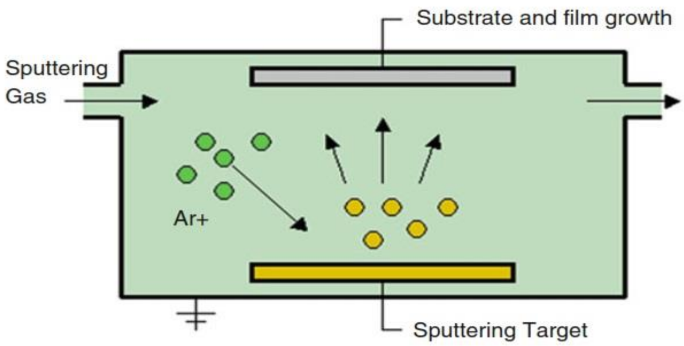

Figure 2.7. *A schematic showing the processing of sputtering deposition (Gao et al., 2016).*

2.6. Design of High-Entropy Alloys

Because of the high number of possible HEAs, seeking for the right composition just by trial and error seem highly impossible. In addition, the increase in the number of elements in an alloy makes the construction of the phase diagram difficult. Therefore, in addition to theoretical modeling computational approaches can be used to study phase formation of HEAs. Initially, some computational approaches such as density functional theory (DFT) calculations and ab initio molecular dynamics (AIMD) simulations had been recommended to study the phase formation of these alloys. However, the required cost and calculation period for these technologies made them not suitable for the design of HEAs. Alternatively, the CAlculation of PHAse Diagrams (CALPHAD), the so-called semi-empirical calculation approach, has been used recently to estimate equilibrium phases in HEAs (Ye et al., 2016).

The CALPHAD method is the most powerful approach to predict phase stability and is the most effective way to prepare multicomponent phase diagrams if there is a reliable thermodynamic database for the relevant system. Since the contributions to the Gibbs energy of a phase mainly consist of binary and ternary systems in CALPHAD models, the CALPHAD method has proven to be unique and superior in its ability to identify multi-component systems (Chen et al., 2018). The CALPHAD method has been applied to a wide range problem of material science beyond the phase diagrams, including solidification, coating, bonding and phase transformation (Gao et al., 2017).

3. STRENGTHENING MECHANISMS IN METALS AND STEELS

Several hardening techniques are available for an engineer, and often the choice depends on the capacity of a material to be adjusted with the mechanical characteristics required for a particular application. The important point in understanding the mechanisms of hardening is the relationship between the displacement movement and the mechanical behavior of metals. As the macroscopic plastic deformation correlated with the motion of a large number of dislocations, the plastic deformability of a metal depends on its ability to move dislocations. Because the hardness and strength (both yield and stress) are related to the ease of occurrence of plastic deformation, the mechanical force can be increased by decreasing the displacement movements; it means, larger mechanical forces will be required to start plastic deformation. In contrast, the more restricted the dislocation motion, the greater is the facility with which a metal may deform, and the softer and weaker it becomes. Almost all strengthening techniques are based on this simple principle: Restricting or preventing dislocation movement makes the material harder and stronger. (Callister and Rethwisch, 2013).

The strengthening of the steel has no different from other metals and it is also controlled by the resistance of the microstructure to the movement of crystal defects known as dislocations when subjected to stress. With a simple tense; higher resistance to dislocation movements causes higher strength values. Many possible combinations of strength and ductility of the steels are produced by forming obstacles to dislocation in the microstructure of the steel and almost all steels, which are designed basically for maximum formability and ultra-high strength, depend on various strengthening mechanisms. For instance, putting various obstacles (such as carbon) to these dislocations and even applying minor changes in the amount of that may cause major changes in the strength values of the same steel family (Krauss, 2016).

In this section, general mechanisms of hardening for single-phase metals as well as steels related strengthening mechanisms are briefly introduced and discussed.

3.1. Strengthening Mechanisms for Single-Phase Metals

3.1.1. Precipitation hardening

The strength of a precipitation or age hardening alloy is controlled by the interaction of the mobile dislocations and the precipitates. In these alloys, stresses in the GP (Guinier-Preston) zones and/or precipitations block the dislocation movement. The GP zones are mostly responsible for the increase in the obtained strength during the first stages of aging procedure, as they cause discontinuation of moving dislocations and/or circulate around dislocations.

There are several ways by which a matrix can be hardened in the presence of precipitates. These methods are generally separated into two categories, including; deforming precipitates and non-deforming precipitates (Courtney, 1990).

3.1.1.1. *Deforming particles*

Coherency hardening, modulus hardening, chemical strengthening, and order strengthening are the sub-categories of this method.

Coherency hardening occurs when the interface between the particles and the matrix is coherent with the parameters, such as particle size, depending on the shape of the particles resulting in a coherency strain which finally leads to an increase in yield strength (Courtney, 1990).

Modulus hardening results from the different shear modulus of the precipitate and the matrix, which leads to an energy change of dislocation line tension when the dislocation line cuts the precipitate. (Courtney, 1990).

Chemical strengthening is related to the surface energy of newly introduced precipitate-matrix interface when the particle is sheared by dislocations. (Courtney, 1990).

Order strengthening happens when the precipitate is ordered structure when the bond energy after shearing is different in respect to before sharing energy bond. (Courtney, 1990).

3.1.1.2. *Non-deforming particles*

In non-deforming particles, the spacing is small enough or the precipitate-matrix interface is disordered, so dislocation bows instead of shears. The strengthening path in this method is related to the effective spacing between particles considering finite particle size (Courtney, 1990).

3.1.2. Strengthening by grain size reduction

The size of the grains is one of the key parameters which influences the mechanical properties. Nearby grains share a common grain boundary but possess different crystallographic orientations. The grain boundary acts as a barrier to dislocation motion when the material is subjected to a plastic deformation for two reasons (Smith and Hashemi, 2006); First of all, the different crystallographic orientations of two grains could be a real barrier, since a dislocation passing to other grain should change its direction, secondly, a discontinuity of slip planes from one grain into the other would make the crystallographic misorientation more difficult.

It should be mentioned that for grain boundaries with high-angle, displacement cannot occur when the grain crosses the boundaries during deformation; instead, dislocations tend to "pile up" at the grain boundaries. These pile-ups create stress concentrations in front of their slip planes, which results in new defects in nearby grains.

Fine-grained materials are harder and stronger than coarse-grained materials. That is because they have a greater total grain boundary area to impede dislocation motion. For many materials, the yield strength σ_y varies with grain size according to Hall–Petch equation (dependence of yield strength on grain size):

$$\sigma_y = \sigma_0 + k_y d^{-1/2} \tag{3.1}$$

According to this equation, the strength of a metal is equal to the frictional stress plus a strengthening factor (k) times the inverse of the square root of the grain size (d). As a result, this equation indicates clearly that reducing the grain size will cause the material to become stronger.

3.1.3. Solid solution hardening

Solid solution hardening involves the addition of other metallic elements and causes distortions because of the atomic size difference of the solvent and the solute metals (Callister and Rethwisch, 2013).

Impurity atoms, which could be both substitutional and/or interstitial atoms, lead to deformation in the lattice and this deformation finally gives the alloys higher strength than their pure forms. The impurity atoms tend to accumulate around dislocations to reduce the total deformation energy. This behavior of impurity atoms increases the amount of stress required for the movement of dislocations and consequently will improve the strength (Callister and Rethwisch, 2013).

Depending on the amount and type of dissolved atoms, solvents can affect the mechanical behavior of a metal on a large scale. In the combination of two or more elements, various elastic, electrical and chemical interactions may occur between the stress fields formed by the dissolved atoms and the dislocations in the matrix; it is believed that when the single-phase microstructure is maintained, elastic interaction is the most important of these interactions (Wu et al., 2017).

As a result, Since the impurity atoms are different in size with surrounding atoms, they can introduce either tensile or compressive lattice strains depending on whether they are smaller or larger than matrix atoms. They disrupt the regular arrangement of ions and make it more difficult for the layers to slide over each other. This makes the alloy stronger and less ductile than the pure one.

3.2. Hardening Mechanisms in Steels

3.2.1. SIP mechanism

The deformation of the austenite steels applied by tensile deformation, which is based on the observation of uniform arrangement and the superior plasticity of austenite, is connected to the homogeneous shear deformation of austenite which is called the shear band-induced plasticity (SIP). Steels of this kind have been stated with following features; 30 μm austenitic grain size, 110 mJ/m^2 SFE (Stacking Fault Energy), 875 MPa tensile strength and 58% elongation (Chen et al., 2017).

shear bands are one of the least understood microstructural properties plastically strained ductile metallic materials, which are formed in a non-crystallographic bandlike deformation region where the highly concentrated plastic flow is present (Anonymous, 2018).

3.2.2. MBIP mechanism

Microband Induced Plasticity (MBIP) is a mechanical property enhancement in a medium to large strain regime due to microband formation in high Mn steels with a relatively high stacking fault energy (Akbari et al, 2009, p.3076).

3.2.3. DSBR mechanism

DSBR (Dynamic Slip Band Refinement) is a deformation mechanism that is seen in Fe-Mn-Al-C austenitic steels.

In the DSBR mechanism, it has been found that the strong sliding plane led to the formation of very thin sliding bands extending throughout the whole grain. During deformation, the slip band structure is becoming much thinner. In the structure where deformation twins are not observed; 40 μm austenite grain size, 85 mJ/m^2 SFE, the tensile strength of 900 MPa and elongation of 68% has been determined (Chen et al., 2017).

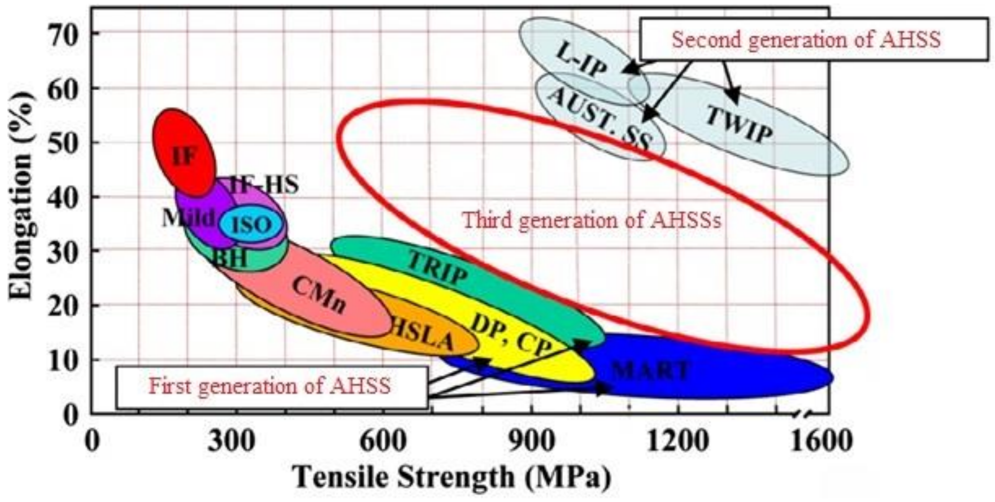

Figure 3.1. *Locations of three generations of AHSS grades in an elongation versus tensile strength chart (Zhao and Jiang, 2018).*

3.3. Advanced High Strength Steels (AHSSs)

Advanced high strength steels (AHSSs) are regarded as the most promising materials for vehicles in the 21st century. AHSSs are complex and sophisticated materials, with microstructures being controlled by precise thermomechanical processing (TMP) technologies. TMP is an established and strategic method for improving the mechanical properties of AHSSs through control of microstructures and is among the most important industrial technologies for producing high-quality AHSSs with the necessary mechanical properties.

3.3.1. Three different generations of AHSSs

Based on the different development stages, AHSSs are generally divided into three generations. Figure 3.1 (Zhao and Jiang, 2018) illustrates the locations of three generations of AHSS in an elongation versus tensile strength chart. The first generation AHSSs include dual phase (DP) steel, transformation-induced plasticity (TRIP) steel, complex phase (CP) steel, and martensitic (MART) steel. This steel family has higher strength and even better ductility without significant cost increase as compared to the conventional high strength steels and have been well developed and used in many applications in the automotive industry (Zhao and Jiang, 2018). The second generation

AHSSs, which include twinning-induced plasticity (TWIP) steel, austenitic stainless steel (AUST.SS) and lightweight steel with induced plasticity (L-IP), is in the upper right corner of the elongation-strength chart and show that these steels have superior mechanical properties. These steels are extremely strong and formable and exhibit an excellent combination of strength and formability to enable them to be used to provide exceptional mass reduction for parts in different shapes, but this AHSS family are highly alloyed with high-cost alloying elements such as chromium and nickel, resulting in a significant increase in production cost, so their extensive selection is restricted. The third generation AHSSs have a better combination of strength and ductility than the first generation one and can be produced at a lower cost than the second generation (Zhao and Jiang, 2018). The third-generation grades are currently under investigation and development. Because they are stronger and more ductile compared to the first generation and more suitable than the second generation, they are considered future opportunities for automotive and other structural applications (Zhao and Jiang, 2018). The mechanical properties of AHSS grades, including DP, TRIP and TWIP steels are compared in Figure 3.2.

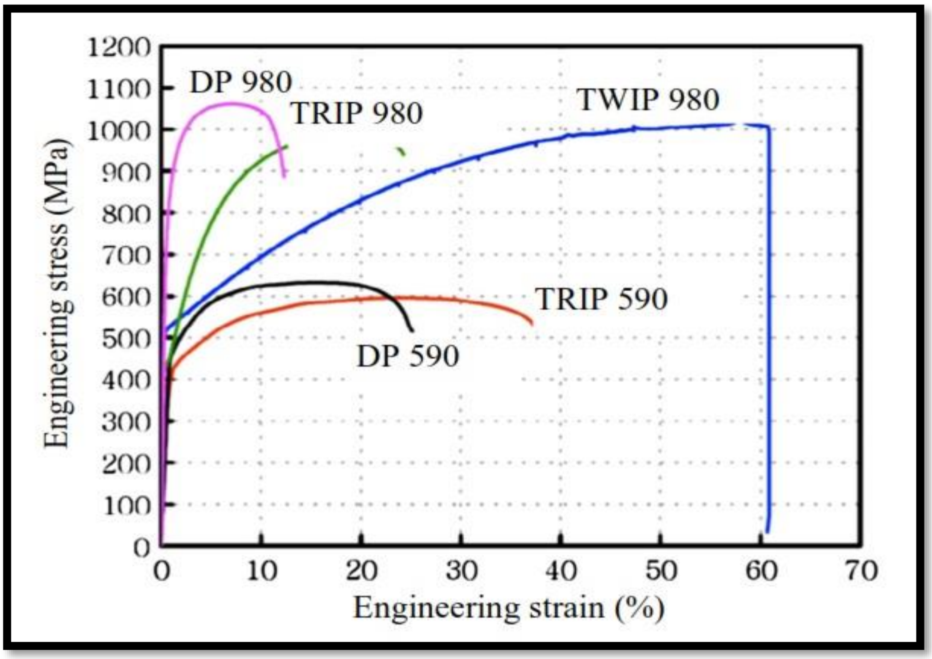

Figure 3.2. *Engineering stress-strain curves of TWIP, TRIP and DP steels (Kwon et al, 2010).*

4. INFLUENCE OF BORON ADDITION ON VARIOUS ALLOYING SYSTEMS IN THE LITERATURE

Grain boundaries can affect some properties of metallic alloys such as mechanical, functional, and kinetic properties. They can be manipulated by the solute decoration that allows energy, mobility, structure, and cohesion related changes or even lead to arising of local phase transformation (Raabe et al., 2014). Grain boundaries (GBs) are defects in metallic alloys that control a wide range of properties, such as tensile strength, fatigue resistance, fracture toughness, strain hardening, brittleness, conductivity, or even corrosion behavior (Rollet et al., 2004). GBs can either weaken (inter-crystalline fracture, stress corrosion cracking) or strengthen (Hall-Petch effect) polycrystalline metallic materials. The involved GB types in both cases greatly affect the specific material response. These observations have led to the concept of grain boundary engineering, aiming to design polycrystals with specific GB distributions (Watanabe and Tsurekawa, 1999; Randle, 2004).

Boron addition proposes a new strategy mostly to enhance the mechanical properties of the single-phase alloys, particularly, through the decoration of the grain boundaries instead of the compositional modification of the bulk. Boron decorates grain boundaries and causes a double way to improve mechanical properties through grain size reduction and interface hardening. These effects increase the coherency of the grain boundary and decelerate grain coarsening, proposing boron-doped grain boundary engineering as an ideal mechanism for the development of various alloys (Seol et al., 2018).

Regarding the mechanisms of this method, firstly, boron increases the load-bearing capacity of each interface by increasing the grain boundary cohesion, which leads to reducing the possibility of catastrophic interface failure in the structural components (Seah, 1980; Wu et al., 1994). Secondly, the interface decoration and reduced grain bound energy generate an enhanced grain boundary drag effect and reduced Gibbs-Thomson force during the recrystallization of polycrystalline materials and capillary-driven grain coarsening, which leads to the refining of grain during heat treatment compared to the undoped alloys. The relevant Hall-Petch effect can improve both the strength and ductility of the materials (Liu et al., 1996; Raabe et al., 2014).

From a practical point of view, boron addition suggests two critical advantages: to improve mechanical properties, firstly, alloying grain boundaries is more efficient than the entire bulk material. Secondly, it is preferable to replace expensive alloying elements such as Ni, Co, and Cr with cheaper grain boundary additives (Seol et al., 2018).

Boron's solubility is usually very low. When introduced in an amount below the critical level, the boron tends to prefer random high-angle grain boundaries. Beyond that level, the formation of boride compounds, such as some of the M_2B borides, can be harmful by the weakening of the GBs (Seol et al., 2018).

4.1. Possible M_2B Metal Borides and Their Structures

Iyer et al. (2019) categorized binary and ternary M_2B boride compounds into three main categories. These are *compounds containing mainly isolated boron atoms*, *structures containing isolated boron atoms and B_n (n = 2- ∞) units* and *structures containing B_n (n =4 - ∞) units and no isolated boron* in which they have divided themselves into six, three and two different M_2B major structures respectively. These structures are shown in Table 4.1.

Table 4.1. *Structure types of compounds with an M:B ratio of 2:1 (Iyer et al., 2019).*

Family group	Type	Space group	Shape	Related to
1.	$CeCo_3B_2$	P6/mmm	tricapped trigonal prismatic	-
	$ErIr_3B_2$	C2/m	tricapped trigonal prismatic	$CeCo_3B_2$
	$ZrCo_3B_2$	$R\bar{3}$	trigonal prismatic	$CeCo_3B_2$
	$(Nd_{0.71}Rh_{0.29})Rh_3B_2$	$P\bar{6}2m$	tricapped trigonal prismatic	$CeCo_3B_2$
	URu_3B_2	$P\bar{3}$	tricapped trigonal prismatic	$CeCo_3B_2$
	$CuAl_2$	I4/mcm	square antiprismatic	-
	Mg_2Cu	Fddd	square antiprismatic	$CuAl_2$
	CuIrB	Fdd2	irregular polyhedra	$CaRh_2B_2$ -LiIrB

	$Cu_2Ir_4B_3$	Cmcm	trigonal prismatic	$ZnIr_4B_3$
	Pt_2B	C2/m	trigonal prismatic	-
	Co_2Si	Pnma	tricapped trigonal prismatic	-
	ZrNiAl	$P\bar{6}2m$	tricapped trigonal prismatic	-
	TiNiSi	Pnma	tricapped trigonal prismatic	Co_2Si
	NbCoB	Pmmn	tricapped trigonal prismatic	ZrNiAl -TiNiSi
2.	$Ti_{1+x}Os_{2-x}RuB_2$	$P\bar{6}2m$	trigonal prismatic	-
	$Ti_{1+x}Rh_{2-x+y}Ir_{3-y}B_3$	Pbam	trigonal prismatic	$Ti_{1+x}Os_{2-x}RuB_2$
	NbRuB	Pmma	trigonal prismatic	-
	HT-$Nb_{1+x}Os_{1-x}B$	Pnma	trigonal prismatic	-
3.	Ni_3ZnB_2	C2/m	tricapped trigonal prismatic	-
	MoAlB	Cmcm	tricapped trigonal prismatic	-

4.2. Case Studies

In this section, we will review the influence of boron addition-in both HEAs and steels-on microstructure and mechanical properties of these alloys.

Seol et al. (2018) published their study on the effect of boron addition on microstructure and mechanical properties of FeMnCrCoNi HEA. A 30 and 100 ppm boron doped FeMnCrCoNi alloy and annealed at a temperature of 800 and 650 ° C for 60 minutes has been studied. As a result, 30 ppm boron doping of single-phase HEA and preventing of metal borides formation increased their yield strength by more than 100% and their ultimate tensile strength by ~40% and up to ~44% grain size reduction without significant loss in the total strain values. Table 4.2 summarize the results of their outstanding study.

Table 4.2. *Effects of boron addition on grain size and mechanical properties of FeMnCrCoNi HEA.*

FeMnCrCoNi alloy	Phase Content	Boron Addition (ppm)	Grain Size (μm)	YS (MPa)	UTS (MPa)	Total Elongation %	Annealing Temperature (°C)
Boron-free	FCC	-	7,6	240	620	68	800
Boron-doped	FCC	30	3,4	630	920	57	800
Boron-doped	FCC	100	3,7	500	790	53	800
Boron-free	FCC	-	2,2	620	810	52	650
Boron-doped	FCC	30	1,8	800	1040	52	650

Wang and Baker (2016) in their study on $Fe_{40.4}Ni_{11.3}Mn_{34.8}Al_{7.5}Cr_6$ HEA investigated the effects of boron addition in as-cast samples without applying rolling and heat treatment operations investigating for its interface hardening effect of boron, where the boron-free alloy has a single phase with particle sizes about 120 μm. Boron-doped alloys were observed to have approximately 120-150 μm grain sizes, contained large long precipitates some greater than 10 μm in length (Table 4.3).

Table 4.3. *Effects of boron addition on mechanical properties of FeNiMnAlCr HEA.*

$Fe_{40.4}Ni_{11.3}Mn_{34.8}Al_{7.5}Cr_6$ alloy	Phase Content	Boron Addition	YS (MPa)	UTS (MPa)	Total Elongation (%)
Boron-free	FCC	-	160	390	40
Boron-doped	FCC	%0,5	175	465	37
Boron-doped	FCC	%1,0	190	530	31

Ferrari et al. (2018) investigated the influence of boron addition on the solidification behavior of double phases AlCoCrFeNi HEA. In their research, the cast AlCoCrFeNi alloy showed a dendritic solidification that forms two different regions (dendritic and interdendritic). The microstructure consists of an Al-Ni rich B2 matrix (primary phase) with BCC precipitates rich in Fe-Cr. While the BCC residues in the dendritic region have a cuboidal morphology, the interdendritic region has a B2/BCC structure with a basket-weave morphology. The interdendritic region also contains small FCC islands. The addition of small boron to produce the $AlCoCrFeNiB_{0.1}$ alloy resulted in the formation of needle-like Cr-rich borides with orthorhombic Cr_2B type structures. Although B2 is the primary phase of this alloy, boron addition changes the final stages of solidification in which BCC, FCC, and Cr_2B-type borides are formed. In general, boron leads to the formation of a hard boride composite and converts the sequence of the matrix/precipitate into a more ductile structure. This may explain why the strength of this alloy is higher than the boron-free alloy while having roughly the same ductility. Due to Ferrari et al. (2018) addition of a small amount of B in HEA containing Cr may result in the formation of hard Cr-rich M_2B type borides, and thus these alloys can perform better performance in terms of wear resistance, corrosion resistance, and strength. Table 4.4 reviews mechanical performances of boron-free and boron-doped AlCoCrFeNi Alloy.

Table 4.4. *The mechanical performances of boron-free and boron-doped AlCoCrFeNi HEA.*

AlCoCrFeNi alloy	Phase Content	Boron Addition	UTS (MPa)	Total Elongation (%)
Boron-free	B2/BCC+FCC	-	1406	23.4
Boron-doped	B2/BCC+FCC+ Cr_2B type borides	%0.1	1730	27

Seol et al. (2018) have also studied the grain size reduction effect of 30 ppm boron edition on $Fe_{40}Mn_{40}Cr_{10}Co_{10}$ HEA. The study showed a reduction of ~ 58% in grain size that results in better mechanical properties- both TS and Total elongation values- can be achieved. Table 4.5 plots briefly the outcomes of this study.

Table 4.5. *Effects of boron addition on grain size and mechanical properties of $Fe_{40}Mn_{40}Cr_{10}Co_{10}$ HEA.*

$Fe_{40}Mn_{40}Cr_{10}Co_{10}$ Alloy	Phase Content	Boron Addition (ppm)	Grain Size (µm)	YS (MPa)	UTS (MPa)	Total Elongation (%)	Annealing Temperature (°C)
Boron-free	FCC	-	7,9	390	770	65	800
Boron-doped	FCC	30	3,3	450	880	73	800

Regarding steels, as a general rule, boron is added to unalloyed and low alloy steels to increase the hardness level of the alloy. Boron-doped steels are generally used when the material meets the mechanical property requirements (such as toughness, abrasion resistance, etc.) but the desired hardness level is insufficient. Boron addition up to 0.01% to austenitic steels increases the high-temperature strength. Boron steels are also used for various applications as wear material and high strength structural steels. The improved cold formability results in better weldability, lower temperatures, and energy savings due to low carbon equivalents and a good curing response are the main advantages of boron steels (Maitrepierre et al., 1979).

Kim and Kwun (1996) studied the influence of boron addition in the cast and mechanical alloyed FeAl (%40 Al) alloy in both room and high temperatures. Although the mechanically alloyed samples had not resulted in better mechanical properties, the boron doped cast samples brought outstanding mechanical properties, as respect to their UTS and total Elongation values. Table 4.6 is summarizing the results of their studies.

Table 4.6. *Mechanical properties of boron free and boron doped FeAl cast and MA FeAl.*

ALLOY	Boron Addition	27 °C (300K)		427 °C (700K)		627 °C (900K)		827 °C (1100K)	
		UTS (MPa)	TE (%)	UTS (MPa)	TE (%)	UTS (MPa)	TE (%)	UTS (MPa)	TE (%)
Boron free CA[1]	-	323	2,8	526,8	14,2	282	34,3	53,9	106,4
Boron doped CA	0,3%	790,4	8,1	705,6	43,5	368	39,8	75,4	128,3
Boron free MA[2]	-	953,8	5,5	924	14,5	392,2	15,2	188,7	8,3
Boron doped MA	0,3%	718,4	4	852,6	15,5	409,1	14,9	150,7	7,9

** 1. CA: Cast alloy, 2.MA: Mechanical alloy*

Brüx et al. (2002) studied the Influence of boron and other elements (in microalloying levels) elements on microstructures and mechanical properties of Fe-6Al steel sheets. Regarding boron addition, UTS of the alloy showed an increase to ~440 MPa, where the boron-free samples showed UTS of ~ 395 MPa at the same condition. On the other hand, boron doped alloys also show better elongation values with respect to boron free samples (Table 4.7).

Table 4.7. *Mechanical properties of 0.002 %, 0.02 %, and boron free Fe-6Al Steel sheets.*

ALLOY	Boron Addition	YS (MPa)	UTS (MPa)	Total Elongation (%)
Boron-free Fe-6Al	-	290	395	26
Boron-doped Fe-6Al	0.002 %	330	440	37
Boron-doped Fe-6Al	0.02 %	285	400	27

Li et al., (2018) studied the influence of boron on mechanical properties of 13% Mn austenitic steel. They showed that the addition of B to 13% Mn TRIP + TWIP steels enhances the yield strength as a result of the formation of hard boride phase but decreased the total elongation for two reasons; One is that the borides are brittle phases and can crack easily under stress. The other reason is that B addition had no influence on deformation mechanism of the experimental steels, but martensite transformation occurred at ends of cracked borides consumed a large number of austenite, which finally contributed to the earlier occurrence of fracture for B-contained steels. The mechanical aspects of their work are summarized in Table 4.8.

Table 4.8. *Mechanical properties of boron free and boron doped hot-rolled 13% Mn metastable austenitic steel.*

ALLOY	Boron Addition	YS (MPa)	UTS (MPa)	Total Elongation (%)
Boron-free	-	485±8.5	1192±18.6	43±1.2
Boron-doped	0.15 %	556±7.2	1206±23.5	38±1.1
Boron-doped	0.30 %	610±8.6	1194±12.8	33±1.6

Uzunsoy (2010) investigated wear behavior of sintered 316L stainless steel with additions of elemental boron. From this study, it can be concluded boron addition improved the performance of 316L stainless steel. The boron addition increased sintered density and hardness as well. Due to Uzunsoy, sintering temperature, time and amount of boron have a significant role to optimize the mechanical properties of boron doped steels. Table 4.9 reviews the mechanical properties of boron doped and boron free sintered 316L stainless steels.

Table 4.9. *Mechanical properties of boron doped 316L stainless steel.*

ALLOY	Boron Addition	Hardness (HRB) average	YS (MPa)	UTS (MPa)
PM 316 L	-	81.3	72.5	99.7
	0.2 %	113.3	83.5	139.5
	0.4 %	119	164.1	347.4
	0.6 %	227.3	227.3	350.2

As a conclusion, boron addition could enhance the mechanical properties of alloys (both HEAs and conventional alloys) due to its grain size reduction and interface hardening effects. On the other hand, amount of added boron has a significant role to optimize the mechanical properties, since the formation of metal borides, especially M_2B, may form brittle participates which can attenuate the effects of boron addition.

5. MATERIALS AND METHODS

The second chapter discusses high entropy alloys (multi-principal element alloys), their core effects, important factors and parameters in the modeling of HEAs and their physical properties. Chapter three reviews strength hardening and ductility enhancement mechanisms of metals and steels. Chapter four argues about the influence of boron addition in both HEAs and conventional alloying systems and provides some numerical values about the effects of boron on grain size and mechanical enhancement of which has obtained in different researches.

In this study, a medium entropy alloy (MEA) [$Fe_{50-x}Mn_{30}Ni_{10}Al_{10}B_x$(x=0-3.32at%)] has been designed based on HEAs concepts. The motivation in the development of this MEA can be described as follows: **firstly**, *Iron* has been chosen as the main alloying element to reduce the cost. **Secondly,** *Manganese* and *Nickel* were selected as the FCC phase stabilizers. **Thirdly**, *Aluminium* is selected as the low-density element which can reduce the density of the alloy. *Boron* is the grain size reduction and interfaces hardening agent of which the effects will be investigated. **In addition**, elements used in this MEA have ideal melting points, and as such, the alloy has the potential to be also studied in high-temperature environments as a further study. Table 5.1 summarizes the physical properties of each selected element.

Table 5.1. *Physical properties of selected elements for the multi-principle alloying system.*

Property	Fe	Mn	Al	Ni	B
Atomic Number	26	25	13	28	5
Molar Mass (g/mol)	55.845	54.938	26.9815	58.6934	10.881
Density (g/cm^3)	7.87	7.47	2.699	8.902	2.3
Atomic Radius (A˚)	1.241	1.35	1.432	1.243	0.88
Melting Point (˚C)	1538	1244	660	1453	2300
VEC	8	7	3	10	3

The boron-free MEA has determined as $Fe_{50}Mn_{30}Al_{10}Ni_{10}$ (in atomic percent) and the addition of boron will detract of the iron atomic percent where the other elements will stay in constant ratios. Table 5.2 shows the atomic and weight percent equivalents of each alloy.

Table 5.2. *Atomic and weight percent equivalent of designed alloys.*

	Fe	***Mn***	***Al***	***Ni***	***B***	**Total**	**Alloy**
wt%	52.71	31.11	5.09	11.08	0.00	100.00	**Boron free**
at%	50.00	30.00	10.00	10.00	0.00	100.00	
wt%	52.66	31.11	5.09	11.08	0.05	100.00	**0.05wt%**
at%	49.85	29.94	9.98	9.98	0.24	100.00	**Boron doped**
wt%	52.51	31.11	5.09	11.08	0.20	100.00	**0.2wt%**
at%	49.42	29.77	9.92	9.92	0.97	100.00	**Boron doped**
wt%	52.21	31.11	5.09	11.08	0.50	100.00	**0.5wt%**
at%	48.57	29.42	9.81	9.81	2.39	100.00	**Boron doped**
wt%	52.01	31.11	5.09	11.08	0.70	100.00	**0.7wt%**
at%	48.02	29.20	9.73	9.73	3.32	100.00	**Boron doped**

This study includes the addition of 0.05, 0.2, 0.5 and 0.7 weight percent of boron to the main MEA alloy and comparing the result of mechanical properties in *as-cast*, rolled, *and annealed* samples as well as determining the grain reduction effect of boron in both as-cast, rolled and annealed samples.

This study consists of five major steps;

1. Design and modeling
2. Casting
3. Thermomechanical treatment
4. Characterization
5. Mechanical tests

In the upcoming sections of this chapter, the methods and mechanism carried out in each step will be discussed in detail.

5.1. Design and Modelling

As discussed in the second and sixth sections of chapter two, modeling of HEAs involves two separate processes. These processes complete each other but for a better understanding of the alloying system and especially phase formation, each of these steps carries an important role in designing of HEAs.

Firstly, in order to determine the eligible compositions in the ($Fe_qMn_yAl_zNi_w$) system, the relevant thermodynamic parameters were calculated by using 5% increments of (q,v,w,y,z) values where $5 \leq q,y,z,w \leq 50$. For this reason, 633 different compositions of the mentioned system have been taken into consideration, which the results have been presented in Appendix 1.

Considering the values of mixing entropy as $-15 < \Delta H_{mix} < +5$ kJ/mol, atomic size difference as $\delta \leq 5.5\%$, Ω parameter as $\Omega > 1.5$ and providing an alloy with a lower density and higher melting point properties (so as calculated theoretical density lower than 7.5 g/cm^3 and calculated melting temperature higher than 1350 ˚C), ten composition have emerged as eligible candidates for the ($Fe_qMn_yAl_zNi_w$) alloying system. Table 5.3 shows the related thermodynamic calculation of these compositions in the order of lower to higher density.

Table 5.3. *Thermodynamic calculations of eligible compositions based on defined parameters in the (FeqMnyAlzNiw) alloying system.*

No	Elements (at%)				Thermodynamic Parameters								
	Fe	Mn	Al	Ni	ΔG_{mix}	ΔS_{conf}	ΔS_{mix}	ΔH_{mix}	δ%	T_m	Ω	VEC	TD[1]
1	50	30	10	10	-19.5849	1.1683	9.5028	-6.72	5.1751	1354	1.91	7.4	7.319
2	50	5	15	30	-22.2015	1.1421	9.2900	-9.51	5.4307	1366	1.33	7.8	7.376
3	50	25	10	15	-20.6242	1.2080	9.8257	-7.22	5.1518	1364	1.86	7.55	7.392
4	45	5	15	35	-22.8425	1.1611	9.4446	-9.98	5.4202	1362	1.29	7.9	7.429
5	45	25	10	20	-21.8763	1.2580	10.2330	-7.96	5.1377	1360	1.75	7.65	7.445
6	45	45	5	5	-15.0673	1.0182	8.2823	-3.82	4.6849	1358	2.94	7.4	7.462
7	50	20	10	20	-21.2076	1.2206	9.9284	-7.56	5.0958	1375	1.81	7.7	7.466
8	50	40	5	5	-14.9865	1.0126	8.2370	-3.68	4.7159	1373	3.07	7.45	7.482
9	40	5	15	40	-23.3016	1.1674	9.4955	-10.41	5.4097	1358	1.24	8	7.482
10	40	25	10	25	-22.8843	1.2899	10.4922	-8.66	5.1235	1356	1.64	7.75	7.498

***1.TD: THEORETICAL DENSITY**

Originally Appendix 1 and Table 5.3 indicate that all calculated alloys are medium entropy alloys as the calculated configurational entropy values are; $0.69R < S^{SS,ideal} < 1.61R$ (Gao et al., 2016), but Ω parameters with values greater than 1.1, ensure that the effect of the mixing entropy is greater than that of the enthalpy of mixing at the melting point, and the high-entropy phase can be formed. The values for enthalpy of mixing and delta (δ) parameter shows that they are in good agreement with suggested value ranges for a HEA which is given in Chapter 2. As a result, $Fe_{50}Mn_{30}Al_{10}Ni_{10}$ MEA has been selected for further investigations as it possesses the lowest density to compare to other MEAs in Table.5.2. It is worthy to mention that, even though VEC value of selected alloy suggests a mixed FCC and BCC phases during solidification since it is $6.87 \leq VEC \leq 8.0$, but it gives no clue about the stability of these phases in different temperatures. To better understanding of phase content and stability of these phases, the pseudo-binary phase diagram of $(Fe_{50}Mn_{30}Al_{10})_{100-x}Ni_x$ MEA has been prepared using the TCFE9 database of Thermo-Calc program (Fig. 5.1).

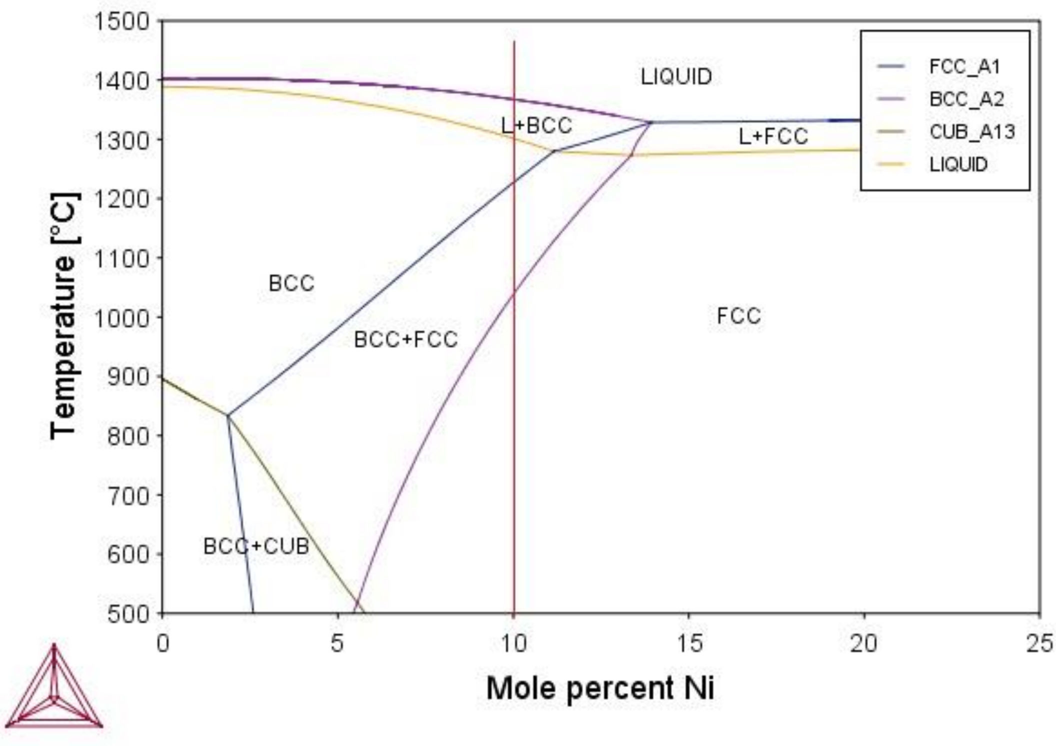

Figure 5.1. *Pseudo-binary phase diagram of $(Fe_{50}Mn_{30}Al_{10})_{100-x}Ni_x$ MEA.*

Fig. 5.2 illustrates the property diagrams of $Fe_{50}Mn_{30}Al_{10}Ni_{10}$ MEA to a better comprehension of the solidification sequence and mole fraction of related phases at different temperatures.

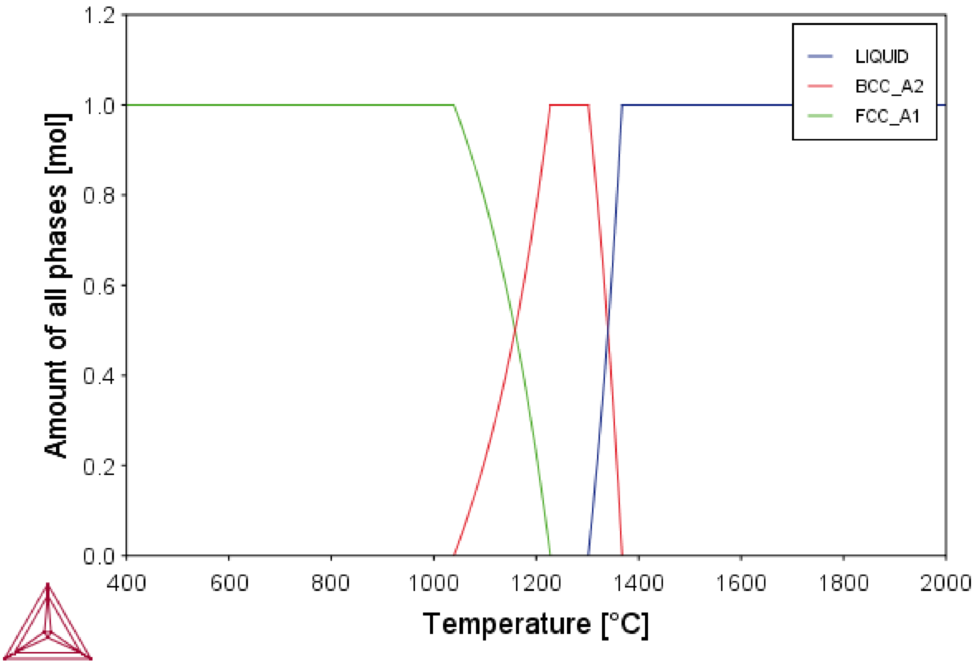

Figure 5.2. *The property diagram of $Fe_{50}Mn_{30}Al_{10}Ni_{10}$, MEA.*

Investigating the relevant phase and property diagrams demonstrates $Fe_{50}Mn_{30}Al_{10}Ni_{10}$ alloy with double phase structure. But more thorough analysis for $Fe_{50}Mn_{30}Al_{10}Ni_{10}$ alloy shows that even though all liquid firstly transforms to BCC structure down to 1200 ˚C, after that point the BCC phase will be replaced with FCC structure and ~1050 ˚C all BCC structure will be totally transformed to FCC structure. Establishing the $Fe_{50}Mn_{30}Al_{10}Ni_{10}$ MEA with a single FCC phase, the further calculation of boron addition to the mentioned MEA has been carried out.

For this reason, it has been decided to study 0.05, 0.2, 0.5 and 0.7 (by wt%) boron addition to $Fe_{50}Mn_{30}Al_{10}Ni_{10}$ MEA. Table 5.4 shows weight percent equivalent for $Fe_{50}Mn_{30}Al_{10}Ni_{10}$ MEA regarded to weight percent addition of boron in upcoming sections.

Table 5.4. *Weight percent equivalent for $Fe_{50}Mn_{30}Al_{10}Ni_{10}$ MEA*

	% at ↔ % wt				
	Fe	**Mn**	**Al**	**Ni**	**Total**
at%	50.00	30.00	10.00	10.00	100.00
wt%	52.71	31.11	5.09	11.08	100.00

In this study, firstly, theoretical modeling, using proposed thermodynamic calculation (Refer to 2.2), has been studied for $Fe_{(52.71-x)}Mn_{31.11}Al_{5.09}Ni_{11.08}B_x$ (x=0.05,0.2,0.5,0.7 wt%) alloying system to ensure whether this alloy carries the primitive thermodynamic principles of HEAs and phase formation rules. The result of the thermodynamic approach has been shown in Table 5.5.

Table 5.5. *Thermodynamic calculation of boron doped $Fe_{50}Mn_{30}Al_{10}Ni_{10}$ MEAs.*

MEA	ΔGmix (kJ/mol)	ΔS_{conf}	ΔS_{mix} (J/K.mol)	ΔH_{mix} (kJ/mol)	δ%	T_m (°C)	Ω	VEC	TD (g/cm^3)
0.05wt% Boron doped	-13.173	1.16810R	9.7116	-6.9339	5.42	1356	1.90	7.39	7.3236
0.2 wt% Boron doped	-13.231	1.16751R	9.7067	-7.5631	6.06	1362	1.75	7.36	7.2864
0.5 wt% Boron doped	-13.343	1.16618R	9.6957	-8.7706	7.14	1375	1.52	7.29	7.2133
0.7 wt% Boron doped	-13.414	1.16520R	9.6875	-9.5393	7.76	1384	1.41	7.25	7.1656

The first column, configurational entropy (ΔS_{conf}), indicates that all designed MEAs are medium entropy alloys (as was in $Fe_{50}Mn_{30}Al_{10}Ni_{10}$ alloy) and the values are $0.69R < S^{SS, ideal} < 1.61R$. In this case, the *Ω* parameter plays an important role, as well, for ensuring that these alloys follow the principles of high entropy alloys. As discussed in Section 2.2, Ω with greater values than 1.1 ensures that during solidification, the effect of the mixing entropy is greater than that of the enthalpy of mixing at the melting temperature, and the high-entropy phase tends to form. Regarding the related values of Ω in Table 5.4, it can result that high entropy principles are satisfied from a thermodynamic point of view.

Refer to Figure 2.2 in Chapter 2, the relation between δ and Ω parameters for first three alloys (i.e. boron-free, 0.05wt% and 0.2wt% boron doped alloys) states that formation of single-phase solid solution or minimum SS phases is possible as the δ and Ω values are ≤ 6.6% and ≥ 1.1 respectively. In the case of the other alloys (i.e. 0.5wt% and 0.7wt% boron doped alloys) with a Ω parameter greater than 1.1 but not satisfied value for δ parameter ≥ 6.6%, the formation of intermetallics like M_2B, in addition to SS phases is estimated.

Values of mixing enthalpy is also in good agreement with the concept of HEAs where Ye at al., (2016) have suggested the formation of a single-phase solid solution corresponds to the region -15 kJ/mol < ΔH_{mix} < 5 kJ/mol which is in line with the summarized results of Zhang et al. (2008).

For all alloys, VEC suggests a mixed FCC and BCC phases since it is in the range of 6.87 and 8.0, but, again, it gives no certainty about the stability of these phases in different temperatures.

Calculated theoretical density suggests ~ 8-9% reduction in density compared to DP 600 steel (where their density is approximately 7.874 g/cm^3) and ~ 6-8% decrease in density compared to HSLA steels (where their density is approximately 7.80 g/cm^3).

For further investigations, the phase diagram (Fig. 5.3) and related property diagrams (Fig. 5.4) of $Fe_{(52.71-x)}Mn_{31.11}Al_{5.09}Ni_{11.08}B_x$ MEAs has been prepared by using the TCFE9 database of Thermo-Calc program.

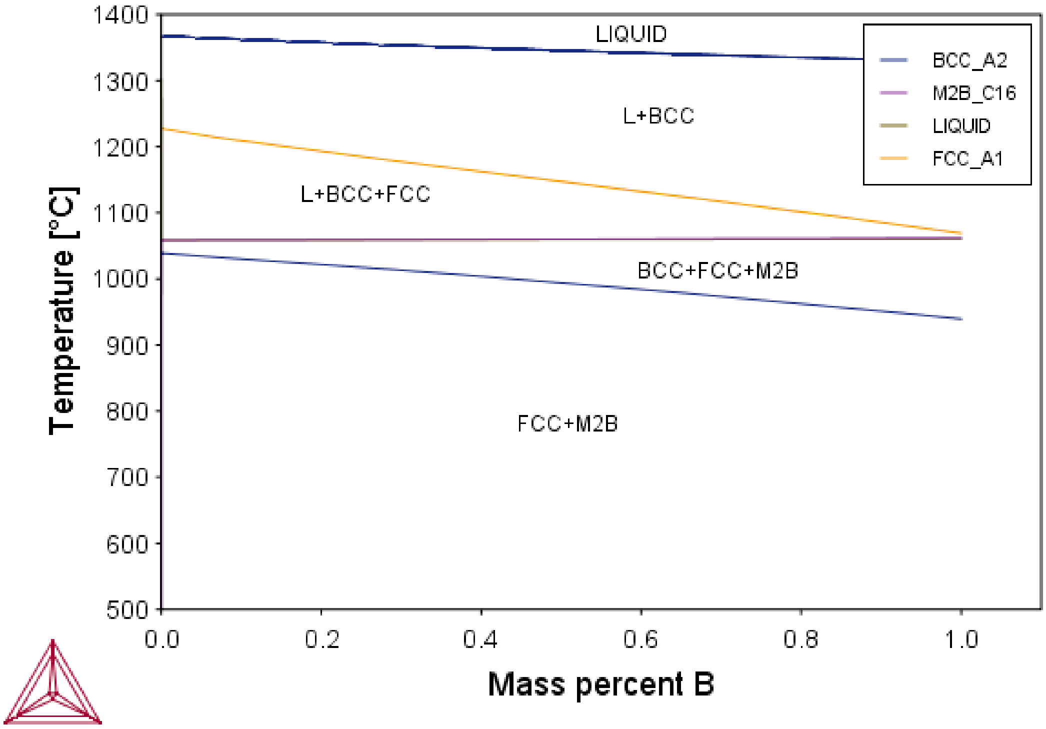

Figure 5.3. *The phase diagram of* $Fe_{(52.71-x)}Mn_{31.11}Al_{5.09}Ni_{11.08}B_x$ *MEA.*

Although the computed property diagrams offer M_2B intermetallic phases for all boron-doped MEAs, which solidifies directly from a liquid solution, it is worthy to mention that CALPHAD simulation neglects the critical boron solubility factor, which specifies about critical solubility level; below this critical level boron tends to prefer random high-angle grain boundaries upon moderate diffusion temperature. Beyond that, the formation of boride compounds could be seen as it leads to a decrease in the Gibbs free energy (Seol et al., 2018; Raabe et al., 2014; Rollet et al., 2004).

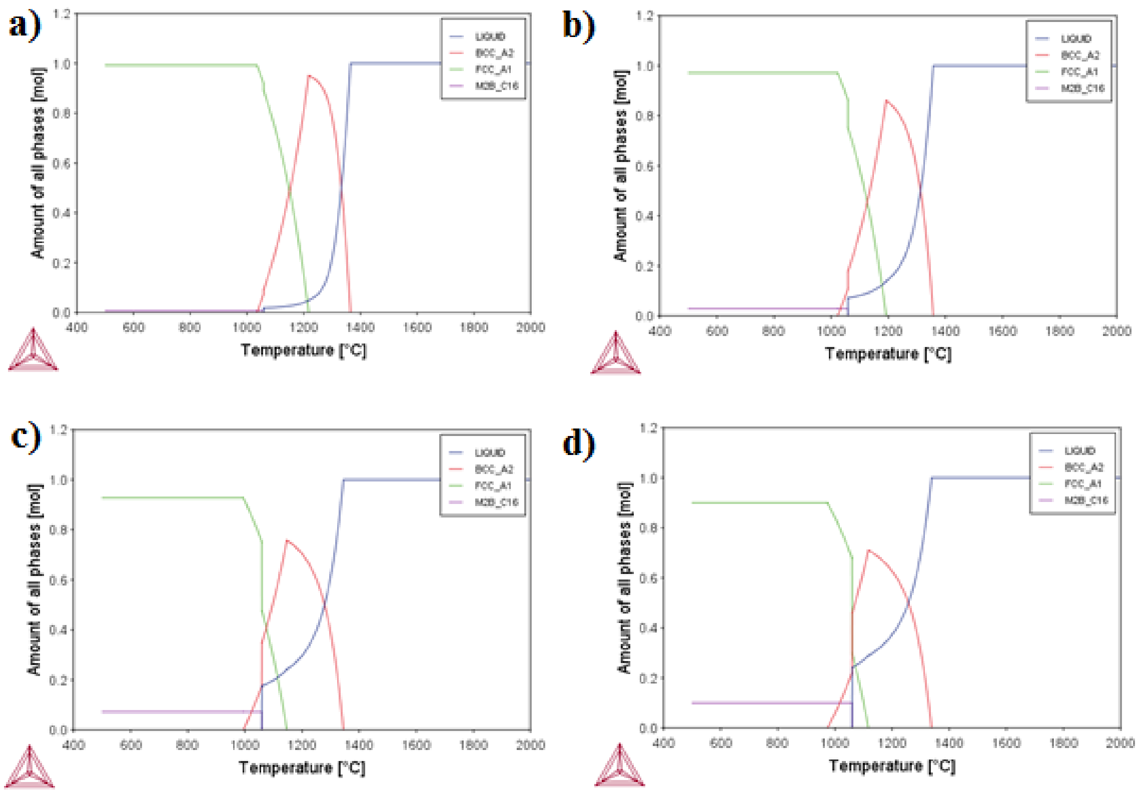

Figure 5.4. *Property diagrams of **a)** 0.05 wt% boron-doped, **b)** 0.2 wt% boron-doped, **c)** 0.5 wt% boron-doped, and **d)** 0.7 wt% boron-doped* $Fe_{(52.71-x)}Mn_{31.11}Al_{5.09}Ni_{11.08}B_x$ *MEAs.*

To sum up, combining extracted information from theoretical modeling with computational approach indicates that these medium entropy alloys correspond with phase formation rules of HEAs and high possibility to form single FCC solid solutions, while with the high amount of boron addition (0.5 and 0.7 wt%) formation of boride compounds is inevitable.

5.2. Melting and Casting

The samples were prepared based on the vacuum arc melting method and copper mold casting. Elements of Fe, Mn, Al, Ni and B with purity higher than 99.9% (Prepared by Alfa Aesar Co.) were used as raw materials. 1 atm Argon gas was injected to the furnace when the vacuum value of the furnace has reached to $6x10^{-1}$ mbar, in which 550 A was applied to melt the elements. The alloys were remelted for four times to ensure the homogeneity and then solidified in a water-cooled copper hearth. The copper molds of 6,5x20x80 mm were used to fabricate the plate-shaped samples.

5.3. Thermomechanical Treatment

Hot-rolling, homogenizing, cold-rolling and annealing processes were committed, respectively, to the as-cast samples. MSE brand furnace (Fig. 5.5) was used for hot rolling, homogenization, and recovery & recrystallization annealing. Hot and cold rolling (Figure 5.6) were both accomplished by the DRM160 brand rolling machine.

Figure 5.5. *The furnace used in hot rolling, homogenization and annealing processes.*

Considering hot rolling, a total of 4 steps of hot rolling were applied to the samples subjected to the 1100 ˚C furnace, preheated by the rate of 10 ℃/min. In the first step, samples were held at 1100 ˚C for 30 minutes and then rolled to reduce the thickness. For the second, third and fourth steps after each round, the samples (also at 1100 ˚C) were held in the furnace for 10, 20 and 20 min, respectively, and then the rolling process was applied. All samples were air cooled after the process was finished. Roughly 52% reduction in thickness was achieved during the final step of hot-rolling. Table 5.6 summarizes the hot-rolling process and final reduction percent for the process.

Figure 5.6. *Durston (DRM160) machine used for rolling processes.*

Homogenization process was carried out after hot rolling. Samples were homogenized at 1000 ˚C for 45 minutes and then quenched in the water.

Table 5.6. *The summary of Hot-rolling process.*

Samples	**Initial thickness (mm)**	**Thickness after Step 1 (mm)**	**Reduction after Step 1**	**Thickness after Step 2 (mm)**	**Reduction after Step 2**	**Thickness after Step 3 (mm)**	**Reduction after Step 3**	**Thickness after Step 4 (mm)**	**Final Reduction**
Boron free	5.65	5.21	%7.79	4.43	%21.59	3.44	%39.11	2.70	**%52.21**
0.05 wt% B	5.65	5.21	%7.79	4.43	%21.59	3.44	%39.11	2.70	**%52.21**
0.2 wt% B	5.70	5.21	%8.6	4.43	%22.28	3.44	%39.65	2.70	**%52.63**
0.5 wt% B	5.60	5.21	%6.96	4.43	%20.89	3.44	%38.57	2.70	**%51.78**
0.7 wt% B	5.68	5.21	%8.27	4.43	%22	3.44	%39.44	2.70	**%52.46**

Further grain refinement was achieved through cold-rolling to a thickness reduction ratio of ~50% of homogenized samples. The cold rolling was made at room temperature and the thickness of all samples was reduced to a total of 4 steps. The results of cold rolling are given in Table 5.7.

Table 5.7. *The summary of the cold-rolling process.*

Samples	Initial thickness (mm)	Thickness after Step 1 (mm)	Reduction after Step 1	Thickness after Step 2 (mm)	Reduction after Step 2	Thickness after Step 3 (mm)	Reduction after Step 3	Thickness after Step 4 (mm)	Final Reduction
Boron free	2.70	2.47	%8.52	1.80	%33.34	1.44	%46.67	1.15	**%57.41**
0.05 wt% B	2.70	2.35	%12.92	1.73	%35.92	1.40	%48.15	1.10	**%59.26**
0.2 wt% B	2.70	2.38	%11.85	1.80	%33.34	1.45	%46.3	1.15	**%57.41**
0.5 wt% B	2.70	2.46	%8.89	1.80	%33.34	1.46	%45.93	1.16	**%57.04**
0.7 wt% B	2.70	2.36	%12.59	1.68	%37.78	1.31	%51.48	1.14	**%57.78**

Thus, to a thickness reduction ratio of ~80% of as-cast samples was achieved after rolling procedure (i.e. hot and cold rolling). The total thickness reduction ratio of the samples is given in Table 5.8.

Table 5.8. *Total thickness reduction ratio after rolling procedure.*

Samples	Initial thickness (mm)	Final thickness (mm)	Total Reduction ratio
Boron free	~ 5.65	~ 1.1	%80.53
0.05 wt% B-doped	~ 5.65	~ 1.1	%80.53
0.2 wt% B-doped	~ 5.70	~ 1.1	%80.70
0.5 wt% B-doped	~ 5.60	~ 1.1	%80.35
0.7 wt% B-doped	~ 5.70	~ 1.1	%80.70

Regarding the phase diagram of $Fe_{(52.71-x)}Mn_{31.11}Al_{5.09}Ni_{11.08}B_x$ (Fig. 5.3) 1000 ˚C was determined as recrystallization temperature since it is the highest temperature in which the alloys face single FCC structure. For recrystallization of boron-doped and undoped samples, the rolled sheets were annealed at a temperature of 1000 ˚C for 30 min and subsequently quenched in water.

After applied deformation and heat treatment procedures, the samples were kept in a mixture of 97% HCl and 3% triethanolamine (by volume) for 90 min (Figure 5.7) and followed by a surface grinding process to remove accumulated oxide layer.

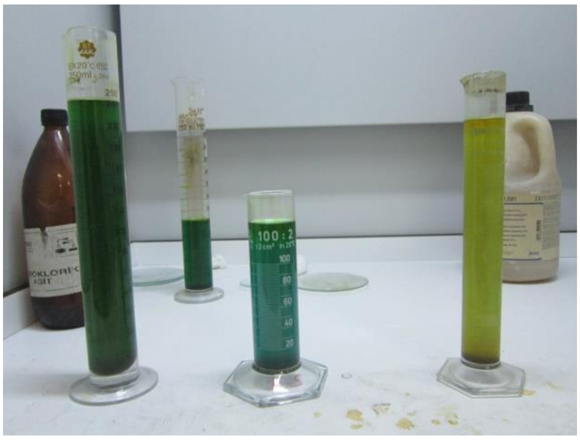

Figure 5.7. *Chemicals used to remove the oxide layer of the samples.*

5.4. Characterization

Characterization studies for the prepared samples (both as-cast and rolled samples) were examined in three main topics as chemical, microstructural and mechanical analysis.

5.4.1. Phase analysis

XRD (X-ray diffraction device) and SEM unit were used for chemical characterization.

5.4.1.1. *X-ray diffraction (XRD) Analysis*

XRD analysis was carried out for both As-Cast (AC) and Deformed and Heat-treated (D&H) samples. The surfaces of the samples were ground with sandpaper of 320 mesh.

The crystal structures were characterized by an X-ray diffractometer (XRD Rigaku-MiniFlex 600), using Cu-Kα radiation scanning from 30˚ to 90˚ for as-cast and 30˚ to 100˚ for D&H samples, at a scanning rate of 2˚/min.

5.4.1.2. *Rietveld analysis*

Rietveld analysis carried out to as-cast samples to calculate the phase amount of MEAs in multiphase structural alloys. Phase fractions were obtained by Rietveld analysis of XRD patterns using the Materials Analysis Using Diffraction (MAUD) program (Lutterotti and Scardi, 1990).

5.4.2. Microstructural characterization

Struers Discotom-5 cutting device and Struers TegraPol-21 device were used for grinding and polishing the samples (Figure 5.8). The specimens used for microstructure analysis were prepared by hot coating. For the grinding process, Metkon brand honeycomb abrasives of 75, 54 and 18 were used respectively, while Buehler brand 1200 mesh paper were benefited as required. Regarding polishing, MDNap 250 mm of Struers brand as the polisher, and 3-micron Magnum-top-duo of the Microdiamant brand as polishing liquid were utilized. The etching was accomplished with a mixture of 25% nitric acid (HNO_3) and 75% pure water.

Figure 5.8. ***a)*** *Struers Discotom-5 cutting device and,* ***b)*** *Struers TegraPol-21 polishing device.*

5.4.2.1. *Optical microscopy (OM)*

The Nikon Eclipse L150 optical microscope equipped with the Clemex Pro image analysis system (Figure 5.9) was used for optical microscopy.

Figure 5.9. *Image analysis system.*

5.4.2.2. *Scanning electron microscope (SEM)*

The SEM images of the AC and D&H samples were prepared by NOVA NANOSEM 650 device.

5.4.3. Mechanical characterization

Mechanical characterization of the samples was carried out by tensile test and microhardness measurement.

5.4.3.1. *Tensile test*

For each MEAs, at least two specimens were prepared based on ASTM E8 Standard (using laser cutting method) to perform tensile tests. The tensile test of the samples was performed using the Shimadzu Autograph AG-IS 250 kN device. The amount of elongation was measured by optical extensometer and the test was applied at a deformation rate of 1.0 mm/min.

5.4.3.2. *Hardness measurement*

The hardness measurements were accomplished by two different methods (i.e. Vickers (HV) and Rockwell (HRC) tests) by applying 50 grams for 10 seconds of load on the Future-Tech FM-700 device. For each sample, at least 10 hardness tests were performed to obtain sufficient statistics.

6. RESULTS, DISCUSSION, AND RECOMMENDATIONS

6.1. Results

6.1.1. OM and SEM Images

The microstructure of all AC and Deformed and heat treated (D&H) samples were examined by optical microscopy and the SEM images. The optical microscope images are ranked in the order of 200x, 500x and 1000x magnifications and are given in Figures 6.1-6.6, on the sequence of the increasing magnification size and operations performed primarily on the samples. Specification of each MEA is indicated in the upper left corner of the microstructure image. Note that the perpendicular surfaces of all samples to the rolling direction was examined in both OM and SEM microstructural characterization.

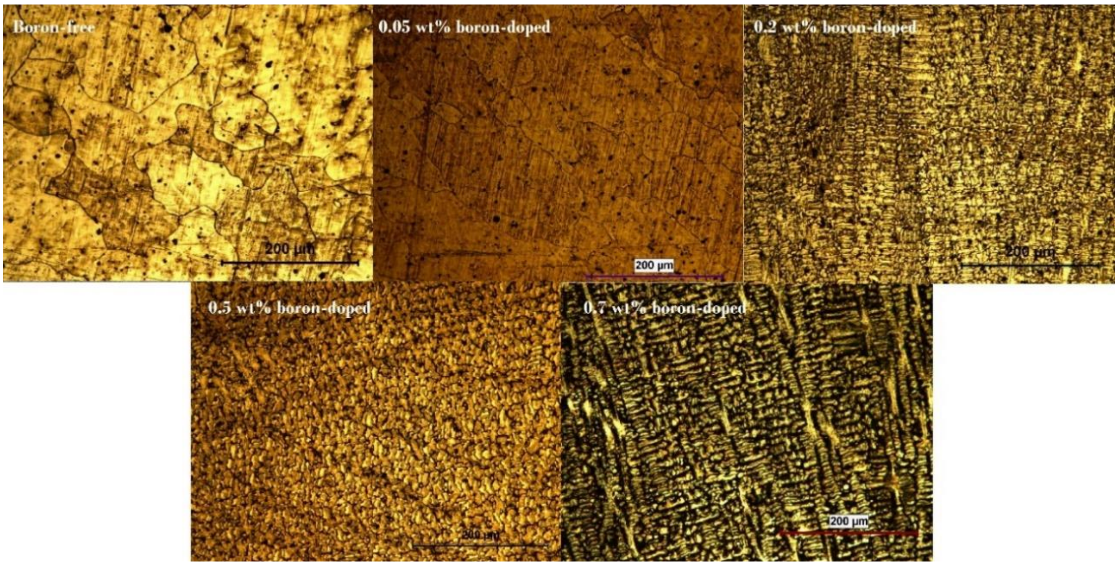

Figure 6.1. *OM images of as-cast samples (200x).*

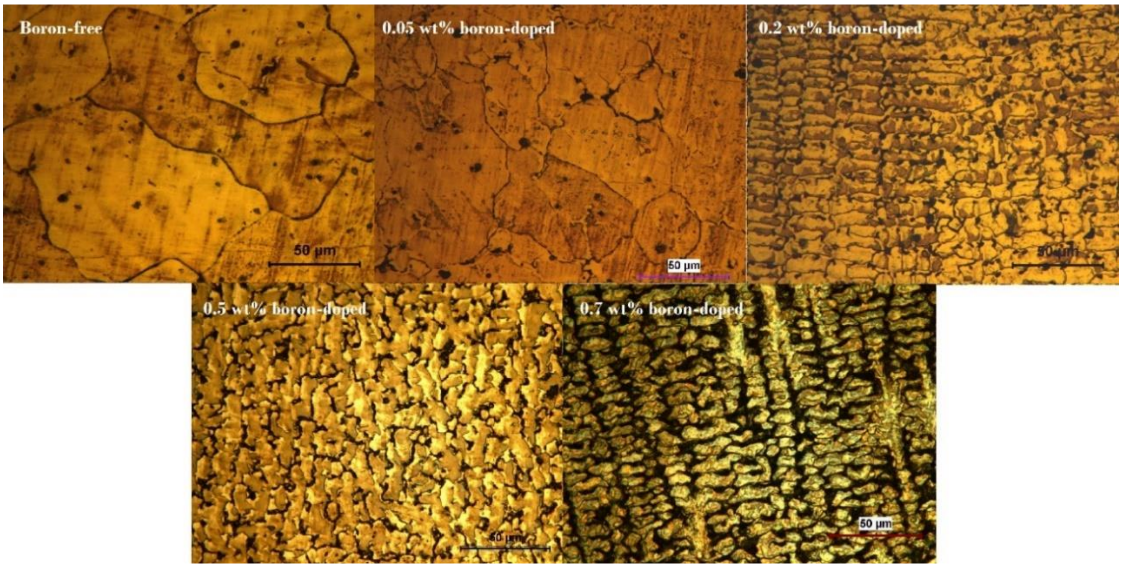

Figure 6.2. *OM images of as-cast samples (500x).*

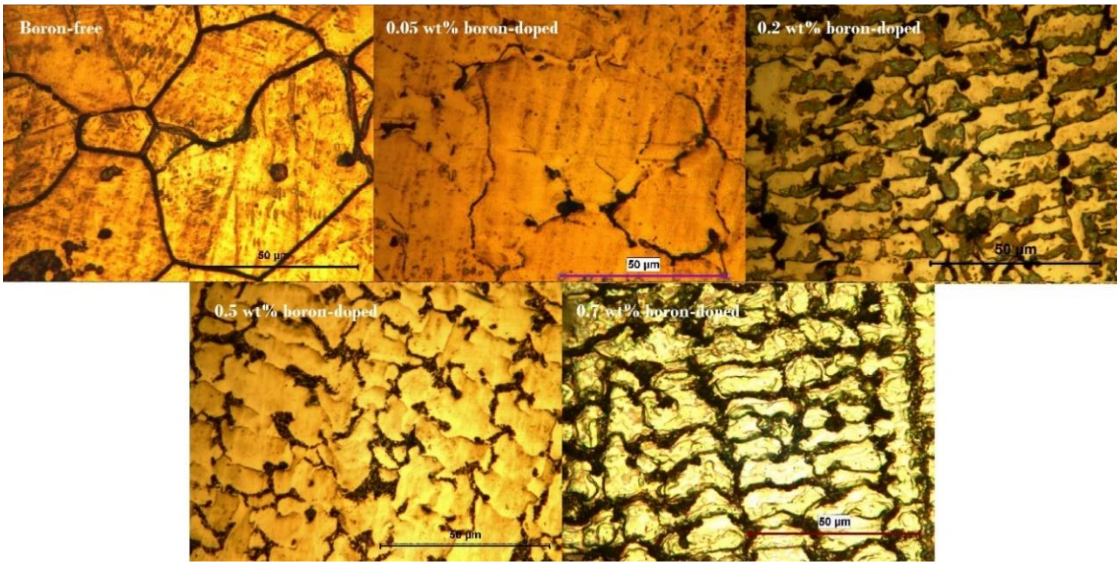

Figure 6.3. *OM images of as-cast samples (1000x).*

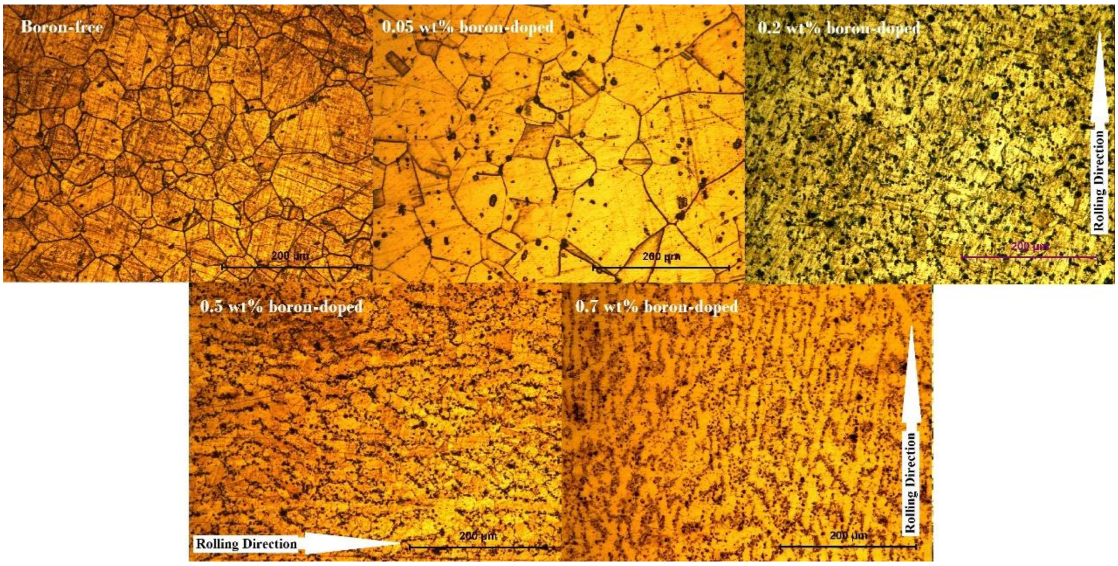

Figure 6.4. *OM images of D&H samples (200x).*

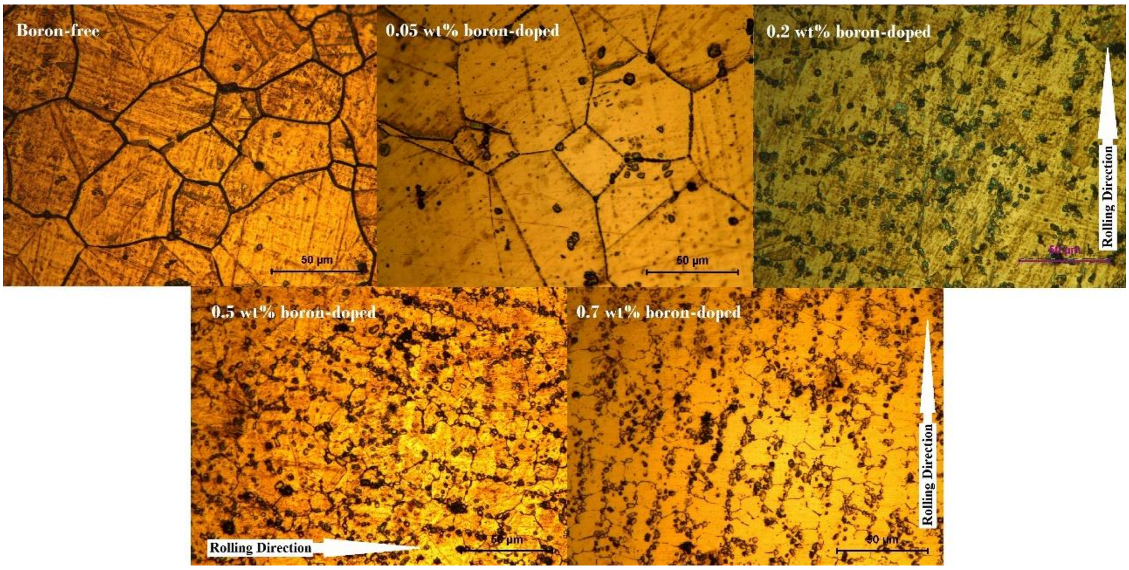

Figure 6.5. *OM images of D&H samples (500x).*

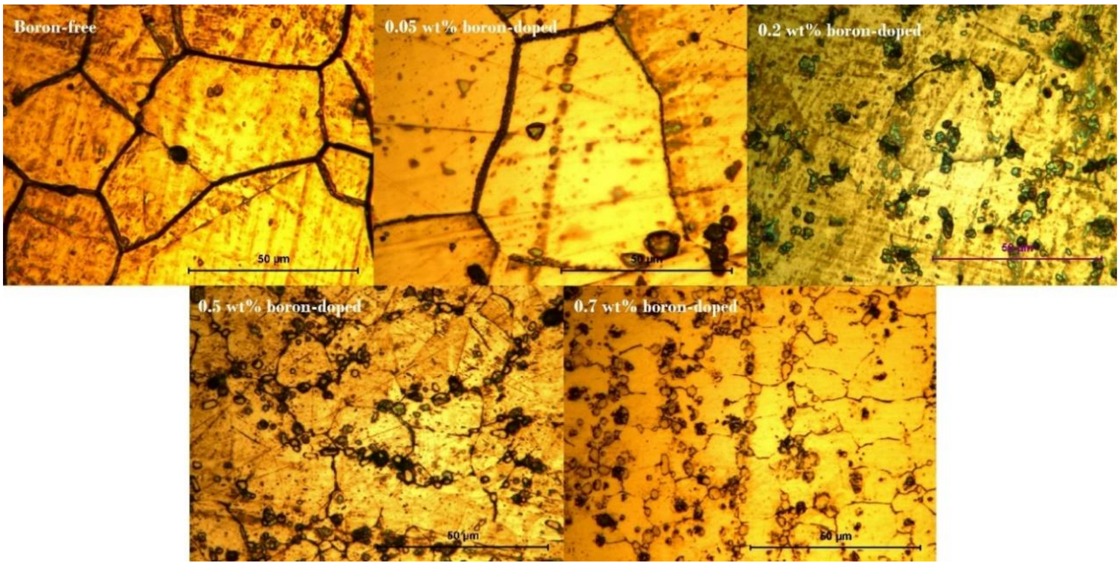

Figure 6.6. *OM images of D&H samples (1000x).*

SEM images of the samples were taken using a secondary electron detector. The SEM images for microstructural analysis are ranked in the order of 250x and 2500x magnifications and presented in Figures 6.7-6.10. The composition code for each sample is located in the upper left corner of the related image.

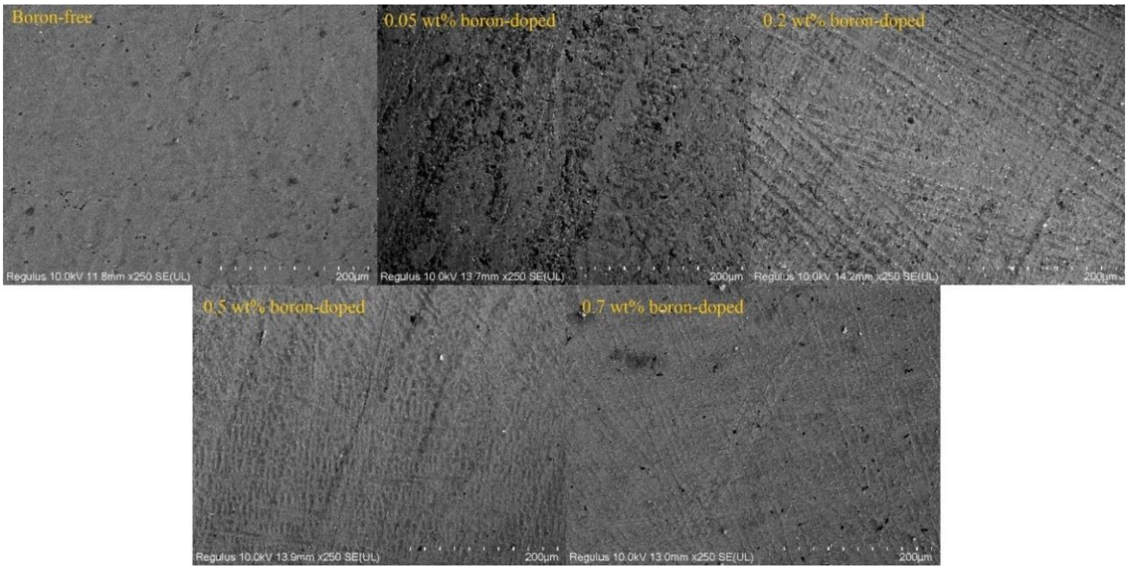

Figure 6.7. *SEM images of as-cast samples (250x).*

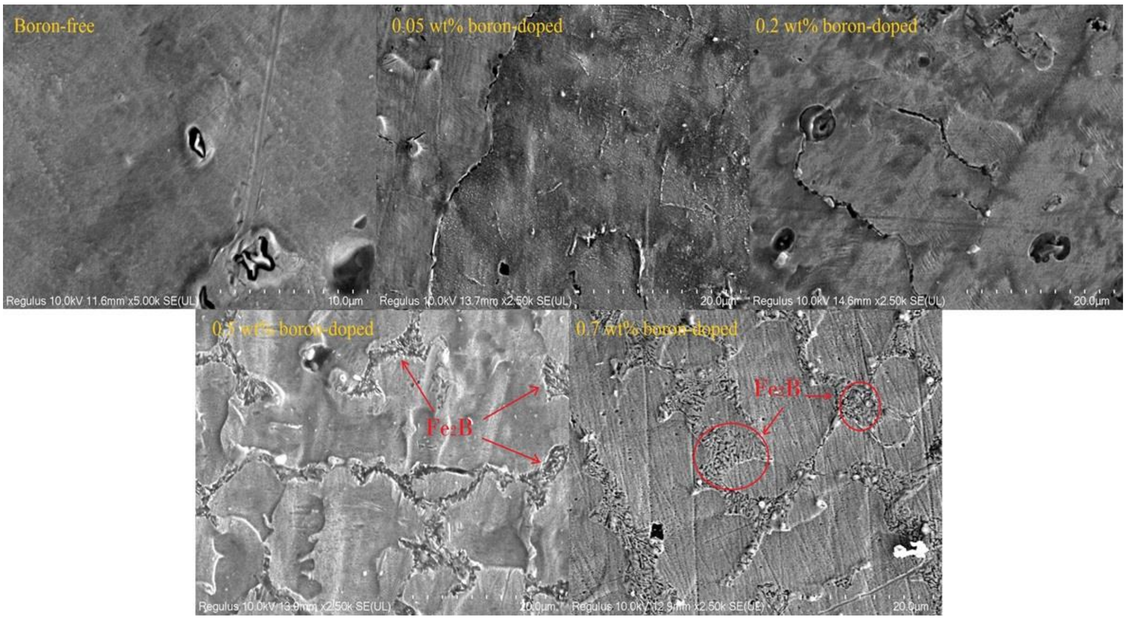

Figure 6.8. *SEM images of as-cast samples (2500x).*

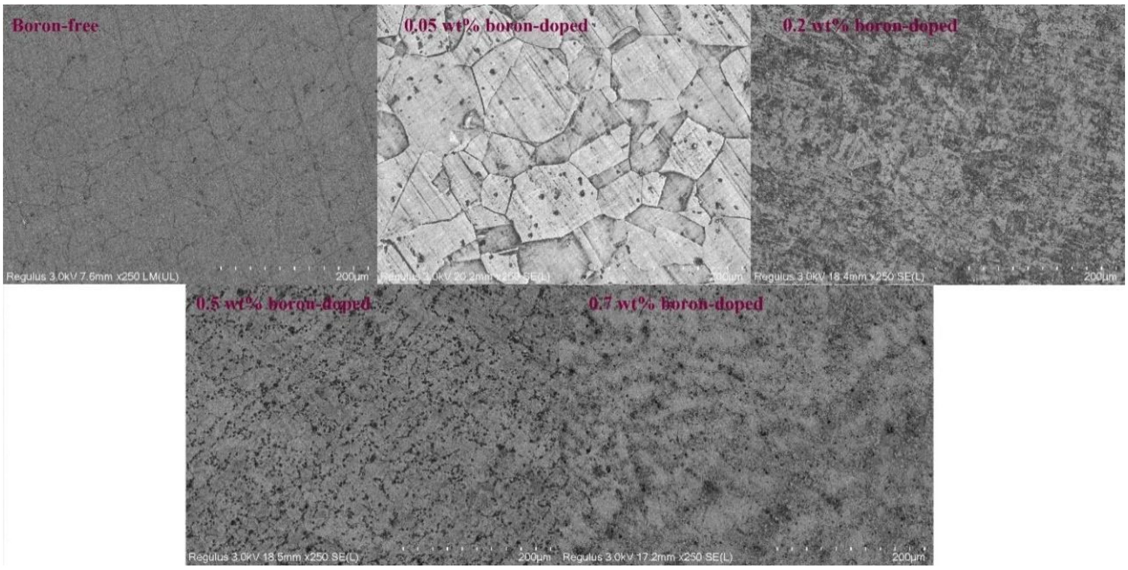

Figure 6.9. *SEM images of D&H samples (250x).*

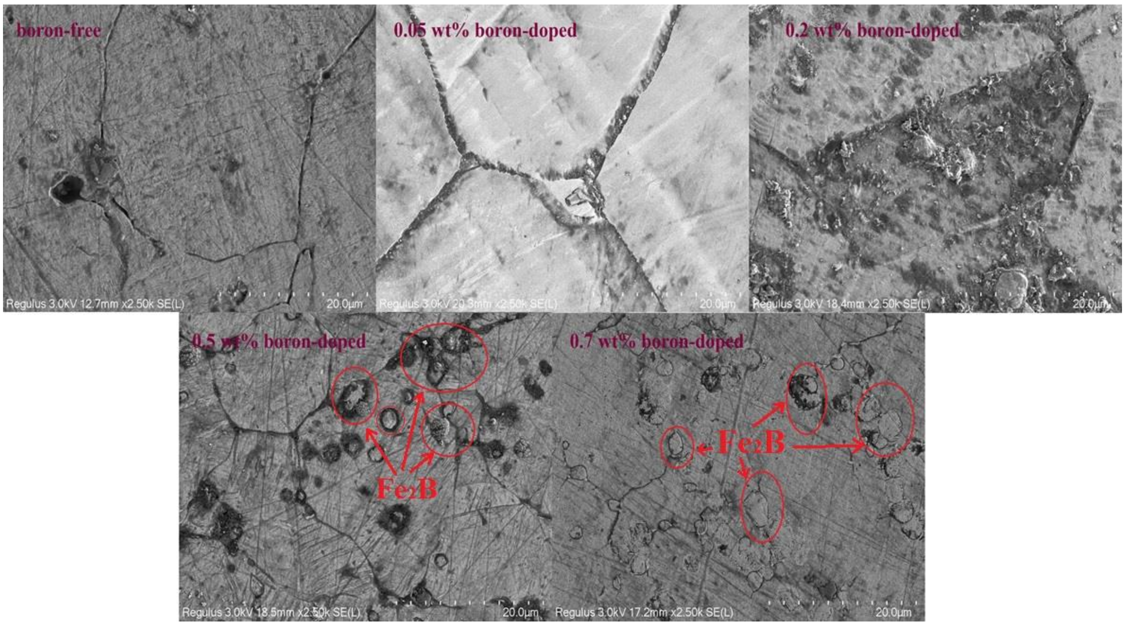

Figure 6.10. *SEM images of D&H samples (2500x).*

For grain size measurements, images with 600x magnifications have been used to calculate the average grain size of each MEA, which is illustrated in Figures 6.11 and 6.12. The composition code for each sample is located in the upper left corner of the related image.

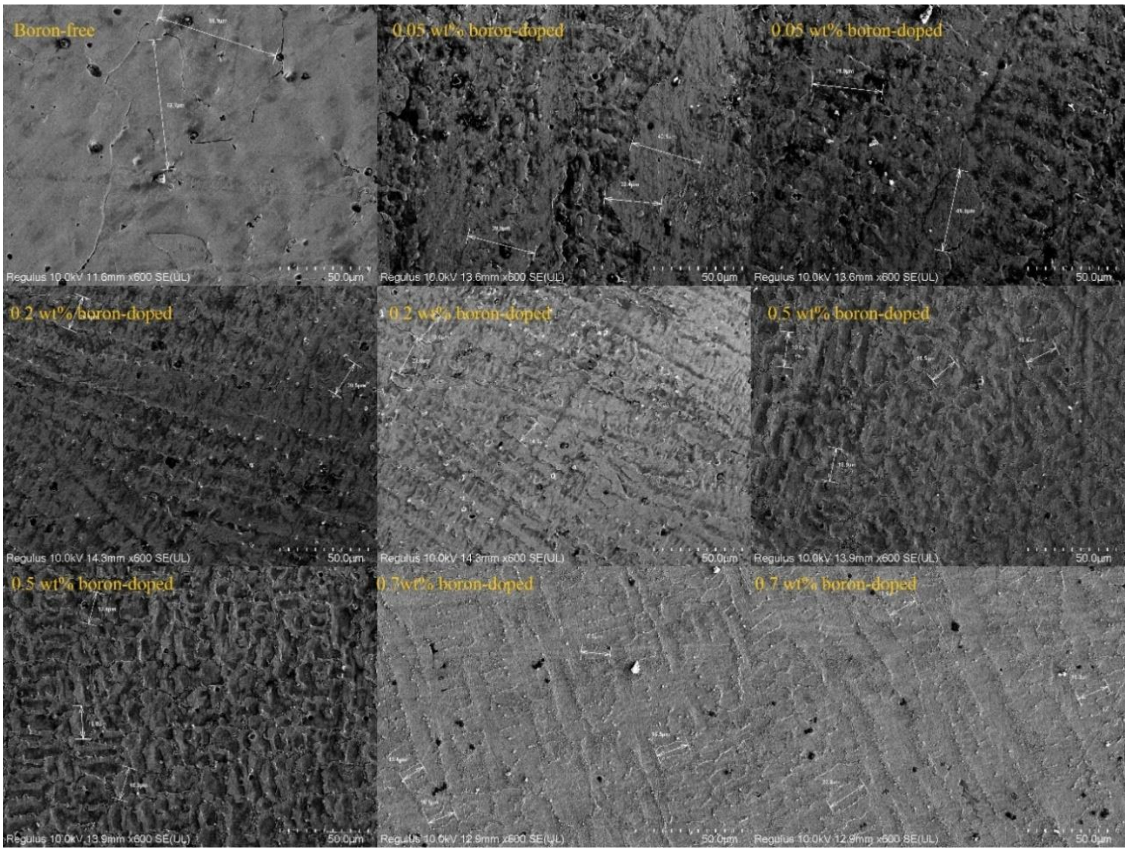

Figure 6.11. *SEM images of as-cast samples (600x). Used for grain size measurements.*

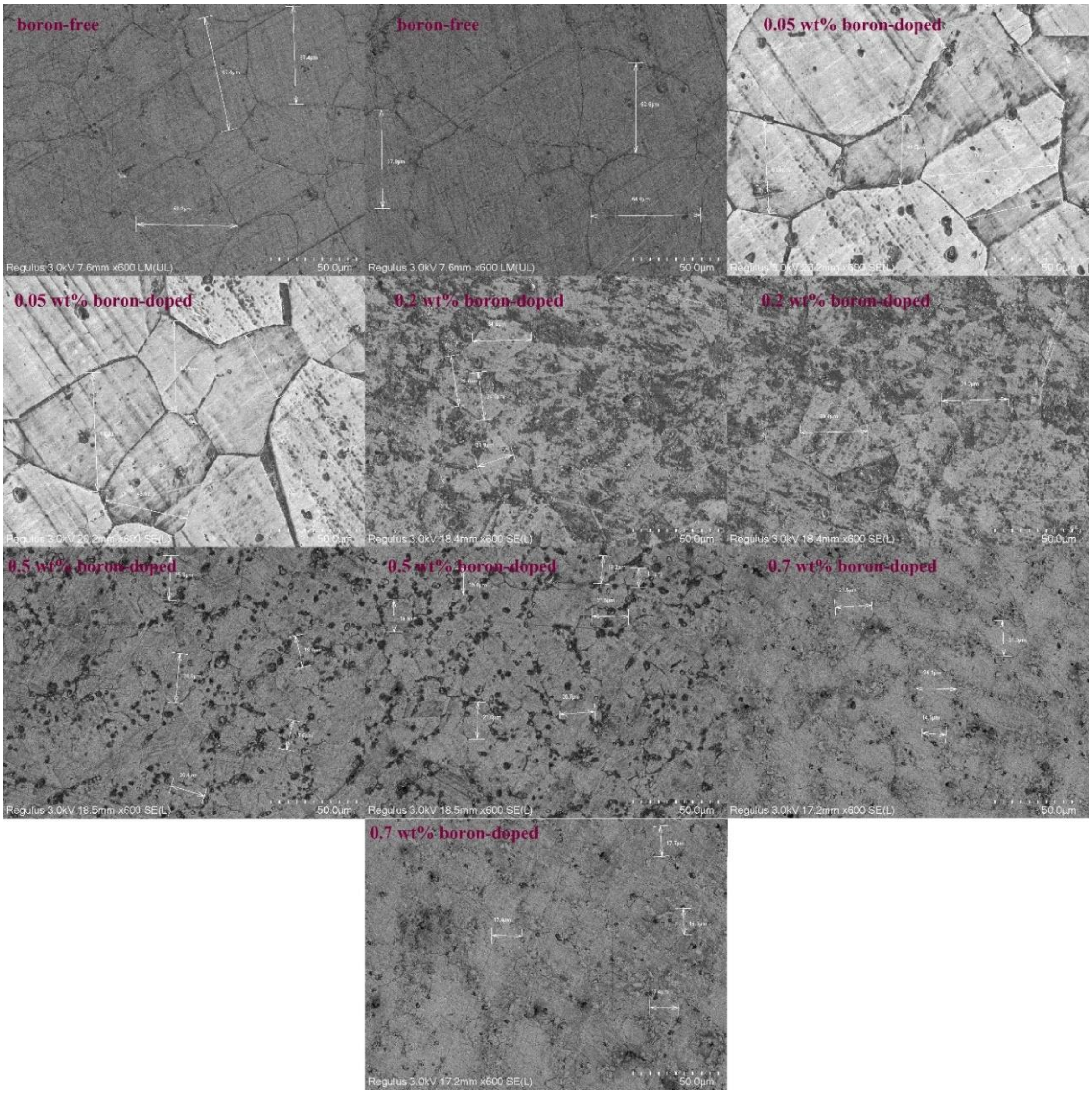

Figure 6.12. *SEM images of D&H samples (600x). Used for grain size measurements.*

6.1.2. XRD and Rietveld studies

The XRD studies carried out for both as-cast and D&H samples. Figure 6.13 and 6.14 illustrates XRD results for as-cast and D&H samples respectively.

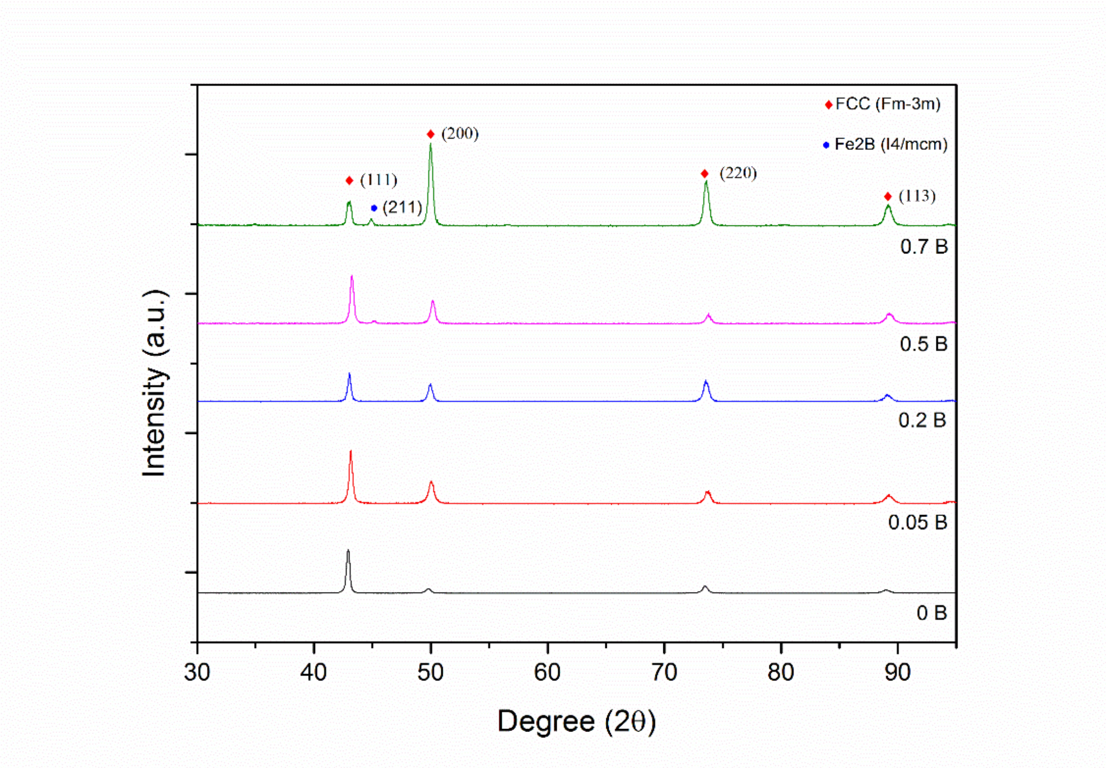

Figure 6.13. *XRD results of as-cast samples.*

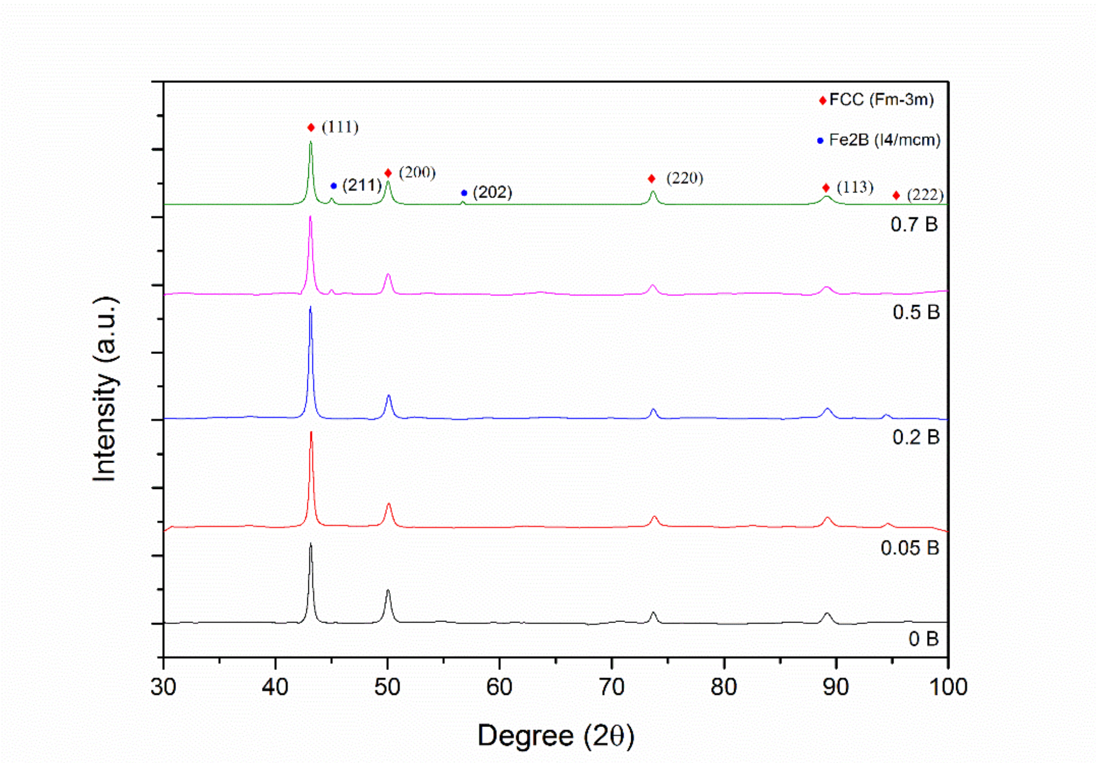

Figure 6.14. *XRD results of D&H samples.*

Just an FCC phase can be indexed on the XRD pattern of the as-cast boron-free alloy. Regarding boron-doped samples, 0.05 and 0.2 wt% boron-doped alloys also show a single FCC structure. For 0.5 and 0.7 wt% boron-doped alloys, Fe_2B with tetragonal structure and I4/mcm space group has been detected as the M_2B intermetallic compound predicted by both theoretical and computational modeling methods. Rietveld Analyses has been carried out to specify the amount of iron boride phase in 0.5 and 0.7 wt% boron-doped alloys in as-cast and D&H samples. Table 6.1 summarizes the result taken from Rietveld analysis.

Table 6.1. *Results of Rietveld analysis for 0.5 and 0.7 wt% Boron doped alloys.*

MEA	Condition	FCC Content (%)	Fe_2B Content (%)	GOF
0.5 wt% B-doped	AC	95.3758	4.6242	1.6493
0.7 wt% B-doped	AC	93.8631	6.1369	1.3212
0.5 wt% B-doped	D&H	97.312	2.688	1.02
0.7 wt% B-doped	D&H	94.563	5.437	1.03

6.1.3. Hardness measurements

The hardness measurements were accomplished by two different methods (i.e. Vickers (HV) and Rockwell (HRC) tests) by applying 50 grams for 10 seconds of load for both as-cast and D&H samples. Table 6.2 and Figures 6.15 represent the results of Hardness tests where for each sample, at least 10 hardness tests were performed to obtain sufficient statistics.

Table 6.2. *The results of Hardness measurement.*

MEAs	As-Cast				D&H			
	HV	SD[1]	HRC	SD	HV	SD	HRC	SD
Boron-free	219	10	15	2	212	10	14	2
0.05 wt% B-doped	267	16	25	3	234	14	19	3
0.2 wt% B-doped	408	78	41	7	249	25	21	5
0.5 wt% B-doped	475	50	47	4	338	17	34	2
0.7 wt% B-doped	538	89	51	6	332	15	32	2

*** 1.SD: Standard Deviation**

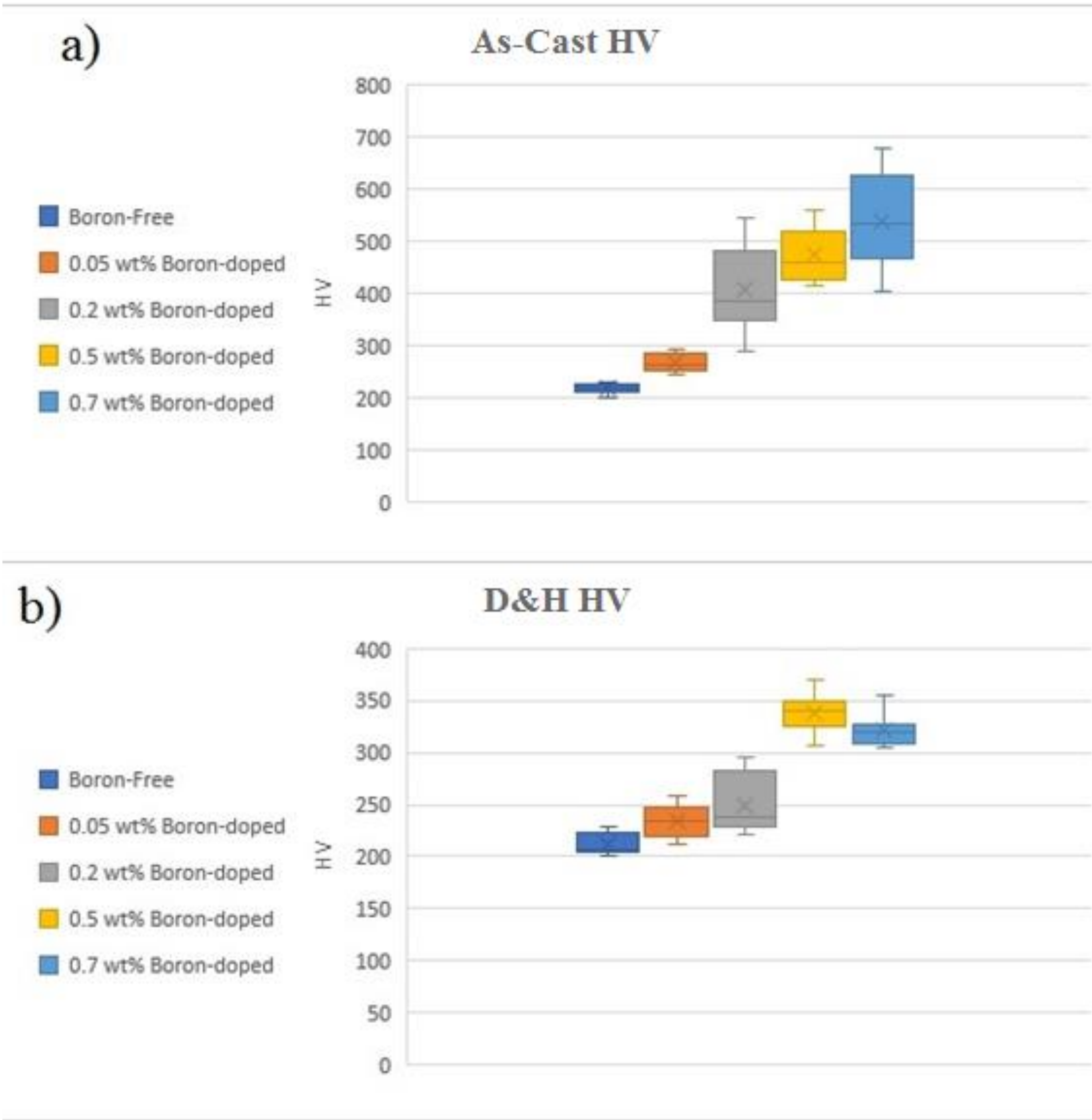

Figure 6.15. *The Hardness measurement results of **a)** as-cast and **b)** D&H samples. (x: average value, —: mean value).*

6.1.4. Tensile test

The tensile tests applied for D&H samples under the load of 250 kN and a deformation rate of 1.0 mm/min. The relevant stress-strain curves of examined samples are presented in Figure 6.16.

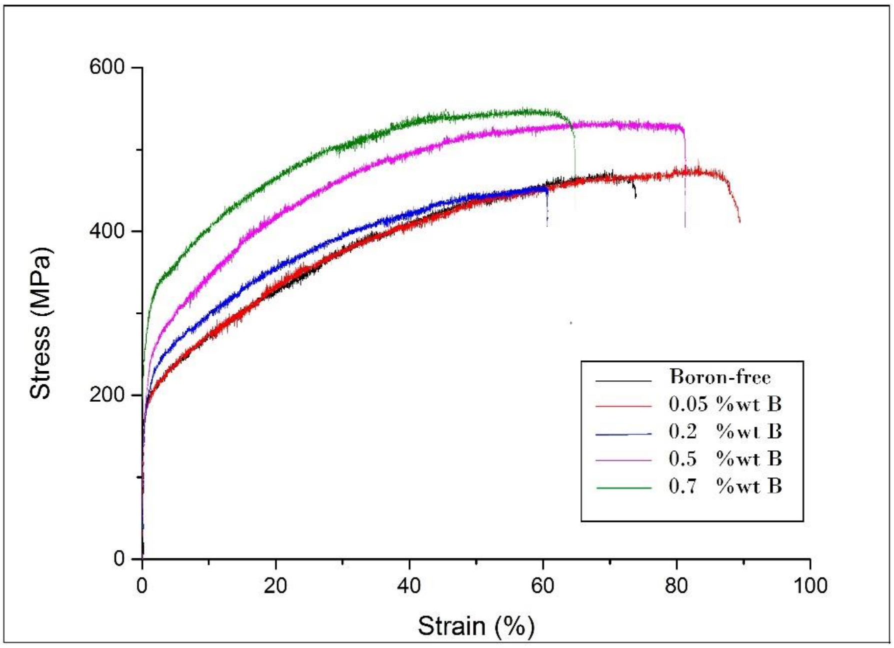

Figure 6.16. *Stress-Strain curves of D&H samples.*

6.1.5. Experimental density

To examine the validity of the theoretical density, the experimental density of the alloys has been calculated using Archimedes Principle. To calculate experimental density at least five measurements have been carried out for each sample and the average value has been taken as the experimental density. Table 6.3 compares the calculated theoretical density and experimental density values.

Table 6.3. *Density values of the samples.*

MEAs	Theoretical density (g/cm^3)	Experimental density (g/cm^3)
Boron-free	7.3361	7.3438
0.05 wt% B-doped	7.3236	7.3255
0.2 wt% B-doped	7.2864	7.281
0.5 wt% B-doped	7.2133	7.2498
0.7 wt% B-doped	7.1656	7.2185

6.2. Discussion

An MEA based on HEA principles has been designed and evaluated. The model proposes that benefiting from high entropy principles, by the enthalpy of mixing values in the range of -15 and 5 kJ/mol and Ω parameters higher than 1.1, it is still possible to obtain a single-phase structure up to 6.6% atomic size difference (δ parameter). Even addition of minor alloying elements (Boron in this case) with a careful arrangement of enthalpy of mixing (ΔH_{mix}), Ω parameter, and (δ) parameter could lead to single solid solution phases. XRD results demonstrate that up to 0.2 wt% boron addition results in a single FCC phase while further boron addition (i.e. 0.5 and 0.7 wt%) leads to exceeding amount of boron compare to the critical level and promotes the formation of metal borides. Rietveld analysis reveals that in 0.5 and 0.7 wt% boron doped alloys in addition to FCC phase, 4.62 and 6.14% Fe_2B phase, respectively, where these amounts decrease to 2.69 and 5.44% in D&H samples. This is thought to stem from higher temperatures and period provided by heat-treatment and annealing process, particularly, to boron atoms to segregate at high angle grain boundaries to reduce the mixing Gibbs free energy. Table 6.4 summarizes the results of chemical, microstructural and mechanical characterization of boron free and boron doped $Fe_{(52.71-x)}Mn_{31.11}Al_{5.09}Ni_{11.08}B_x$ MEAs.

Earlier chemical and microstructural characterizations showed that further boron addition not only induces a second intermetallic phase but also it changes the solidification behavior of the system, where after 0.2 wt% boron addition there is no sign of equiaxed grains, and a dendritic structure take place. 0.5 and 0.7 wt% boron additions, to produce $Fe_{(52.71-x)}Mn_{31.11}Al_{5.09}Ni_{11.08}B_x$ alloys lead to the formation of needle-like tetragonal Fe_2B-type structures in as-cast samples. The volume fraction of the boride phase increases as the boron content increases. Although the FCC phase is also the primary phase of the alloy, the boron addition modifies solidification behavior of the system, where FCC and Fe_2B-type boride are formed simultaneously during solidification. The final structure of thermomechanical treated samples is composed of a dendritic region with Fe_2B precipitates where the interdendritic region of as-cast samples have been spheroidized and precipitated at the grain boundaries as well as within the FCC matrix through the thermomechanical process.

Table 6.4. *The summary of chemical, microstructural and mechanical characterization of boron free and boron doped MEAs*

MEA	Condition	Phase content	Microstructure	Grain Size (μm)	HRC	YS (MPa)	UTS (MPa)	TE (%)
Boron-free	AC	FCC	Equiaxed grains	71.8	15	151	476.0	70.4
	D&T	FCC	Equiaxed grains	59.75	14			
0.05 wt% B-doped	AC	FCC	Equiaxed grains	39.72	25	155	488.8	83.2
	D&T	FCC	Equiaxed grains	54.1	19			
0.2 wt% B-doped	AC	FCC	Dendritic	19.3	41	170	458.5	64.3
	D&T	FCC	Dendritic	32.12	21			
0.5 wt% B-doped	AC	FCC+Fe_2B	Dendritic	18.6	47	185	537.8	81.3
	D&T	FCC+Fe_2B	Dendritic	22.62	34			
0.7 wt% B-doped	AC	FCC+Fe_2B	Dendritic	16.51	51	225.5	543.3	64.8
	D&T	FCC+Fe_2B	Dendritic	18.61	31			

Coupling the CALPHAD simulation to the microstructural characterization, the following solidification sequence was proposed to both boron-free and boron-containing alloys: the sample starts to solidify with the formation of BCC grains, segregating Fe, Mn, Al, Ni and B into the liquid. At the final stages, FCC takes place as a final structure where with further boron addition (higher than 0.05 in this case) FCC dendrites and Fe_2B-type borides (in 0.5 and 0.7 wt% boron-doped alloys) solidifies. The morphology of the alloys generally depends on its freezing range, the temperature gradient in the liquid, the heat extraction and the surface energy (Jung et al., 2007, Park et al., 2004). Where the other parameters for the all fabricated alloys are the same, the surface energy is thought to be the key parameter in the transition of equiaxed grains to the dendritic structure. It is thought that by further boron addition (≥ 0.2 wt%), boron atoms increase the surface energy and induce an energy barrier which causes anisotropic grain growth in the favored directions leading to dendritic structures.

The Table 6.4 shows that boron addition has a positive effect on grain size reduction where just by 0.05 wt% boron addition the grain size has been almost halved (from 71.8μm to 39.7 μm) compare to boron free as-cast sample. Moreover, it is observed that as the boron level increases, the hardness value increases, the same mechanism which is used in low alloy steels to increase the hardness level.

The 0.7 wt% b-doped alloy shows the highest yield and ultimate tensile properties. The thermomechanical process resulted in increasing the yield strength by ~ 50% (from 151 MPa to 222.5 MPa) and ultimate tensile strength by ~15% (from 476 MPa to 543 MPa) -both in 0.7 wt% boron doped alloy- at comparable ductility. The improvement of room-temperature tensile properties demonstrates the success of the proposed GB alloying strategy and positive effect of spheroidized iron boride intermetallics for MEAs. Just by 0.05 wt% boron addition both yield and ultimate tensile properties of the alloy has been improved due to effective grain size reduction at even better ductility. However, the transition of the equiaxed grains to the dendritic microstructure has decreased the tensile property and ductility of the alloy, regardless of the finer grains compare to 0.05 wt% alloy. Smaller dendrites generally lead to higher ductility of the product (as in the case of 0.5 wt% b-doped alloy compare to 0.2 wt% b-doped alloy). On the other hand, the finer dendrites in the presence of spheroidized iron borides have enhanced the mechanical properties of the alloy. Although further amounts of Fe_2B intermetallic phase (5.4% in 0.7 wt% b-doped alloy compares to 2.7% in 0.5 wt% b-doped alloy due to Rietveld analysis) has improved mechanical properties of the alloy, it has caused a decrease in ductility due to the higher amount of brittle iron boride intermetallics.

The results show that segregation of boron at GBs is an efficient site-specific manipulation method that allows optimization of the strengths through grain size reduction and enhanced GB cohesion without sacrificing ductility. Overall, boron leads to the formation of a composite with hard borides and changes the matrix/precipitate order to a more ductile configuration. This can explain why the strength of this alloy is higher than the boron-free alloy while having roughly the same ductility.

Regarding the obtained results, it could be said that this method is also applicable to other MEAs as well as HEAs with single FCC phase since it improves the GB properties without affecting the bulk deformation mechanisms.

6.3. Recommendations

For $Fe_{50}Mn_{30}Al_{10}Ni_{10}$ (at%) MEA it seems that due to its low yield and ultimate strength further studies based on various strengthening mechanism should be carried out to obtain higher mechanical properties.

More thorough investigations on heat treatment procedure and the thermomechanical process should take place to a better understanding of thermomechanical behavior and also better control of the grain size of the alloy.

More microstructural analysis should be carried out to understand the transition mechanism and texture change via boron addition.

REFERENCES

Akbari, S., Imlau, J., Prahl, U., Bleck, W. (2009). *Derivation and Variation in Composition-Dependent Stacking Fault Energy Maps Based on Subregular Solution Model in High-Manganese Steels*. Metallurgical and Materials Transactions A, Vols:40A, p.3076.

Alaneme, K.K., Bodunrin, M.O., Oke, S. R. (2016). *Processing Alloy Composition and Phase Transition Effect on the Mechanical and Corrosion Properties of High Entropy Alloys: a Review*. Journal of Materials Research and Technology, Vols:5, p.4.

Anonymous (2018). *Shear Band Formation During Cold Rolling of Metals.* http://www.dierkraabe.com/shear-banding/, accessed on 12.12.2018.

Anonymous (2019). *Boron in Steels*, http://ispatguru.com/boron-in-steels/ . accessed on 01.03.2019.

Anonymous (2019b). *Boron in Steels: part two*. https://www.totalmateria.com/page.aspx?ID=CheckArticle&site=kts&NM=214 , accessed on 03.03.2019.

Beladi, H., Timokhina, I.B., Estrin, Y., Kim, J., De Cooman, B.C., Kim, S.K. (2011). *Orientation dependence of twinning and strain hardening behaviour of a high manganese twinning induced plasticity steel with polycrystalline structure*. Acta Mater., Vols:59, p.7787–7799.

Benito, J.A., Cobo, R., Lei, W., Calvo, J., Cabrera, J.M. (2016). *Stress-strain response and microstructural evolution of a FeMnCAl TWIP steel during tension compression tests.* Mater Sci Eng:A, Vols:655, p.310–320.

Boyer, H.E. and Gall, T.L. (1985). *Metals handbook*. Desk ed. Metals Park, Ohio: American Society for Metals.

Brüx, U., Frommeyer, G., Jimenez, J. (2002). *Light-weight steels based on iron-aluminium - Influence of micro alloying elements (B, Ti, Nb) on microstructures, textures and mechanical properties*. Steel Res, Vols:73, p.543-548.

Callister, W.D. and Rethwisch, D.G. (2013). *Material science and engineering an introduction*. Weily, p.213-215.

Cantor, B., Chang, I.T.H., Knight, P., Vincent, A.J.B. (2004). *Microstructural development in equiatomic multicomponent alloys*. Mater Sci Eng A, Vols:375–377, p.213–218.

Chaiberge, M. (2011). *New Trends and Developments in Automotive System Engineering*. p.107,109,https://www.intechopen.com/books/new-trends-and-developments-inautomotive-system-engineering/high-mn-twip-steels-for-automotive-applications, accessed on 02.02.2019.

Chen, H.L., Mao, H., Chen, Q. (2018). *Database Development and Calphad Calculations for High Entropy Alloys: Challenges, Strategies and Tips*. Material Chemistry and Physics, Vols:210, p.279-290.

Chen, S., Rana, R., Haldar, A., Ray, R.J. (2017). *Current State of Fe-Mn-Al-C Low Density Steel.* Progress in Material Science, Vols:89.

Courtney, T.H. (1990). *Mechanical Behavior of Materials.* New York: McGraw-Hill Publ. Co. p.198-205.

De Knijf, D., Petrov, R., Föjer, C., Kestens, L.A.I (2014). *Effect of fresh martensite on the stability of retained austenite in quenching and partitioning steels*. Mater Sci Eng: A, Vols:615, p.107–115.

Demeri, M.Y. (2013). *Advanced high-strength steels: science, technology, and applications.* ASM International.

Emadoddin, E., Akbarzadeh, A., Daneshi, G. (2006). *Effect of intercritical annealing on retained austenite characterization in textured TRIP-assisted steel sheet*. Mater Charact, Vols:57, p.408–413.

Gao, M.C., Yeh, J.W., Liaw, P. K., Zhang, Y. [Editors]; (2016). *High-Entropy Alloys: Fundamentals and Applications*. Springer International Publishing, Switzerland.

Gao, M.C., Zhang, C., Gao, P., Zhang, F., Ouyang, L.Z. (2017). *Thermodynamics of Concentrated Solid Solution Alloys*. Current Opinion Solid State and Material Science, Vols:21, p.238-251.

Guo, S., Ng, C., Lu, J., Liu, C.T. (2011). *Effect of valence electron concentration on stability of fcc or bcc phase in high entropy alloys*. Journal of applied physics, Vols:109, Issue 10.

Hall, J.N. and Fekete, J.R. (2017). *Steels for auto bodies: a general overview*. In: Rana R, Singh SB, editors. Automotive steels: design, metallurgy, processing and applications. Elsevier, p.19–45.

Hamada, A.S. (2007). *Manufacturing, mechanical properties and corrosion behaviour of high-Mn TWIP steels*. Oulu University Press.

Gutierrez-Urrutia, I. and Raabe, D. (2012). *Multistage strain hardening through dislocation substructure and twinning in a high strength and ductile weight-reduced Fe–Mn–Al–C steel*. Acta Mater. Vols: 60, p.5791-5802.

Iyer, A.K., Zhang, Y., Scheifers, J.P., Fokwa, B. P. T. (2019). *Structural variations, relationships and properties of M2B metal borides*. Journal of Solid State Chemistry, Vols:270, p.618–635.

Juan, C.C., Hsu, C.Y., Tsai, C.W., Wang, W.R., Sheu, T.S., Yeh, J.W., Chen, S.K. (2013). *On microstructure and mechanical performance of AlCoCrFeMo0.5Nix high-entropy alloys*. Intermetallics, Vols:32, p.401–407.

Jung, I.-H., Bang, W., Kim, I. J., Sung, H.-J., Park, W.-J. et al. (2007). *Mg coil production via strip casting and coil rolling technologies.* Proceedings of Magnesium Technology, TMS, pp. 85–88

Kao, Y.F., Chen, S.K., Chen, T.J., Chu, P.C., Yeh, J.W., Lin, S.J. (2011). *Electrical, magnetic, and hall properties of AlxCoCrFeNi high-entropy alloys*. J Alloys Compd, Vols:509, p.607–1614.

Kim, M.H. and Kwun, S.I. (1996). *Tensile properties of cast and mechanically alloyed FeAl with high boron content*. Scr. Mater., vol. 35, no. 3, pp. 317–322.

Krauss, G (2016). *Strengthening Mechanism in Steels*. Reference Module in Materials Science and Materials Engineering.

Kwon, O., Lee, K., Kim, G., Chin, K.G. (2010). *New trends in advanced high strength steel developments for automotive applications*. Materials Science Forum, Vols: 638-642, pp. 136-141.

Li, C., Li, F., Liang, J., Cao, R., Zhao, Z. (2018). *Effects of boron on mechanical properties of a hot-rolled 13% Mn metastable austenitic steel*. Mater Lett, Vols:233, p.314-317.

Liu, C.T., George, E.P., Oliver, W.C. (1996). *Grain-boundary fracture and boron effect in Ni3Si alloys*. Intermetallics, Vols: 4, p.77-83.

Liu, H., Lu, X., Jin, X., Dong, H., Shi, J. (2011). *Enhanced mechanical properties of a hot stamped advanced high-strength steel treated by quenching and partitioning process*. Scr Mater, Vols:64, p.749–752.

Luo, H., Shi, J., Wang, C., Cao, W., Sun, X., Dong, H. (2011). *Experimental and numerical analysis on formation of stable austenite during the intercritical annealing of 5Mn steel*. Acta Mater, Vols:59, p.4002–4014.

Lutterotti, L., and Scardi, P. (1990). *Simultaneous structure and size-strain refinement by the Rietveld method*. *Journal of Applied Crystallography* (23): 246-52.

Maffei, B., Salvatore, W., Valentini, R. (2007). *Dual-phase steel rebars for high-ductile r.c. structures, part 1: microstructural and mechanical characterization of steel rebars.* Eng Struct, Vols:29,3325–3332.

Maitrepierre, P.h., Rofes-Vernis, J., Thivellier, D. (1979). *Structure-properties relationships in boron steels*. Boron in Steel, p.1-18

Mallick, P.K. (2010). *Materials Design and Manufacturing for Lightweight Vehicles*. Woodhead Publishing Limited, p.50.

Matlock, D.K., Speer, J.G., De Moor, E., Gibbs, P.J. (2012). *Resent developments in advanced high strength sheet steels for automotive applications: an overview*. JESTECH, Vols:15(1), p.1–12.

Miracle, D.B. and Senkov, O.N. (2017). *A critical review of high entropy alloys and related concepts*. Acta Materialia, Vols:122, p.448-51.

Murty, B.S., Yeh, J.W., Ranganathan, S. (2014). *High-entropy Alloys*. Butterworth-Heinmann (Elsevier), London.

Nakada, N., Arakawa, Y., Park, K.S., Tsuchiyama, T., Takaki, S. (2012). *Dual phase structure formed by partial reversion of cold-deformed martensite*. Mater Sci Eng:A, Vols:553, p.128–133.

Oh, H.S., Ma, D., Leyson, G.P., Grabowski, B., Park, E.S. (2016). *Lattice Distortions in the FeCoNiCrMn High Entropy Alloy Studied by Theory and Experiment*. Entropy, 18, 9, 321, https://www.mdpi.com/1099-4300/18/9/321 , accessed on: 28.11.2018.

Park, K.T., Kim, G., Kim, S., Lee, S., Hwang, S., Lee, C. (2010). *On the transitions of deformation modes of fully austenitic steels at room temperature*. Met. Mater. Int., Vols:16, p.1.

Park, S. S., Jung G. Lee, Hak C. Lee and Nack J. Kim (2004). *Development of wrought Mg alloys via strip casting*. TMS, Magnesium Technology, 107–112.

Paschoal, J.O.A., Kleykamp, H., Thummler, H. (1983). *Phase equilibria in the quaternary molybdenum-ruthenium-rhodium-palladium system*. Z. Met. Vols:74, p.652.

Raabe, D., Herbig, M., Sandlobes, S., Li, Y., Tytko, D., Kuzmina, M., Ponge, D., Choi P.- P (2014). *Grain boundary segregation engineering in metallic alloys: a pathway to the design of interfaces*. Curr. Opin. Solid State Mater. Sci, Vols:18, p.253-261.

Raabe, D., Sandlöbes, S., Millán, J., Ponge, D., Assadi, H., Herbig, M., et al. (2013). *Segregation engineering enables nanoscale martensite to austenite phase transformation at grain boundaries: a pathway to ductile martensite*. Acta Mater, Vols:61, p.6123–6152.

Rana, R. (2014). *Low-density steels*. JOM, Vols:66, Issue 9, p.1730–1733.

Rana, R. and Singh, S.B. (2017). *Automotive Steels Design, Metallurgy, Processing and Applications*, Woodhead Publishing Series in Metals and Surface Engineering, Vols:317, p.326-330.

Randle, V. (2004). *Twinning-related grain boundary engineering*. Acta Mater, Vols:52, p.4067–4081.

Rollet, A.D., Gottstein, G., Shvindlerman, L.S., Molodov, D.A. (2004). *Grain boundary mobility – a brief review*. Z Metallkd, Vols:95, p.226–299.

Seah, M.P. (1980). *Adsorption-induced interface decohesion*. Acta Metall, Vols:28, p.955-962.

Seol, J.B., Bae, J.W., Li, Z., Chan Han, J., Kim, J.G., Raabe, D., Kim, H. S. (2018). *Boron doped ultrastrong and ductile high-entropy alloys*. Acta Materialia, Vols:151, p.366–376.

Shi, J., Sun, X., Wang, M., Hui, W., Dong, H., Cao, W. (2010). *Enhanced work-hardening behavior and mechanical properties in ultrafine-grained steels with large fractioned metastable austenite*. Scr Mater, Vols:63, p.815–818.

Shome, M. and Tumuluru, M. (2015). *Welding and Joining of Advanced High Strength Steels*. Woodhead Publishing, p.21.

Smith, W.F. and Hashemi, J. (2006). *Foundations of Materials Science and Engineering* (4th ed.). McGraw-Hill.

Sohn, S.S., Song, H., Suh, B.C., Kwa,k J.H., Lee, B.J., Kim, N.J., et al. (2015). *Novel ultra-high-strength (ferrite + austenite) duplex lightweight steels achieved by fine dislocation substructures (Taylor lattices), grain refinement, and partial recrystallization*. Acta Mater., Vols:96, p.301–310.

Sologub, O., Salamakha, L., Rogl, P., Stoger, B., Bauer, E., Bernardi, J., Giester, G., Waas, M., Svagera, R. (2015). *Pt-B system revisited: Pt2B, a new structure type of binary borides, ternary WAI12-type derivative borides*. Inorg. Chem. 54 (22), p.10958–10965.

Speer, J.G., De Moor, E., Findley, K.O., Matlock, D.K., De Cooman, B.C., Edmonds, D.V. (2011). *Analysis of microstructure evolution in quenching and partitioning automotive sheet steel*. Metallurgical and Materials Transactions A, Vols:42, p.3591–3601.

Speer, J.G., Matlock, D.K., De Cooman, B.C., Schroth, J.G. (2003). *Carbon partitioning into austenite after martensite transformation*. Acta Mater, Vols:51, p.2611–2622.

Springer, H., Belde, M., Raabe, D. (2013). *Bulk combinatorial design of ductile martensitic stainless steels through confined martensite-to-austenite reversio*n. Mater Sci Eng: A, Vols:582, p.235–244.

Thomas, G.A., Speer, J.G., Matlock, D.K. (2011). *Quenched and partitioned microstructures produced via Gleeble simulations of hot-strip mill cooling practices*. Metallurgical and Materials Transactions A, Vols:42, p.3652–3659.

Toji, Y., Miyamoto, G., Raabe, D. (2015). *Carbon partitioning during quenching and partitioning heat treatment accompanied by carbide precipitation*. Acta Mater., Vols:86, p.137–147.

Tomlin, I. A. and Kaloshkin, S. D. (2015). *High entropy alloys—semi-impossible regular solid solutions*. Mat. Sci. Technol., Vols:31, p.1231-1234.

Tong, C.J., Chen, Y.L., Chen, S.K., Yeh, J.W., Shun, T.T., Tsau, C.H., Lin, S.J., Chang, S.Y. (2005). *Microstructure characterization of AlxCoCrCuFeNi high-entropy alloy system with multiprincipal elements*. Metall Mater Trans A, Vols:36A, p.881–893.

Tsai, K.Y., Tsai, M.H., Yeh, J.W. (2013). *Sluggish diffusion in Co-Cr-Fe-Mn-Ni high-entropy alloys*. Acta Mater, Vols:61, p.4887–4898.

Tsai, M.H. and Yeh, J.W. (2014). *High-Entropy Alloys: A Critical Review*. Materials Research Letters, 2, 3, p.107-123.

Uzunsoy D (2010). *Investigation of dry sliding wear properties of boron doped powder metallurgy 316L stainless steel*. Mater Des, Vols:31(8), p.3896-3900.

Vercammen, S., Blanpain, B., De Cooman, B.C., Wollants, P. (2004). *Cold rolling behaviour of an austenitic Fe-30Mn-3Al-3Si TWIP-steel: the importance of deformation twinning*. Acta Mater, Vol:52, p.2005–2012.

Wang, M.M., Tasan, C.C., Ponge, D., Dippel, A.Ch., Raabe, D. (2015). *Nanolaminate transformation-induced plasticity–twinning-induced plasticity steel with dynamic strain partitioning and enhanced damage resistance*. Acta Mater, Vols:85, p.216–228.

Wang, Z. and Baker, I. (2016). *Interstitial strengthening of a f.c.c. FeNiMnAlCr high entropy alloy*. Materials Letters, 180, p.153–156.

Watanabe, T. and Tsurekawa, S. (1999). *The control of brittleness and development of desirable mechanical properties in polycrystalline systems by grain boundary engineering*. Acta Mater, Vols:47, p.4171–4185.

Welsch, E., Ponge, D., Haghighat, S.M.H., Sandlöbes, S., Choi, P. (2016). *Strain Hardening by Dynamic Slip Band Refinement in a High Mn Lightweight Steel*. Acta Mater., Vols:116.

WordAutoSteel; June 2009, *Advanced high strength steel (AHSS) application guidelines* (version 4.1).

Wu R, Freeman AJ, Olson GB (1994), *First principles determination of the effects of phosphorus and boron on iron grain boundary cohesion*, Science15, p.376-380.

Wu, Z., Troparevsky, M.C., Gao, Y.F., Morris, J.R., Stocks, G.M., et al. (2017). *Phase Stability, Physical Properties and Strengthening Mechanisms of Concentrated Solid-Solution Alloys*. Current Opinion in Solid State and Materials Science, Vols:21.

Yang, X. and Zhang, Y. (2012). *Prediction of high-entropy stabilized solid-solution in multicomponent alloys*. Mater Chem Phys, Vols:132(2–3), p.233–238.

Yeh, J.W. (2006), *Recent Progress in High Entropy Alloys*. Ann. Chim. Sci. Mat.Vols:31, p.633-648.

Yeh, J.W., Chen, S.K., Gan, J.Y., Lin, S.J., Chin, T.S., Shun, T.T., Tsau, C.H., Chang, S.Y. (2004). *Nanostructured high-entropy alloys with multiple principal elements: novel alloy design concepts and outcomes*. Adv Eng Mater, Vols:6, p.299–303.

Yeh, J.W., Chen, S.K., Gan, J.Y., Lin, S.J., Chin, T.S., Shun, T.T., Tsau, C.H., Chang, S.Y. (2004-b). *Formation of simple crystal structures in solid-solution alloys with multi-principal metallic elements*. Metall Mater Trans A, Vols:35A, p.2533–2536.

Yen, H.W., Huang, M., Scott, C.P., Yang, J.R. (2012). *Interactions between deformation-induced defects and carbides in a vanadium-containing TWIP steel*. Scripta Materialia, Vols:66, p.1018–1023.

Yoo, J. and Park, K.T. (2008). *Microband-induced plasticity in high Mn-Al-C light steel*. Mater. Sci. and Eng., Vols: A496, p.417.

Zhang, J., Ding, H., Wang, C., Zhao, J., Ding, T. (2013). *Work hardening behaviors of a low carbon Nb-microalloyed Si-Mn quenching-partitioning steel with different cooling styles after partitioning*. Mater Sci Eng:A, Vols:585, p.132–138.

Zhang, Y., Lu, Z.P., Ma, S.G., Liaw, P.K., Tang, Z., Cheng, Y.Q., Gao, M.C. (2014). *Guidelines in predicting phase formation of high-entropy alloys*. MRS Commun, Vols:4, p.57–62.

Zhang, Y., Zhou, Y.J., Lin, J.P., Chen, G.L., Liaw, P.K. (2008). *Solid-solution phase formation rules for multi-component alloys*. Adv Eng Mater, Vols:10, Issue:6, p.534–538.

Zhao, J. and Jiang, Z. (2018). *Thermomechanical processing of advanced high strength steels*. Progress in Materials Science, Vols:94, p.174–242.

Zhao, J., Jiang. Z., Lee, C.S. (2014). *Functions of tungsten alloying in microalloyed stee*ls. Nova Science Publishers.

Appendix 1

Thermodynamic calculations for all possible combinations of $Fe_qMn_yAl_zNi_w$ (5≤q,y,z,w≤50) medium entropy alloys by 5% incerments.

No	(at %)				Thermodynamic Parameters								
	Fe	Mn	Al	Ni	ΔG_{mix} (KJ/mol)	ΔS_{conf}	ΔS_{mix} (J/K.mol)	ΔH_{mix} (KJ/mol)	δ%	T_m (˚C)	Ω	VEC	Density (g/cm³)
1	5	5	40	50	-30.305	1.013	8.237	-21	6.784	1129.65	0.443	6.95	6.303
2	5	5	45	45	-30.448	1.018	8.282	-21.42	6.806	1090	0.421	6.6	5.994
3	5	5	50	40	-30.052	1.013	8.237	-21.4	6.757	1050.35	0.404	6.25	5.684
4	5	10	35	50	-30.943	1.094	8.899	-20.63	6.567	1158.9	0.500	7.15	6.540
5	5	10	40	45	-31.448	1.106	8.995	-21.38	6.626	1119.25	0.471	6.8	6.230
6	5	10	45	40	-31.401	1.106	8.995	-21.69	6.610	1079.6	0.448	6.45	5.920
7	5	10	50	35	-30.815	1.094	8.899	-21.56	6.521	1039.95	0.429	6.1	5.610
8	5	15	30	50	-30.918	1.142	9.290	-19.88	6.325	1188.15	0.555	7.35	6.776
9	5	15	35	45	-31.807	1.161	9.445	-20.96	6.424	1148.5	0.518	7	6.466
10	5	15	40	40	-32.129	1.167	9.496	-21.6	6.443	1108.85	0.487	6.65	6.157
11	5	15	45	35	-31.898	1.161	9.445	-21.8	6.387	1069.2	0.463	6.3	5.847
12	5	15	50	30	-31.125	1.142	9.290	-21.56	6.257	1029.55	0.444	5.95	5.537
13	5	20	25	50	-30.284	1.165	9.475	-18.75	6.053	1217.4	0.615	7.55	7.013
14	5	20	30	45	-31.581	1.192	9.697	-20.16	6.196	1177.75	0.567	7.2	6.703
15	5	20	35	40	-32.291	1.206	9.807	-21.13	6.255	1138.1	0.528	6.85	6.393
16	5	20	40	35	-32.432	1.206	9.807	-21.66	6.234	1098.45	0.497	6.5	6.083
17	5	20	45	30	-32.018	1.192	9.697	-21.75	6.136	1058.8	0.472	6.15	5.773
18	5	20	50	25	-31.056	1.165	9.475	-21.4	5.961	1019.15	0.451	5.8	5.464

19	5	25	20	50	-29.052	1.165	9.475	-17.24	5.748	1246.65	0.685	7.75	7.249
20	5	25	25	45	-30.783	1.202	9.779	-18.98	5.941	1207	0.622	7.4	6.939
21	5	25	30	40	-31.903	1.224	9.957	-20.28	6.042	1167.35	0.573	7.05	6.629
22	5	25	35	35	-32.434	1.231	10.015	-21.14	6.059	1127.7	0.534	6.7	6.320
23	5	25	40	30	-32.393	1.224	9.957	-21.56	5.995	1088.05	0.502	6.35	6.010
24	5	25	45	25	-31.793	1.202	9.779	-21.54	5.853	1048.4	0.476	6	5.700
25	5	25	50	20	-30.638	1.165	9.475	-21.08	5.629	1008.75	0.453	5.65	5.390
26	5	30	15	50	-27.203	1.142	9.290	-15.35	5.404	1275.9	0.772	7.95	7.485
27	5	30	20	45	-29.408	1.192	9.697	-17.42	5.654	1236.25	0.688	7.6	7.176
28	5	30	25	40	-30.964	1.224	9.957	-19.05	5.802	1196.6	0.625	7.25	6.866
29	5	30	30	35	-31.905	1.240	10.083	-20.24	5.860	1156.95	0.576	6.9	6.556
30	5	30	35	30	-32.256	1.240	10.083	-20.99	5.833	1117.3	0.537	6.55	6.246
31	5	30	40	25	-32.030	1.224	9.957	-21.3	5.725	1077.65	0.504	6.2	5.936
32	5	30	45	20	-31.236	1.192	9.697	-21.17	5.534	1038	0.475	5.85	5.627
33	5	30	50	15	-29.875	1.142	9.290	-20.6	5.254	998.35	0.450	5.5	5.317
34	5	35	10	50	-24.695	1.094	8.899	-13.08	5.011	1305.15	0.888	8.15	7.722
35	5	35	15	45	-27.432	1.161	9.445	-15.48	5.329	1265.5	0.772	7.8	7.412
36	5	35	20	40	-29.461	1.206	9.807	-17.44	5.531	1225.85	0.689	7.45	7.102
37	5	35	25	35	-30.840	1.231	10.015	-18.96	5.635	1186.2	0.627	7.1	6.792
38	5	35	30	30	-31.601	1.240	10.083	-20.04	5.648	1146.55	0.577	6.75	6.483
39	5	35	35	25	-31.765	1.231	10.015	-20.68	5.576	1106.9	0.536	6.4	6.173
40	5	35	40	20	-31.346	1.206	9.807	-20.88	5.419	1067.25	0.501	6.05	5.863
41	5	35	45	15	-30.345	1.161	9.445	-20.64	5.172	1027.6	0.470	5.7	5.553
42	5	35	50	10	-28.752	1.094	8.899	-19.96	4.826	987.95	0.440	5.35	5.243
43	5	40	5	50	-21.421	1.013	8.237	-10.43	4.557	1334.4	1.054	8.35	7.958
44	5	40	10	45	-24.807	1.106	8.995	-13.16	4.958	1294.75	0.885	8	7.648
45	5	40	15	40	-27.368	1.167	9.496	-15.45	5.224	1255.1	0.771	7.65	7.339

46	5	40	20	35	-29.219	1.206	9.807	-17.3	5.379	1215.45	0.689	7.3	7.029
47	5	40	25	30	-30.417	1.224	9.957	-18.71	5.437	1175.8	0.626	6.95	6.719
48	5	40	30	25	-30.992	1.224	9.957	-19.68	5.404	1136.15	0.575	6.6	6.409
49	5	40	35	20	-30.963	1.206	9.807	-20.21	5.283	1096.5	0.532	6.25	6.099
50	5	40	40	15	-30.335	1.167	9.496	-20.3	5.071	1056.85	0.494	5.9	5.790
51	5	40	45	10	-29.100	1.106	8.995	-19.95	4.760	1017.2	0.459	5.55	5.480
52	5	40	50	5	-27.212	1.013	8.237	-19.16	4.332	977.55	0.420	5.2	5.170
53	5	45	5	45	-21.426	1.018	8.282	-10.46	4.531	1324	1.048	8.2	7.885
54	5	45	10	40	-24.633	1.106	8.995	-13.08	4.874	1284.35	0.883	7.85	7.575
55	5	45	15	35	-27.016	1.161	9.445	-15.26	5.089	1244.7	0.770	7.5	7.265
56	5	45	20	30	-28.686	1.192	9.697	-17	5.196	1205.05	0.687	7.15	6.955
57	5	45	25	25	-29.697	1.202	9.779	-18.3	5.206	1165.4	0.623	6.8	6.646
58	5	45	30	20	-30.077	1.192	9.697	-19.16	5.123	1125.75	0.570	6.45	6.336
59	5	45	35	15	-29.838	1.161	9.445	-19.58	4.947	1086.1	0.524	6.1	6.026
60	5	45	40	10	-28.973	1.106	8.995	-19.56	4.672	1046.45	0.481	5.75	5.716
61	5	45	45	5	-27.439	1.018	8.282	-19.1	4.281	1006.8	0.437	5.4	5.406
62	5	50	5	40	-21.150	1.013	8.237	-10.33	4.469	1313.6	1.047	8.05	7.811
63	5	50	10	35	-24.177	1.094	8.899	-12.84	4.756	1273.95	0.883	7.7	7.502
64	5	50	15	30	-26.377	1.142	9.290	-14.91	4.920	1234.3	0.769	7.35	7.192
65	5	50	20	25	-27.859	1.165	9.475	-16.54	4.978	1194.65	0.684	7	6.882
66	5	50	25	20	-28.673	1.165	9.475	-17.73	4.937	1155	0.617	6.65	6.572
67	5	50	30	15	-28.842	1.142	9.290	-18.48	4.800	1115.35	0.561	6.3	6.262
68	5	50	35	10	-28.363	1.094	8.899	-18.79	4.561	1075.7	0.509	5.95	5.953
69	5	50	40	5	-27.194	1.013	8.237	-18.66	4.208	1036.05	0.457	5.6	5.643
70	10	5	35	50	-29.913	1.094	8.899	-19.47	6.703	1173.55	0.536	7.2	6.560
71	10	5	40	45	-30.400	1.106	8.995	-20.2	6.802	1133.9	0.505	6.85	6.250
72	10	5	45	40	-30.333	1.106	8.995	-20.49	6.826	1094.25	0.480	6.5	5.941

73	10	5	50	35	-29.725	1.094	8.899	-20.34	6.778	1054.6	0.461	6.15	5.631
74	10	10	30	50	-30.230	1.168	9.503	-18.8	6.445	1202.8	0.608	7.4	6.797
75	10	10	35	45	-31.093	1.187	9.657	-19.86	6.585	1163.15	0.566	7.05	6.487
76	10	10	40	40	-31.387	1.194	9.708	-20.48	6.646	1123.5	0.533	6.7	6.177
77	10	10	45	35	-31.127	1.187	9.657	-20.66	6.631	1083.85	0.507	6.35	5.867
78	10	10	50	30	-30.323	1.168	9.503	-20.4	6.545	1044.2	0.486	6	5.557
79	10	15	25	50	-29.856	1.208	9.826	-17.75	6.156	1232.05	0.682	7.6	7.033
80	10	15	30	45	-31.122	1.235	10.048	-19.14	6.343	1192.4	0.626	7.25	6.723
81	10	15	35	40	-31.799	1.249	10.158	-20.09	6.443	1152.75	0.583	6.9	6.413
82	10	15	40	35	-31.906	1.249	10.158	-20.6	6.464	1113.1	0.549	6.55	6.104
83	10	15	45	30	-31.456	1.235	10.048	-20.67	6.410	1073.45	0.522	6.2	5.794
84	10	15	50	25	-30.458	1.208	9.826	-20.3	6.283	1033.8	0.500	5.85	5.484
85	10	20	20	50	-28.843	1.221	9.928	-16.32	5.832	1261.3	0.767	7.8	7.269
86	10	20	25	45	-30.541	1.258	10.233	-18.04	6.071	1221.65	0.693	7.45	6.960
87	10	20	30	40	-31.625	1.280	10.410	-19.32	6.216	1182	0.637	7.1	6.650
88	10	20	35	35	-32.119	1.287	10.469	-20.16	6.276	1142.35	0.593	6.75	6.340
89	10	20	40	30	-32.039	1.280	10.410	-20.56	6.257	1102.7	0.558	6.4	6.030
90	10	20	45	25	-31.398	1.258	10.233	-20.52	6.161	1063.05	0.530	6.05	5.720
91	10	20	50	20	-30.201	1.221	9.928	-20.04	5.989	1023.4	0.507	5.7	5.411
92	10	25	15	50	-27.191	1.208	9.826	-14.51	5.466	1290.55	0.874	8	7.506
93	10	25	20	45	-29.360	1.258	10.233	-16.56	5.766	1250.9	0.773	7.65	7.196
94	10	25	25	40	-30.879	1.290	10.492	-18.17	5.960	1211.25	0.699	7.3	6.886
95	10	25	30	35	-31.781	1.305	10.619	-19.34	6.063	1171.6	0.643	6.95	6.576
96	10	25	35	30	-32.090	1.305	10.619	-20.07	6.081	1131.95	0.599	6.6	6.267
97	10	25	40	25	-31.821	1.290	10.492	-20.36	6.020	1092.3	0.563	6.25	5.957
98	10	25	45	20	-30.982	1.258	10.233	-20.21	5.880	1052.65	0.533	5.9	5.647
99	10	25	50	15	-29.573	1.208	9.826	-19.62	5.659	1013	0.507	5.55	5.337

100	10	30	10	50	-24.862	1.168	9.503	-12.32	5.049	1319.8	1.018	8.2	7.742
101	10	30	15	45	-27.563	1.235	10.048	-14.7	5.422	1280.15	0.875	7.85	7.432
102	10	30	20	40	-29.554	1.280	10.410	-16.64	5.673	1240.5	0.776	7.5	7.123
103	10	30	25	35	-30.891	1.305	10.619	-18.14	5.823	1200.85	0.703	7.15	6.813
104	10	30	30	30	-31.609	1.314	10.687	-19.2	5.882	1161.2	0.646	6.8	6.503
105	10	30	35	25	-31.729	1.305	10.619	-19.82	5.858	1121.55	0.601	6.45	6.193
106	10	30	40	20	-31.263	1.280	10.410	-20	5.752	1081.9	0.563	6.1	5.883
107	10	30	45	15	-30.213	1.235	10.048	-19.74	5.563	1042.25	0.531	5.75	5.574
108	10	30	50	10	-28.568	1.168	9.503	-19.04	5.287	1002.6	0.500	5.4	5.264
109	10	35	5	50	-21.755	1.094	8.899	-9.75	4.565	1349.05	1.231	8.4	7.979
110	10	35	10	45	-25.105	1.187	9.657	-12.46	5.029	1309.4	1.015	8.05	7.669
111	10	35	15	40	-27.628	1.249	10.158	-14.73	5.348	1269.75	0.876	7.7	7.359
112	10	35	20	35	-29.437	1.287	10.469	-16.56	5.552	1230.1	0.778	7.35	7.049
113	10	35	25	30	-30.591	1.305	10.619	-17.95	5.657	1190.45	0.704	7	6.739
114	10	35	30	25	-31.120	1.305	10.619	-18.9	5.673	1150.8	0.647	6.65	6.430
115	10	35	35	20	-31.042	1.287	10.469	-19.41	5.603	1111.15	0.599	6.3	6.120
116	10	35	40	15	-30.364	1.249	10.158	-19.48	5.448	1071.5	0.559	5.95	5.810
117	10	35	45	10	-29.075	1.187	9.657	-19.11	5.205	1031.85	0.521	5.6	5.500
118	10	35	50	5	-27.130	1.094	8.899	-18.3	4.863	992.2	0.482	5.25	5.190
119	10	40	5	45	-21.882	1.106	8.995	-9.84	4.576	1338.65	1.224	8.25	7.905
120	10	40	10	40	-25.051	1.194	9.708	-12.44	4.978	1299	1.014	7.9	7.595
121	10	40	15	35	-27.392	1.249	10.158	-14.6	5.245	1259.35	0.876	7.55	7.286
122	10	40	20	30	-29.017	1.280	10.410	-16.32	5.402	1219.7	0.778	7.2	6.976
123	10	40	25	25	-29.981	1.290	10.492	-17.6	5.461	1180.05	0.703	6.85	6.666
124	10	40	30	20	-30.312	1.280	10.410	-18.44	5.430	1140.4	0.644	6.5	6.356
125	10	40	35	15	-30.021	1.249	10.158	-18.84	5.312	1100.75	0.593	6.15	6.046
126	10	40	40	10	-29.102	1.194	9.708	-18.8	5.103	1061.1	0.548	5.8	5.737

127	10	40	45	5	-27.508	1.106	8.995	-18.32	4.796	1021.45	0.502	5.45	5.427
128	10	45	5	40	-21.718	1.106	8.995	-9.77	4.551	1328.25	1.223	8.1	7.832
129	10	45	10	35	-24.704	1.187	9.657	-12.26	4.895	1288.6	1.015	7.75	7.522
130	10	45	15	30	-26.860	1.235	10.048	-14.31	5.111	1248.95	0.877	7.4	7.212
131	10	45	20	25	-28.295	1.258	10.233	-15.92	5.220	1209.3	0.777	7.05	6.902
132	10	45	25	20	-29.059	1.258	10.233	-17.09	5.232	1169.65	0.700	6.7	6.593
133	10	45	30	15	-29.175	1.235	10.048	-17.82	5.152	1130	0.637	6.35	6.283
134	10	45	35	10	-28.640	1.187	9.657	-18.11	4.979	1090.35	0.581	6	5.973
135	10	45	40	5	-27.411	1.106	8.995	-17.96	4.708	1050.7	0.526	5.65	5.663
136	10	50	5	35	-21.268	1.094	8.899	-9.54	4.491	1317.85	1.229	7.95	7.758
137	10	50	10	30	-24.066	1.168	9.503	-11.92	4.779	1278.2	1.019	7.6	7.449
138	10	50	15	25	-26.030	1.208	9.826	-13.86	4.945	1238.55	0.878	7.25	7.139
139	10	50	20	20	-27.263	1.221	9.928	-15.36	5.005	1198.9	0.775	6.9	6.829
140	10	50	25	15	-27.810	1.208	9.826	-16.42	4.966	1159.25	0.694	6.55	6.519
141	10	50	30	10	-27.679	1.168	9.503	-17.04	4.832	1119.6	0.624	6.2	6.209
142	10	50	35	5	-26.831	1.094	8.899	-17.22	4.597	1079.95	0.558	5.85	5.900
143	15	5	30	50	-29.030	1.142	9.290	-17.72	6.538	1217.45	0.638	7.45	6.817
144	15	5	35	45	-29.884	1.161	9.445	-18.76	6.720	1177.8	0.593	7.1	6.507
145	15	5	40	40	-30.167	1.167	9.496	-19.36	6.821	1138.15	0.558	6.75	6.198
146	15	5	45	35	-29.895	1.161	9.445	-19.52	6.846	1098.5	0.531	6.4	5.888
147	15	5	50	30	-29.077	1.142	9.290	-19.24	6.800	1058.85	0.511	6.05	5.578
148	15	10	25	50	-29.000	1.208	9.826	-16.75	6.230	1246.7	0.731	7.65	7.054
149	15	10	30	45	-30.249	1.235	10.048	-18.12	6.461	1207.05	0.669	7.3	6.744
150	15	10	35	40	-30.908	1.249	10.158	-19.05	6.603	1167.4	0.622	6.95	6.434
151	15	10	40	35	-30.995	1.249	10.158	-19.54	6.665	1127.75	0.586	6.6	6.124
152	15	10	45	30	-30.524	1.235	10.048	-19.59	6.653	1088.1	0.558	6.25	5.814
153	15	10	50	25	-29.502	1.208	9.826	-19.2	6.568	1048.45	0.537	5.9	5.505

154	15	15	20	50	-28.244	1.238	10.067	-15.4	5.885	1275.95	0.834	7.85	7.290
155	15	15	25	45	-29.922	1.275	10.371	-17.1	6.172	1236.3	0.750	7.5	6.980
156	15	15	30	40	-30.983	1.297	10.549	-18.36	6.361	1196.65	0.688	7.15	6.670
157	15	15	35	35	-31.452	1.304	10.607	-19.18	6.463	1157	0.640	6.8	6.361
158	15	15	40	30	-31.346	1.297	10.549	-19.56	6.485	1117.35	0.603	6.45	6.051
159	15	15	45	25	-30.677	1.275	10.371	-19.5	6.433	1077.7	0.573	6.1	5.741
160	15	15	50	20	-29.450	1.238	10.067	-19	6.308	1038.05	0.550	5.75	5.431
161	15	20	15	50	-26.809	1.238	10.067	-13.67	5.496	1305.2	0.961	8.05	7.526
162	15	20	20	45	-28.955	1.288	10.474	-15.7	5.848	1265.55	0.844	7.7	7.217
163	15	20	25	40	-30.448	1.320	10.733	-17.29	6.089	1225.9	0.761	7.35	6.907
164	15	20	30	35	-31.322	1.335	10.860	-18.44	6.235	1186.25	0.699	7	6.597
165	15	20	35	30	-31.602	1.335	10.860	-19.15	6.296	1146.6	0.650	6.65	6.287
166	15	20	40	25	-31.301	1.320	10.733	-19.42	6.279	1106.95	0.612	6.3	5.977
167	15	20	45	20	-30.429	1.288	10.474	-19.25	6.186	1067.3	0.581	5.95	5.668
168	15	20	50	15	-28.985	1.238	10.067	-18.64	6.016	1027.65	0.555	5.6	5.358
169	15	25	10	50	-24.672	1.208	9.826	-11.56	5.051	1334.45	1.134	8.25	7.763
170	15	25	15	45	-27.349	1.275	10.371	-13.92	5.482	1294.8	0.965	7.9	7.453
171	15	25	20	40	-29.312	1.320	10.733	-15.84	5.784	1255.15	0.850	7.55	7.143
172	15	25	25	35	-30.619	1.345	10.941	-17.32	5.980	1215.5	0.768	7.2	6.833
173	15	25	30	30	-31.306	1.354	11.010	-18.36	6.083	1175.85	0.705	6.85	6.524
174	15	25	35	25	-31.392	1.345	10.941	-18.96	6.104	1136.2	0.656	6.5	6.214
175	15	25	40	20	-30.889	1.320	10.733	-19.12	6.045	1096.55	0.616	6.15	5.904
176	15	25	45	15	-29.801	1.275	10.371	-18.84	5.907	1056.9	0.582	5.8	5.594
177	15	25	50	10	-28.115	1.208	9.826	-18.12	5.689	1017.25	0.552	5.45	5.284
178	15	30	5	50	-21.739	1.142	9.290	-9.07	4.534	1363.7	1.397	8.45	7.999
179	15	30	10	45	-25.064	1.235	10.048	-11.76	5.065	1324.05	1.131	8.1	7.689
180	15	30	15	40	-27.559	1.297	10.549	-14.01	5.439	1284.4	0.967	7.75	7.380

181	15	30	20	35	-29.337	1.335	10.860	-15.82	5.692	1244.75	0.854	7.4	7.070
182	15	30	25	30	-30.458	1.354	11.010	-17.19	5.843	1205.1	0.772	7.05	6.760
183	15	30	30	25	-30.951	1.354	11.010	-18.12	5.905	1165.45	0.708	6.7	6.450
184	15	30	35	20	-30.836	1.335	10.860	-18.61	5.882	1125.8	0.657	6.35	6.140
185	15	30	40	15	-30.117	1.297	10.549	-18.66	5.779	1086.15	0.614	6	5.831
186	15	30	45	10	-28.786	1.235	10.048	-18.27	5.593	1046.5	0.576	5.65	5.521
187	15	30	50	5	-26.794	1.142	9.290	-17.44	5.319	1006.85	0.536	5.3	5.211
188	15	35	5	45	-22.001	1.161	9.445	-9.22	4.582	1353.3	1.386	8.3	7.926
189	15	35	10	40	-25.144	1.249	10.158	-11.8	5.047	1313.65	1.131	7.95	7.616
190	15	35	15	35	-27.453	1.304	10.607	-13.94	5.367	1274	0.969	7.6	7.306
191	15	35	20	30	-29.045	1.335	10.860	-15.64	5.573	1234.35	0.857	7.25	6.996
192	15	35	25	25	-29.972	1.345	10.941	-16.9	5.679	1194.7	0.773	6.9	6.687
193	15	35	30	20	-30.263	1.335	10.860	-17.72	5.697	1155.05	0.708	6.55	6.377
194	15	35	35	15	-29.931	1.304	10.607	-18.1	5.629	1115.4	0.654	6.2	6.067
195	15	35	40	10	-28.967	1.249	10.158	-18.04	5.477	1075.75	0.606	5.85	5.757
196	15	35	45	5	-27.326	1.161	9.445	-17.54	5.237	1036.1	0.558	5.5	5.447
197	15	40	5	40	-21.962	1.167	9.496	-9.21	4.594	1342.9	1.385	8.15	7.852
198	15	40	10	35	-24.918	1.249	10.158	-11.68	4.997	1303.25	1.133	7.8	7.543
199	15	40	15	30	-27.039	1.297	10.549	-13.71	5.266	1263.6	0.972	7.45	7.233
200	15	40	20	25	-28.437	1.320	10.733	-15.3	5.424	1223.95	0.859	7.1	6.923
201	15	40	25	20	-29.161	1.320	10.733	-16.45	5.485	1184.3	0.773	6.75	6.613
202	15	40	30	15	-29.234	1.297	10.549	-17.16	5.457	1144.65	0.704	6.4	6.303
203	15	40	35	10	-28.654	1.249	10.158	-17.43	5.341	1105	0.644	6.05	5.994
204	15	40	40	5	-27.376	1.167	9.496	-17.26	5.135	1065.35	0.586	5.7	5.684
205	15	45	5	35	-21.625	1.161	9.445	-9.04	4.570	1332.5	1.392	8	7.779
206	15	45	10	30	-24.391	1.235	10.048	-11.4	4.916	1292.85	1.140	7.65	7.469
207	15	45	15	25	-26.317	1.275	10.371	-13.32	5.134	1253.2	0.976	7.3	7.159

208	15	45	20	20	-27.511	1.288	10.474	-14.8	5.244	1213.55	0.859	6.95	6.850
209	15	45	25	15	-28.015	1.275	10.371	-15.84	5.259	1173.9	0.769	6.6	6.540
210	15	45	30	10	-27.837	1.235	10.048	-16.44	5.181	1134.25	0.693	6.25	6.230
211	15	45	35	5	-26.938	1.161	9.445	-16.6	5.011	1094.6	0.623	5.9	5.920
212	15	50	5	30	-20.992	1.142	9.290	-8.71	4.512	1322.1	1.410	7.85	7.706
213	15	50	10	25	-23.561	1.208	9.826	-10.96	4.802	1282.45	1.150	7.5	7.396
214	15	50	15	20	-25.281	1.238	10.067	-12.77	4.969	1242.8	0.980	7.15	7.086
215	15	50	20	15	-26.252	1.238	10.067	-14.14	5.031	1203.15	0.857	6.8	6.776
216	15	50	25	10	-26.502	1.208	9.826	-15.07	4.995	1163.5	0.759	6.45	6.466
217	15	50	30	5	-26.001	1.142	9.290	-15.56	4.864	1123.85	0.671	6.1	6.157
218	20	5	25	50	-27.701	1.165	9.475	-15.75	6.277	1261.35	0.759	7.7	7.074
219	20	5	30	45	-28.947	1.192	9.697	-17.1	6.553	1221.7	0.693	7.35	6.764
220	20	5	35	40	-29.602	1.206	9.807	-18.01	6.737	1182.05	0.644	7	6.454
221	20	5	40	35	-29.683	1.206	9.807	-18.48	6.839	1142.4	0.606	6.65	6.145
222	20	5	45	30	-29.204	1.192	9.697	-18.51	6.866	1102.75	0.578	6.3	5.835
223	20	5	50	25	-28.173	1.165	9.475	-18.1	6.822	1063.1	0.556	5.95	5.525
224	20	10	20	50	-27.294	1.221	9.928	-14.48	5.909	1290.6	0.885	7.9	7.310
225	20	10	25	45	-28.961	1.258	10.233	-16.16	6.245	1250.95	0.792	7.55	7.001
226	20	10	30	40	-30.010	1.280	10.410	-17.4	6.478	1211.3	0.725	7.2	6.691
227	20	10	35	35	-30.466	1.287	10.469	-18.2	6.621	1171.65	0.674	6.85	6.381
228	20	10	40	30	-30.344	1.280	10.410	-18.56	6.685	1132	0.635	6.5	6.071
229	20	10	45	25	-29.658	1.258	10.233	-18.48	6.674	1092.35	0.605	6.15	5.761
230	20	10	50	20	-28.412	1.221	9.928	-17.96	6.591	1052.7	0.582	5.8	5.452
231	20	15	15	50	-26.116	1.238	10.067	-12.83	5.494	1319.85	1.036	8.1	7.547
232	20	15	20	45	-28.249	1.288	10.474	-14.84	5.900	1280.2	0.904	7.75	7.237
233	20	15	25	40	-29.725	1.320	10.733	-16.41	6.189	1240.55	0.811	7.4	6.927
234	20	15	30	35	-30.581	1.335	10.860	-17.54	6.378	1200.9	0.744	7.05	6.617

235	20	15	35	30	-30.841	1.335	10.860	-18.23	6.482	1161.25	0.692	6.7	6.308
236	20	15	40	25	-30.518	1.320	10.733	-18.48	6.506	1121.6	0.651	6.35	5.998
237	20	15	45	20	-29.622	1.288	10.474	-18.29	6.456	1081.95	0.620	6	5.688
238	20	15	50	15	-28.152	1.238	10.067	-17.66	6.333	1042.3	0.594	5.65	5.378
239	20	20	10	50	-24.194	1.221	9.928	-10.8	5.018	1349.1	1.240	8.3	7.783
240	20	20	15	45	-26.855	1.288	10.474	-13.14	5.511	1309.45	1.044	7.95	7.473
241	20	20	20	40	-28.799	1.332	10.836	-15.04	5.864	1269.8	0.915	7.6	7.164
242	20	20	25	35	-30.086	1.358	11.044	-16.5	6.106	1230.15	0.823	7.25	6.854
243	20	20	30	30	-30.749	1.366	11.112	-17.52	6.254	1190.5	0.755	6.9	6.544
244	20	20	35	25	-30.810	1.358	11.044	-18.1	6.317	1150.85	0.702	6.55	6.234
245	20	20	40	20	-30.281	1.332	10.836	-18.24	6.302	1111.2	0.660	6.2	5.924
246	20	20	45	15	-29.163	1.288	10.474	-17.94	6.210	1071.55	0.626	5.85	5.615
247	20	20	50	10	-27.445	1.221	9.928	-17.2	6.043	1031.9	0.596	5.5	5.305
248	20	25	5	50	-21.449	1.165	9.475	-8.39	4.461	1378.35	1.557	8.5	8.020
249	20	25	10	45	-24.759	1.258	10.233	-11.06	5.066	1338.7	1.239	8.15	7.710
250	20	25	15	40	-27.233	1.320	10.733	-13.29	5.498	1299.05	1.049	7.8	7.400
251	20	25	20	35	-28.989	1.358	11.044	-15.08	5.801	1259.4	0.922	7.45	7.090
252	20	25	25	30	-30.084	1.376	11.194	-16.43	5.998	1219.75	0.831	7.1	6.780
253	20	25	30	25	-30.550	1.376	11.194	-17.34	6.104	1180.1	0.762	6.75	6.471
254	20	25	35	20	-30.405	1.358	11.044	-17.81	6.126	1140.45	0.707	6.4	6.161
255	20	25	40	15	-29.655	1.320	10.733	-17.84	6.069	1100.8	0.662	6.05	5.851
256	20	25	45	10	-28.289	1.258	10.233	-17.43	5.934	1061.15	0.623	5.7	5.541
257	20	25	50	5	-26.258	1.165	9.475	-16.58	5.718	1021.5	0.584	5.35	5.231
258	20	30	5	45	-21.865	1.192	9.697	-8.6	4.549	1367.95	1.542	8.35	7.946
259	20	30	10	40	-24.988	1.280	10.410	-11.16	5.081	1328.3	1.239	8	7.636
260	20	30	15	35	-27.274	1.335	10.860	-13.28	5.457	1288.65	1.054	7.65	7.327
261	20	30	20	30	-28.839	1.366	11.112	-14.96	5.711	1249	0.928	7.3	7.017

262	20	30	25	25	-29.738	1.376	11.194	-16.2	5.864	1209.35	0.836	6.95	6.707
263	20	30	30	20	-29.998	1.366	11.112	-17	5.927	1169.7	0.765	6.6	6.397
264	20	30	35	15	-29.632	1.335	10.860	-17.36	5.906	1130.05	0.707	6.25	6.087
265	20	30	40	10	-28.631	1.280	10.410	-17.28	5.805	1090.4	0.657	5.9	5.778
266	20	30	45	5	-26.949	1.192	9.697	-16.76	5.622	1050.75	0.608	5.55	5.468
267	20	35	5	40	-21.963	1.206	9.807	-8.65	4.598	1357.55	1.539	8.2	7.873
268	20	35	10	35	-24.897	1.287	10.469	-11.1	5.064	1317.9	1.243	7.85	7.563
269	20	35	15	30	-26.991	1.335	10.860	-13.11	5.386	1278.25	1.059	7.5	7.253
270	20	35	20	25	-28.359	1.358	11.044	-14.68	5.593	1238.6	0.932	7.15	6.943
271	20	35	25	20	-29.051	1.358	11.044	-15.81	5.701	1198.95	0.838	6.8	6.634
272	20	35	30	15	-29.090	1.335	10.860	-16.5	5.721	1159.3	0.763	6.45	6.324
273	20	35	35	10	-28.471	1.287	10.469	-16.75	5.655	1119.65	0.700	6.1	6.014
274	20	35	40	5	-27.151	1.206	9.807	-16.56	5.506	1080	0.640	5.75	5.704
275	20	40	5	35	-21.751	1.206	9.807	-8.54	4.611	1347.15	1.547	8.05	7.799
276	20	40	10	30	-24.492	1.280	10.410	-10.88	5.016	1307.5	1.251	7.7	7.490
277	20	40	15	25	-26.388	1.320	10.733	-12.78	5.286	1267.85	1.065	7.35	7.180
278	20	40	20	20	-27.549	1.332	10.836	-14.24	5.446	1228.2	0.935	7	6.870
279	20	40	25	15	-28.017	1.320	10.733	-15.26	5.509	1188.55	0.836	6.65	6.560
280	20	40	30	10	-27.800	1.280	10.410	-15.84	5.483	1148.9	0.755	6.3	6.250
281	20	40	35	5	-26.858	1.206	9.807	-15.98	5.369	1109.25	0.681	5.95	5.941
282	20	45	5	30	-21.233	1.192	9.697	-8.27	4.590	1336.75	1.567	7.9	7.726
283	20	45	10	25	-23.773	1.258	10.233	-10.5	4.936	1297.1	1.264	7.55	7.416
284	20	45	15	20	-25.460	1.288	10.474	-12.29	5.156	1257.45	1.072	7.2	7.106
285	20	45	20	15	-26.395	1.288	10.474	-13.64	5.268	1217.8	0.935	6.85	6.797
286	20	45	25	10	-26.606	1.258	10.233	-14.55	5.285	1178.15	0.829	6.5	6.487
287	20	45	30	5	-26.060	1.192	9.697	-15.02	5.209	1138.5	0.735	6.15	6.177
288	20	50	5	25	-20.407	1.165	9.475	-7.84	4.533	1326.35	1.603	7.75	7.653

289	20	50	10	20	-22.735	1.221	9.928	-9.96	4.824	1286.7	1.283	7.4	7.343
290	20	50	15	15	-24.194	1.238	10.067	-11.64	4.994	1247.05	1.078	7.05	7.033
291	20	50	20	10	-24.868	1.221	9.928	-12.88	5.057	1207.4	0.931	6.7	6.723
292	20	50	25	5	-24.744	1.165	9.475	-13.68	5.024	1167.75	0.809	6.35	6.413
293	25	5	20	50	-25.927	1.165	9.475	-13.56	5.903	1305.25	0.912	7.95	7.331
294	25	5	25	45	-27.597	1.202	9.779	-15.22	6.290	1265.6	0.813	7.6	7.021
295	25	5	30	40	-28.646	1.224	9.957	-16.44	6.568	1225.95	0.742	7.25	6.711
296	25	5	35	35	-29.101	1.231	10.015	-17.22	6.754	1186.3	0.690	6.9	6.402
297	25	5	40	30	-28.977	1.224	9.957	-17.56	6.857	1146.65	0.650	6.55	6.092
298	25	5	45	25	-28.286	1.202	9.779	-17.46	6.886	1107	0.620	6.2	5.782
299	25	5	50	20	-27.033	1.165	9.475	-16.92	6.843	1067.35	0.598	5.85	5.472
300	25	10	15	50	-25.102	1.208	9.826	-11.99	5.458	1334.5	1.094	8.15	7.567
301	25	10	20	45	-27.230	1.258	10.233	-13.98	5.923	1294.85	0.948	7.8	7.258
302	25	10	25	40	-28.700	1.290	10.492	-15.53	6.260	1255.2	0.848	7.45	6.948
303	25	10	30	35	-29.547	1.305	10.619	-16.64	6.494	1215.55	0.776	7.1	6.638
304	25	10	35	30	-29.796	1.305	10.619	-17.31	6.639	1175.9	0.721	6.75	6.328
305	25	10	40	25	-29.462	1.290	10.492	-17.54	6.704	1136.25	0.680	6.4	6.018
306	25	10	45	20	-28.551	1.258	10.233	-17.33	6.695	1096.6	0.648	6.05	5.709
307	25	10	50	15	-27.065	1.208	9.826	-16.68	6.614	1056.95	0.623	5.7	5.399
308	25	15	10	50	-23.440	1.208	9.826	-10.04	4.947	1363.75	1.335	8.35	7.804
309	25	15	15	45	-26.092	1.275	10.371	-12.36	5.507	1324.1	1.111	8	7.494
310	25	15	20	40	-28.026	1.320	10.733	-14.24	5.915	1284.45	0.968	7.65	7.184
311	25	15	25	35	-29.300	1.345	10.941	-15.68	6.205	1244.8	0.869	7.3	6.874
312	25	15	30	30	-29.948	1.354	11.010	-16.68	6.396	1205.15	0.795	6.95	6.565
313	25	15	35	25	-29.992	1.345	10.941	-17.24	6.501	1165.5	0.740	6.6	6.255
314	25	15	40	20	-29.444	1.320	10.733	-17.36	6.527	1125.85	0.696	6.25	5.945
315	25	15	45	15	-28.305	1.275	10.371	-17.04	6.479	1086.2	0.661	5.9	5.635

316	25	15	50	10	-26.563	1.208	9.826	-16.28	6.357	1046.55	0.632	5.55	5.325
317	25	20	5	50	-20.908	1.165	9.475	-7.71	4.344	1393	1.712	8.55	8.040
318	25	20	10	45	-24.209	1.258	10.233	-10.36	5.031	1353.35	1.337	8.2	7.730
319	25	20	15	40	-26.670	1.320	10.733	-12.57	5.525	1313.7	1.122	7.85	7.421
320	25	20	20	35	-28.411	1.358	11.044	-14.34	5.880	1274.05	0.981	7.5	7.111
321	25	20	25	30	-29.488	1.376	11.194	-15.67	6.124	1234.4	0.882	7.15	6.801
322	25	20	30	25	-29.934	1.376	11.194	-16.56	6.273	1194.75	0.808	6.8	6.491
323	25	20	35	20	-29.767	1.358	11.044	-17.01	6.338	1155.1	0.750	6.45	6.181
324	25	20	40	15	-28.992	1.320	10.733	-17.02	6.324	1115.45	0.703	6.1	5.872
325	25	20	45	10	-27.599	1.258	10.233	-16.59	6.235	1075.8	0.664	5.75	5.562
326	25	20	50	5	-25.537	1.165	9.475	-15.72	6.070	1036.15	0.625	5.4	5.252
327	25	25	5	45	-21.501	1.202	9.779	-7.98	4.475	1382.6	1.694	8.4	7.967
328	25	25	10	40	-24.611	1.290	10.492	-10.52	5.080	1342.95	1.339	8.05	7.657
329	25	25	15	35	-26.880	1.345	10.941	-12.62	5.514	1303.3	1.130	7.7	7.347
330	25	25	20	30	-28.426	1.376	11.194	-14.28	5.818	1263.65	0.991	7.35	7.037
331	25	25	25	25	-29.302	1.386	11.276	-15.5	6.017	1224	0.890	7	6.728
332	25	25	30	20	-29.538	1.376	11.194	-16.28	6.125	1184.35	0.814	6.65	6.418
333	25	25	35	15	-29.145	1.345	10.941	-16.62	6.148	1144.7	0.754	6.3	6.108
334	25	25	40	10	-28.114	1.290	10.492	-16.52	6.093	1105.05	0.702	5.95	5.798
335	25	25	45	5	-26.399	1.202	9.779	-15.98	5.960	1065.4	0.652	5.6	5.488
336	25	30	5	40	-21.752	1.224	9.957	-8.09	4.564	1372.2	1.689	8.25	7.893
337	25	30	10	35	-24.670	1.305	10.619	-10.52	5.097	1332.55	1.345	7.9	7.584
338	25	30	15	30	-26.744	1.354	11.010	-12.51	5.474	1292.9	1.138	7.55	7.274
339	25	30	20	25	-28.089	1.376	11.194	-14.06	5.730	1253.25	0.998	7.2	6.964
340	25	30	25	20	-28.755	1.376	11.194	-15.17	5.884	1213.6	0.896	6.85	6.654
341	25	30	30	15	-28.765	1.354	11.010	-15.84	5.949	1173.95	0.816	6.5	6.344
342	25	30	35	10	-28.115	1.305	10.619	-16.07	5.930	1134.3	0.750	6.15	6.035

343	25	30	40	5	-26.759	1.224	9.957	-15.86	5.831	1094.65	0.687	5.8	5.725
344	25	35	5	35	-21.678	1.231	10.015	-8.04	4.614	1361.8	1.696	8.1	7.820
345	25	35	10	30	-24.399	1.305	10.619	-10.36	5.082	1322.15	1.355	7.75	7.510
346	25	35	15	25	-26.272	1.345	10.941	-12.24	5.405	1282.5	1.146	7.4	7.200
347	25	35	20	20	-27.406	1.358	11.044	-13.68	5.613	1242.85	1.003	7.05	6.891
348	25	35	25	15	-27.845	1.345	10.941	-14.68	5.723	1203.2	0.897	6.7	6.581
349	25	35	30	10	-27.595	1.305	10.619	-15.24	5.745	1163.55	0.811	6.35	6.271
350	25	35	35	5	-26.616	1.231	10.015	-15.36	5.682	1123.9	0.733	6	5.961
351	25	40	5	30	-21.285	1.224	9.957	-7.83	4.629	1351.4	1.718	7.95	7.747
352	25	40	10	25	-23.803	1.290	10.492	-10.04	5.035	1311.75	1.371	7.6	7.437
353	25	40	15	20	-25.464	1.320	10.733	-11.81	5.307	1272.1	1.156	7.25	7.127
354	25	40	20	15	-26.368	1.320	10.733	-13.14	5.468	1232.45	1.007	6.9	6.817
355	25	40	25	10	-26.545	1.290	10.492	-14.03	5.533	1192.8	0.892	6.55	6.507
356	25	40	30	5	-25.961	1.224	9.957	-14.48	5.509	1153.15	0.793	6.2	6.198
357	25	45	5	25	-20.574	1.202	9.779	-7.46	4.609	1341	1.758	7.8	7.673
358	25	45	10	20	-22.877	1.258	10.233	-9.56	4.957	1301.35	1.393	7.45	7.363
359	25	45	15	15	-24.305	1.275	10.371	-11.22	5.178	1261.7	1.166	7.1	7.054
360	25	45	20	10	-24.945	1.258	10.233	-12.44	5.292	1222.05	1.005	6.75	6.744
361	25	45	25	5	-24.783	1.202	9.779	-13.22	5.311	1182.4	0.875	6.4	6.434
362	25	50	5	20	-19.537	1.165	9.475	-6.93	4.554	1330.6	1.819	7.65	7.600
363	25	50	10	15	-21.604	1.208	9.826	-8.92	4.847	1290.95	1.422	7.3	7.290
364	25	50	15	10	-22.765	1.208	9.826	-10.47	5.018	1251.3	1.174	6.95	6.980
365	25	50	20	5	-23.060	1.165	9.475	-11.58	5.083	1211.65	0.991	6.6	6.670
366	30	5	15	50	-23.684	1.142	9.290	-11.15	5.388	1349.15	1.124	8.2	7.588
367	30	5	20	45	-25.819	1.192	9.697	-13.12	5.915	1309.5	0.968	7.85	7.278
368	30	5	25	40	-27.293	1.224	9.957	-14.65	6.304	1269.85	0.863	7.5	6.968
369	30	5	30	35	-28.144	1.240	10.083	-15.74	6.583	1230.2	0.788	7.15	6.658

370	30	5	35	30	-28.394	1.240	10.083	-16.39	6.770	1190.55	0.732	6.8	6.349
371	30	5	40	25	-28.059	1.224	9.957	-16.6	6.875	1150.9	0.690	6.45	6.039
372	30	5	45	20	-27.146	1.192	9.697	-16.37	6.905	1111.25	0.658	6.1	5.729
373	30	5	50	15	-25.655	1.142	9.290	-15.7	6.865	1071.6	0.634	5.75	5.419
374	30	10	10	50	-22.379	1.168	9.503	-9.28	4.836	1378.4	1.411	8.4	7.824
375	30	10	15	45	-25.032	1.235	10.048	-11.58	5.470	1338.75	1.162	8.05	7.514
376	30	10	20	40	-26.964	1.280	10.410	-13.44	5.936	1299.1	1.006	7.7	7.205
377	30	10	25	35	-28.234	1.305	10.619	-14.86	6.275	1259.45	0.900	7.35	6.895
378	30	10	30	30	-28.876	1.314	10.687	-15.84	6.511	1219.8	0.823	7	6.585
379	30	10	35	25	-28.912	1.305	10.619	-16.38	6.657	1180.15	0.765	6.65	6.275
380	30	10	40	20	-28.353	1.280	10.410	-16.48	6.724	1140.5	0.720	6.3	5.965
381	30	10	45	15	-27.202	1.235	10.048	-16.14	6.716	1100.85	0.685	5.95	5.656
382	30	10	50	10	-25.444	1.168	9.503	-15.36	6.637	1061.2	0.657	5.6	5.346
383	30	15	5	50	-20.107	1.142	9.290	-7.03	4.178	1407.65	1.860	8.6	8.061
384	30	15	10	45	-23.406	1.235	10.048	-9.66	4.959	1368	1.423	8.25	7.751
385	30	15	15	40	-25.862	1.297	10.549	-11.85	5.520	1328.35	1.182	7.9	7.441
386	30	15	20	35	-27.595	1.335	10.860	-13.6	5.930	1288.7	1.029	7.55	7.131
387	30	15	25	30	-28.662	1.354	11.010	-14.91	6.221	1249.05	0.922	7.2	6.821
388	30	15	30	25	-29.095	1.354	11.010	-15.78	6.414	1209.4	0.844	6.85	6.512
389	30	15	35	20	-28.913	1.335	10.860	-16.21	6.520	1169.75	0.784	6.5	6.202
390	30	15	40	15	-28.121	1.297	10.549	-16.2	6.548	1130.1	0.736	6.15	5.892
391	30	15	45	10	-26.707	1.235	10.048	-15.75	6.502	1090.45	0.696	5.8	5.582
392	30	15	50	5	-24.622	1.142	9.290	-14.86	6.382	1050.8	0.657	5.45	5.272
393	30	20	5	45	-20.910	1.192	9.697	-7.36	4.356	1397.25	1.841	8.45	7.987
394	30	20	10	40	-24.013	1.280	10.410	-9.88	5.044	1357.6	1.430	8.1	7.677
395	30	20	15	35	-26.272	1.335	10.860	-11.96	5.540	1317.95	1.197	7.75	7.368
396	30	20	20	30	-27.805	1.366	11.112	-13.6	5.896	1278.3	1.044	7.4	7.058

397	30	20	25	25	-28.666	1.376	11.194	-14.8	6.141	1238.65	0.937	7.05	6.748
398	30	20	30	20	-28.884	1.366	11.112	-15.56	6.292	1199	0.856	6.7	6.438
399	30	20	35	15	-28.470	1.335	10.860	-15.88	6.358	1159.35	0.793	6.35	6.128
400	30	20	40	10	-27.416	1.280	10.410	-15.76	6.347	1119.7	0.740	6	5.819
401	30	20	45	5	-25.674	1.192	9.697	-15.2	6.259	1080.05	0.689	5.65	5.509
402	30	25	5	40	-21.338	1.224	9.957	-7.53	4.488	1386.85	1.834	8.3	7.914
403	30	25	10	35	-24.245	1.305	10.619	-9.94	5.095	1347.2	1.439	7.95	7.604
404	30	25	15	30	-26.306	1.354	11.010	-11.91	5.530	1307.55	1.209	7.6	7.294
405	30	25	20	25	-27.633	1.376	11.194	-13.44	5.836	1267.9	1.056	7.25	6.984
406	30	25	25	20	-28.279	1.376	11.194	-14.53	6.036	1228.25	0.946	6.9	6.675
407	30	25	30	15	-28.266	1.354	11.010	-15.18	6.145	1188.6	0.862	6.55	6.365
408	30	25	35	10	-27.590	1.305	10.619	-15.39	6.171	1148.95	0.793	6.2	6.055
409	30	25	40	5	-26.205	1.224	9.957	-15.16	6.117	1109.3	0.729	5.85	5.745
410	30	30	5	35	-21.419	1.240	10.083	-7.54	4.578	1376.45	1.841	8.15	7.840
411	30	30	10	30	-24.126	1.314	10.687	-9.84	5.113	1336.8	1.452	7.8	7.531
412	30	30	15	25	-25.981	1.354	11.010	-11.7	5.491	1297.15	1.221	7.45	7.221
413	30	30	20	20	-27.094	1.366	11.112	-13.12	5.748	1257.5	1.065	7.1	6.911
414	30	30	25	15	-27.508	1.354	11.010	-14.1	5.905	1217.85	0.951	6.75	6.601
415	30	30	30	10	-27.231	1.314	10.687	-14.64	5.971	1178.2	0.860	6.4	6.291
416	30	30	35	5	-26.220	1.240	10.083	-14.74	5.954	1138.55	0.779	6.05	5.982
417	30	35	5	30	-21.164	1.240	10.083	-7.39	4.631	1366.05	1.864	8	7.767
418	30	35	10	25	-23.665	1.305	10.619	-9.58	5.099	1326.4	1.470	7.65	7.457
419	30	35	15	20	-25.304	1.335	10.860	-11.33	5.424	1286.75	1.233	7.3	7.147
420	30	35	20	15	-26.183	1.335	10.860	-12.64	5.634	1247.1	1.071	6.95	6.838
421	30	35	25	10	-26.331	1.305	10.619	-13.51	5.745	1207.45	0.949	6.6	6.528
422	30	35	30	5	-25.715	1.240	10.083	-13.94	5.768	1167.8	0.845	6.25	6.218
423	30	40	5	25	-20.578	1.224	9.957	-7.08	4.647	1355.65	1.906	7.85	7.694

424	30	40	10	20	-22.860	1.280	10.410	-9.16	5.054	1316	1.496	7.5	7.384
425	30	40	15	15	-24.264	1.297	10.549	-10.8	5.327	1276.35	1.247	7.15	7.074
426	30	40	20	10	-24.874	1.280	10.410	-12	5.490	1236.7	1.073	6.8	6.764
427	30	40	25	5	-24.679	1.224	9.957	-12.76	5.557	1197.05	0.934	6.45	6.454
428	30	45	5	20	-19.655	1.192	9.697	-6.61	4.628	1345.25	1.974	7.7	7.620
429	30	45	10	15	-21.699	1.235	10.048	-8.58	4.978	1305.6	1.529	7.35	7.310
430	30	45	15	10	-22.831	1.235	10.048	-10.11	5.200	1265.95	1.258	7	7.001
431	30	45	20	5	-23.092	1.192	9.697	-11.2	5.316	1226.3	1.062	6.65	6.691
432	30	50	5	15	-18.381	1.142	9.290	-5.98	4.575	1334.85	2.074	7.55	7.547
433	30	50	10	10	-20.148	1.168	9.503	-7.84	4.869	1295.2	1.570	7.2	7.237
434	30	50	15	5	-20.924	1.142	9.290	-9.26	5.042	1255.55	1.260	6.85	6.927
435	35	5	10	50	-20.917	1.094	8.899	-8.52	4.681	1393.05	1.455	8.45	7.845
436	35	5	15	45	-23.582	1.161	9.445	-10.8	5.399	1353.4	1.184	8.1	7.535
437	35	5	20	40	-25.523	1.206	9.807	-12.64	5.927	1313.75	1.019	7.75	7.225
438	35	5	25	35	-26.800	1.231	10.015	-14.04	6.318	1274.1	0.909	7.4	6.915
439	35	5	30	30	-27.447	1.240	10.083	-15	6.598	1234.45	0.830	7.05	6.606
440	35	5	35	25	-27.486	1.231	10.015	-15.52	6.787	1194.8	0.771	6.7	6.296
441	35	5	40	20	-26.928	1.206	9.807	-15.6	6.893	1155.15	0.726	6.35	5.986
442	35	5	45	15	-25.775	1.161	9.445	-15.24	6.925	1115.5	0.691	6	5.676
443	35	5	50	10	-24.014	1.094	8.899	-14.44	6.886	1075.85	0.663	5.65	5.366
444	35	10	5	50	-19.007	1.094	8.899	-6.35	3.954	1422.3	1.993	8.65	8.081
445	35	10	10	45	-22.313	1.187	9.657	-8.96	4.846	1382.65	1.490	8.3	7.771
446	35	10	15	40	-24.772	1.249	10.158	-11.13	5.482	1343	1.226	7.95	7.462
447	35	10	20	35	-26.504	1.287	10.469	-12.86	5.950	1303.35	1.061	7.6	7.152
448	35	10	25	30	-27.569	1.305	10.619	-14.15	6.290	1263.7	0.948	7.25	6.842
449	35	10	30	25	-27.998	1.305	10.619	-15	6.527	1224.05	0.867	6.9	6.532
450	35	10	35	20	-27.809	1.287	10.469	-15.41	6.675	1184.4	0.805	6.55	6.222

451	35	10	40	15	-27.008	1.249	10.158	-15.38	6.743	1144.75	0.756	6.2	5.913
452	35	10	45	10	-25.582	1.187	9.657	-14.91	6.737	1105.1	0.716	5.85	5.603
453	35	10	50	5	-23.481	1.094	8.899	-14	6.660	1065.45	0.677	5.5	5.293
454	35	15	5	45	-20.075	1.161	9.445	-6.74	4.188	1411.9	1.978	8.5	8.008
455	35	15	10	40	-23.179	1.249	10.158	-9.24	4.970	1372.25	1.509	8.15	7.698
456	35	15	15	35	-25.435	1.304	10.607	-11.3	5.533	1332.6	1.251	7.8	7.388
457	35	15	20	30	-26.961	1.335	10.860	-12.92	5.944	1292.95	1.087	7.45	7.078
458	35	15	25	25	-27.813	1.345	10.941	-14.1	6.237	1253.3	0.973	7.1	6.769
459	35	15	30	20	-28.020	1.335	10.860	-14.84	6.431	1213.65	0.888	6.75	6.459
460	35	15	35	15	-27.592	1.304	10.607	-15.14	6.539	1174	0.822	6.4	6.149
461	35	15	40	10	-26.522	1.249	10.158	-15	6.569	1134.35	0.768	6.05	5.839
462	35	15	45	5	-24.759	1.161	9.445	-14.42	6.524	1094.7	0.717	5.7	5.529
463	35	20	5	40	-20.714	1.206	9.807	-6.97	4.368	1401.5	1.972	8.35	7.934
464	35	20	10	35	-23.617	1.287	10.469	-9.36	5.057	1361.85	1.523	8	7.625
465	35	20	15	30	-25.669	1.335	10.860	-11.31	5.554	1322.2	1.270	7.65	7.315
466	35	20	20	25	-26.985	1.358	11.044	-12.82	5.912	1282.55	1.105	7.3	7.005
467	35	20	25	20	-27.617	1.358	11.044	-13.89	6.159	1242.9	0.988	6.95	6.695
468	35	20	30	15	-27.587	1.335	10.860	-14.52	6.311	1203.25	0.900	6.6	6.385
469	35	20	35	10	-26.891	1.287	10.469	-14.71	6.379	1163.6	0.828	6.25	6.076
470	35	20	40	5	-25.482	1.206	9.807	-14.46	6.369	1123.95	0.762	5.9	5.766
471	35	25	5	35	-20.972	1.231	10.015	-7.04	4.501	1391.1	1.979	8.2	7.861
472	35	25	10	30	-23.671	1.305	10.619	-9.32	5.109	1351.45	1.540	7.85	7.551
473	35	25	15	25	-25.513	1.345	10.941	-11.16	5.546	1311.8	1.286	7.5	7.241
474	35	25	20	20	-26.610	1.358	11.044	-12.56	5.853	1272.15	1.119	7.15	6.932
475	35	25	25	15	-27.005	1.345	10.941	-13.52	6.055	1232.5	0.997	6.8	6.622
476	35	25	30	10	-26.706	1.305	10.619	-14.04	6.165	1192.85	0.902	6.45	6.312
477	35	25	35	5	-25.669	1.231	10.015	-14.12	6.193	1153.2	0.818	6.1	6.002

478	35	30	5	30	-20.872	1.240	10.083	-6.95	4.593	1380.7	2.003	8.05	7.788
479	35	30	10	25	-23.360	1.305	10.619	-9.12	5.128	1341.05	1.561	7.7	7.478
480	35	30	15	20	-24.983	1.335	10.860	-10.85	5.508	1301.4	1.303	7.35	7.168
481	35	30	20	15	-25.842	1.335	10.860	-12.14	5.767	1261.75	1.129	7	6.858
482	35	30	25	10	-25.967	1.305	10.619	-12.99	5.925	1222.1	0.999	6.65	6.548
483	35	30	30	5	-25.323	1.240	10.083	-13.4	5.993	1182.45	0.890	6.3	6.239
484	35	35	5	25	-20.423	1.231	10.015	-6.7	4.647	1370.3	2.048	7.9	7.714
485	35	35	10	20	-22.690	1.287	10.469	-8.76	5.116	1330.65	1.590	7.55	7.404
486	35	35	15	15	-24.073	1.304	10.607	-10.38	5.442	1291	1.319	7.2	7.095
487	35	35	20	10	-24.660	1.287	10.469	-11.56	5.654	1251.35	1.133	6.85	6.785
488	35	35	25	5	-24.435	1.231	10.015	-12.3	5.767	1211.7	0.987	6.5	6.475
489	35	40	5	20	-19.626	1.206	9.807	-6.29	4.664	1359.9	2.120	7.75	7.641
490	35	40	10	15	-21.651	1.249	10.158	-8.24	5.073	1320.25	1.627	7.4	7.331
491	35	40	15	10	-22.758	1.249	10.158	-9.75	5.347	1280.6	1.334	7.05	7.021
492	35	40	20	5	-22.989	1.206	9.807	-10.82	5.512	1240.95	1.125	6.7	6.711
493	35	45	5	15	-18.465	1.161	9.445	-5.72	4.647	1349.5	2.228	7.6	7.567
494	35	45	10	10	-20.210	1.187	9.657	-7.56	4.998	1309.85	1.673	7.25	7.258
495	35	45	15	5	-20.956	1.161	9.445	-8.96	5.222	1270.2	1.339	6.9	6.948
496	35	50	5	10	-16.907	1.094	8.899	-4.99	4.596	1339.1	2.388	7.45	7.494
497	35	50	10	5	-18.284	1.094	8.899	-6.72	4.891	1299.45	1.721	7.1	7.184
498	40	5	5	50	-17.506	1.013	8.237	-5.67	3.662	1436.95	2.088	8.7	8.102
499	40	5	10	45	-20.829	1.106	8.995	-8.26	4.690	1397.3	1.522	8.35	7.792
500	40	5	15	40	-23.302	1.167	9.496	-10.41	5.410	1357.65	1.238	8	7.482
501	40	5	20	35	-25.045	1.206	9.807	-12.12	5.940	1318	1.066	7.65	7.172
502	40	5	25	30	-26.118	1.224	9.957	-13.39	6.331	1278.35	0.951	7.3	6.862
503	40	5	30	25	-26.553	1.224	9.957	-14.22	6.613	1238.7	0.867	6.95	6.553
504	40	5	35	20	-26.369	1.206	9.807	-14.61	6.803	1199.05	0.805	6.6	6.243

505	40	5	40	15	-25.569	1.167	9.496	-14.56	6.911	1159.4	0.756	6.25	5.933
506	40	5	45	10	-24.142	1.106	8.995	-14.07	6.944	1119.75	0.716	5.9	5.623
507	40	5	50	5	-22.037	1.013	8.237	-13.14	6.907	1080.1	0.677	5.55	5.313
508	40	10	5	45	-18.952	1.106	8.995	-6.12	3.963	1426.55	2.097	8.55	8.028
509	40	10	10	40	-22.064	1.194	9.708	-8.6	4.857	1386.9	1.566	8.2	7.718
510	40	10	15	35	-24.325	1.249	10.158	-10.64	5.494	1347.25	1.286	7.85	7.409
511	40	10	20	30	-25.853	1.280	10.410	-12.24	5.963	1307.6	1.112	7.5	7.099
512	40	10	25	25	-26.704	1.290	10.492	-13.4	6.305	1267.95	0.993	7.15	6.789
513	40	10	30	20	-26.907	1.280	10.410	-14.12	6.543	1228.3	0.906	6.8	6.479
514	40	10	35	15	-26.474	1.249	10.158	-14.4	6.692	1188.65	0.838	6.45	6.169
515	40	10	40	10	-25.395	1.194	9.708	-14.24	6.762	1149	0.783	6.1	5.860
516	40	10	45	5	-23.619	1.106	8.995	-13.64	6.758	1109.35	0.732	5.75	5.550
517	40	15	5	40	-19.857	1.167	9.496	-6.41	4.198	1416.15	2.098	8.4	7.955
518	40	15	10	35	-22.762	1.249	10.158	-8.78	4.982	1376.5	1.592	8.05	7.645
519	40	15	15	30	-24.812	1.297	10.549	-10.71	5.546	1336.85	1.317	7.7	7.335
520	40	15	20	25	-26.123	1.320	10.733	-12.2	5.959	1297.2	1.141	7.35	7.025
521	40	15	25	20	-26.748	1.320	10.733	-13.25	6.253	1257.55	1.019	7	6.716
522	40	15	30	15	-26.707	1.297	10.549	-13.86	6.448	1217.9	0.927	6.65	6.406
523	40	15	35	10	-25.998	1.249	10.158	-14.03	6.558	1178.25	0.853	6.3	6.096
524	40	15	40	5	-24.572	1.167	9.496	-13.76	6.589	1138.6	0.786	5.95	5.786
525	40	20	5	35	-20.326	1.206	9.807	-6.54	4.379	1405.75	2.108	8.25	7.881
526	40	20	10	30	-23.022	1.280	10.410	-8.8	5.070	1366.1	1.616	7.9	7.572
527	40	20	15	25	-24.857	1.320	10.733	-10.62	5.569	1326.45	1.341	7.55	7.262
528	40	20	20	20	-25.944	1.332	10.836	-12	5.928	1286.8	1.162	7.2	6.952
529	40	20	25	15	-26.326	1.320	10.733	-12.94	6.176	1247.15	1.034	6.85	6.642
530	40	20	30	10	-26.010	1.280	10.410	-13.44	6.329	1207.5	0.935	6.5	6.332
531	40	20	35	5	-24.953	1.206	9.807	-13.5	6.399	1167.85	0.848	6.15	6.023

532	40	25	5	30	-20.403	1.224	9.957	-6.51	4.514	1395.35	2.134	8.1	7.808
533	40	25	10	25	-22.884	1.290	10.492	-8.66	5.124	1355.7	1.643	7.75	7.498
534	40	25	15	20	-24.495	1.320	10.733	-10.37	5.561	1316.05	1.362	7.4	7.188
535	40	25	20	15	-25.340	1.320	10.733	-11.64	5.870	1276.4	1.177	7.05	6.879
536	40	25	25	10	-25.446	1.290	10.492	-12.47	6.073	1236.75	1.041	6.7	6.569
537	40	25	30	5	-24.779	1.224	9.957	-12.86	6.185	1197.1	0.927	6.35	6.259
538	40	30	5	25	-20.109	1.224	9.957	-6.32	4.607	1384.95	2.182	7.95	7.735
539	40	30	10	20	-22.365	1.280	10.410	-8.36	5.144	1345.3	1.675	7.6	7.425
540	40	30	15	15	-23.733	1.297	10.549	-9.96	5.525	1305.65	1.383	7.25	7.115
541	40	30	20	10	-24.299	1.280	10.410	-11.12	5.785	1266	1.185	6.9	6.805
542	40	30	25	5	-24.050	1.224	9.957	-11.84	5.945	1226.35	1.031	6.55	6.495
543	40	35	5	20	-19.450	1.206	9.807	-5.97	4.662	1374.55	2.258	7.8	7.661
544	40	35	10	15	-21.459	1.249	10.158	-7.9	5.133	1334.9	1.716	7.45	7.351
545	40	35	15	10	-22.547	1.249	10.158	-9.39	5.461	1295.25	1.401	7.1	7.042
546	40	35	20	5	-22.753	1.206	9.807	-10.44	5.674	1255.6	1.179	6.75	6.732
547	40	40	5	15	-18.413	1.167	9.496	-5.46	4.682	1364.15	2.372	7.65	7.588
548	40	40	10	10	-20.139	1.194	9.708	-7.28	5.091	1324.5	1.766	7.3	7.278
549	40	40	15	5	-20.860	1.167	9.496	-8.66	5.367	1284.85	1.409	6.95	6.968
550	40	45	5	10	-16.967	1.106	8.995	-4.79	4.666	1353.75	2.542	7.5	7.514
551	40	45	10	5	-18.321	1.106	8.995	-6.5	5.018	1314.1	1.819	7.15	7.205
552	40	50	5	5	-15.025	1.013	8.237	-3.96	4.617	1343.35	2.794	7.35	7.441
553	45	5	5	45	-17.436	1.018	8.282	-5.5	3.669	1441.2	2.170	8.6	8.049
554	45	5	10	40	-20.567	1.106	8.995	-7.96	4.699	1401.55	1.584	8.25	7.739
555	45	5	15	35	-22.843	1.161	9.445	-9.98	5.420	1361.9	1.289	7.9	7.429
556	45	5	20	30	-24.382	1.192	9.697	-11.56	5.952	1322.25	1.109	7.55	7.119
557	45	5	25	25	-25.243	1.202	9.779	-12.7	6.345	1282.6	0.988	7.2	6.810
558	45	5	30	20	-25.453	1.192	9.697	-13.4	6.628	1242.95	0.899	6.85	6.500

559	45	5	35	15	-25.025	1.161	9.445	-13.66	6.819	1203.3	0.832	6.5	6.190
560	45	5	40	10	-23.947	1.106	8.995	-13.48	6.929	1163.65	0.777	6.15	5.880
561	45	5	45	5	-22.169	1.018	8.282	-12.86	6.964	1124	0.724	5.8	5.570
562	45	10	5	40	-18.720	1.106	8.995	-5.85	3.972	1430.8	2.200	8.45	7.975
563	45	10	10	35	-21.635	1.187	9.657	-8.2	4.867	1391.15	1.638	8.1	7.666
564	45	10	15	30	-23.690	1.235	10.048	-10.11	5.506	1351.5	1.343	7.75	7.356
565	45	10	20	25	-25.004	1.258	10.233	-11.58	5.976	1311.85	1.159	7.4	7.046
566	45	10	25	20	-25.628	1.258	10.233	-12.61	6.319	1272.2	1.032	7.05	6.736
567	45	10	30	15	-25.585	1.235	10.048	-13.2	6.559	1232.55	0.938	6.7	6.426
568	45	10	35	10	-24.870	1.187	9.657	-13.35	6.710	1192.9	0.863	6.35	6.117
569	45	10	40	5	-23.434	1.106	8.995	-13.06	6.781	1153.25	0.794	6	5.807
570	45	15	5	35	-19.455	1.161	9.445	-6.04	4.208	1420.4	2.221	8.3	7.902
571	45	15	10	30	-22.154	1.235	10.048	-8.28	4.994	1380.75	1.676	7.95	7.592
572	45	15	15	25	-23.989	1.275	10.371	-10.08	5.559	1341.1	1.380	7.6	7.282
573	45	15	20	20	-25.071	1.288	10.474	-11.44	5.973	1301.45	1.192	7.25	6.973
574	45	15	25	15	-25.446	1.275	10.371	-12.36	6.269	1261.8	1.059	6.9	6.663
575	45	15	30	10	-25.121	1.235	10.048	-12.84	6.466	1222.15	0.956	6.55	6.353
576	45	15	35	5	-24.048	1.161	9.445	-12.88	6.577	1182.5	0.867	6.2	6.043
577	45	20	5	30	-19.743	1.192	9.697	-6.07	4.391	1410	2.253	8.15	7.829
578	45	20	10	25	-22.223	1.258	10.233	-8.2	5.083	1370.35	1.710	7.8	7.519
579	45	20	15	20	-23.828	1.288	10.474	-9.89	5.583	1330.7	1.409	7.45	7.209
580	45	20	20	15	-24.662	1.288	10.474	-11.14	5.943	1291.05	1.214	7.1	6.899
581	45	20	25	10	-24.756	1.258	10.233	-11.95	6.193	1251.4	1.072	6.75	6.589
582	45	20	30	5	-24.071	1.192	9.697	-12.32	6.348	1211.75	0.954	6.4	6.280
583	45	25	5	25	-19.627	1.202	9.779	-5.94	4.527	1399.6	2.304	8	7.755
584	45	25	10	20	-21.876	1.258	10.233	-7.96	5.138	1359.95	1.748	7.65	7.445
585	45	25	15	15	-23.233	1.275	10.371	-9.54	5.577	1320.3	1.435	7.3	7.136

586	45	25	20	10	-23.785	1.258	10.233	-10.68	5.887	1280.65	1.227	6.95	6.826
587	45	25	25	5	-23.516	1.202	9.779	-11.38	6.092	1241	1.066	6.6	6.516
588	45	30	5	20	-19.122	1.192	9.697	-5.65	4.622	1389.2	2.384	7.85	7.682
589	45	30	10	15	-21.121	1.235	10.048	-7.56	5.160	1349.55	1.794	7.5	7.372
590	45	30	15	10	-22.192	1.235	10.048	-9.03	5.542	1309.9	1.458	7.15	7.062
591	45	30	20	5	-22.378	1.192	9.697	-10.06	5.804	1270.25	1.224	6.8	6.752
592	45	35	5	15	-18.222	1.161	9.445	-5.2	4.678	1378.8	2.504	7.7	7.608
593	45	35	10	10	-19.933	1.187	9.657	-7	5.150	1339.15	1.848	7.35	7.299
594	45	35	15	5	-20.633	1.161	9.445	-8.36	5.479	1299.5	1.468	7	6.989
595	45	40	5	10	-16.899	1.106	8.995	-4.59	4.699	1368.4	2.682	7.55	7.535
596	45	40	10	5	-18.233	1.106	8.995	-6.28	5.110	1328.75	1.903	7.2	7.225
597	45	45	5	5	-15.067	1.018	8.282	-3.82	4.685	1358	2.944	7.4	7.462
598	50	5	5	40	-17.196	1.013	8.237	-5.29	3.677	1445.45	2.251	8.5	7.996
599	50	5	10	35	-20.130	1.094	8.899	-7.62	4.708	1405.8	1.642	8.15	7.686
600	50	5	15	30	-22.202	1.142	9.290	-9.51	5.431	1366.15	1.335	7.8	7.376
601	50	5	20	25	-23.528	1.165	9.475	-10.96	5.963	1326.5	1.147	7.45	7.066
602	50	5	25	20	-24.162	1.165	9.475	-11.97	6.358	1286.85	1.019	7.1	6.757
603	50	5	30	15	-24.126	1.142	9.290	-12.54	6.643	1247.2	0.924	6.75	6.447
604	50	5	35	10	-23.416	1.094	8.899	-12.67	6.836	1207.55	0.848	6.4	6.137
605	50	5	40	5	-21.980	1.013	8.237	-12.36	6.946	1167.9	0.778	6.05	5.827
606	50	10	5	35	-18.311	1.094	8.899	-5.54	3.980	1435.05	2.305	8.35	7.922
607	50	10	10	30	-21.020	1.168	9.503	-7.76	4.877	1395.4	1.709	8	7.613
608	50	10	15	25	-22.861	1.208	9.826	-9.54	5.518	1355.75	1.396	7.65	7.303
609	50	10	20	20	-23.947	1.221	9.928	-10.88	5.989	1316.1	1.201	7.3	6.993
610	50	10	25	15	-24.322	1.208	9.826	-11.78	6.334	1276.45	1.065	6.95	6.683
611	50	10	30	10	-23.993	1.168	9.503	-12.24	6.575	1236.8	0.960	6.6	6.373
612	50	10	35	5	-22.914	1.094	8.899	-12.26	6.727	1197.15	0.869	6.25	6.064

613	50	15	5	30	-18.865	1.142	9.290	-5.63	4.218	1424.65	2.351	8.2	7.849
614	50	15	10	25	-21.349	1.208	9.826	-7.74	5.005	1385	1.758	7.85	7.539
615	50	15	15	20	-22.953	1.238	10.067	-9.41	5.572	1345.35	1.439	7.5	7.229
616	50	15	20	15	-23.784	1.238	10.067	-10.64	5.987	1305.7	1.235	7.15	6.920
617	50	15	25	10	-23.870	1.208	9.826	-11.43	6.284	1266.05	1.088	6.8	6.610
618	50	15	30	5	-23.173	1.142	9.290	-11.78	6.483	1226.4	0.967	6.45	6.300
619	50	20	5	25	-18.960	1.165	9.475	-5.56	4.402	1414.25	2.410	8.05	7.776
620	50	20	10	20	-21.208	1.221	9.928	-7.56	5.096	1374.6	1.805	7.7	7.466
621	50	20	15	15	-22.558	1.238	10.067	-9.12	5.597	1334.95	1.474	7.35	7.156
622	50	20	20	10	-23.100	1.221	9.928	-10.24	5.959	1295.3	1.256	7	6.846
623	50	20	25	5	-22.817	1.165	9.475	-10.92	6.210	1255.65	1.089	6.65	6.536
624	50	25	5	20	-18.631	1.165	9.475	-5.33	4.540	1403.85	2.495	7.9	7.702
625	50	25	10	15	-20.624	1.208	9.826	-7.22	5.152	1364.2	1.857	7.55	7.392
626	50	25	15	10	-21.685	1.208	9.826	-8.67	5.592	1324.55	1.501	7.2	7.083
627	50	25	20	5	-21.854	1.165	9.475	-9.68	5.904	1284.9	1.258	6.85	6.773
628	50	30	5	15	-17.885	1.142	9.290	-4.94	4.636	1393.45	2.620	7.75	7.629
629	50	30	10	10	-19.585	1.168	9.503	-6.72	5.175	1353.8	1.914	7.4	7.319
630	50	30	15	5	-20.268	1.142	9.290	-8.06	5.559	1314.15	1.515	7.05	7.009
631	50	35	5	10	-16.698	1.094	8.899	-4.39	4.694	1383.05	2.804	7.6	7.555
632	50	35	10	5	-18.015	1.094	8.899	-6.06	5.167	1343.4	1.973	7.25	7.246
633	50	40	5	5	-14.987	1.013	8.237	-3.68	4.716	1372.65	3.072	7.45	7.482